NRC·CNRC

NRC Publications Archive
Archives des publications du CNRC

Short-time creep of ice

Zaretskii, Y. K.; Chumichev, B. D.

For the publisher's version, please access the DOI link below./ Pour consulter la version de l'éditeur, utilisez le lien DOI ci-dessous.

Publisher's version / Version de l'éditeur:
https://doi.org/10.4224/20359126
Technical Translation (National Research Council of Canada), 1985

NRC Publications Archive Record / Notice des Archives des publications du CNRC :
https://nrc-publications.canada.ca/eng/view/object/?id=93e88f60-0865-4325-8b91-d68c3fa4ee63
https://publications-cnrc.canada.ca/fra/voir/objet/?id=93e88f60-0865-4325-8b91-d68c3fa4ee63

Access and use of this website and the material on it are subject to the Terms and Conditions set forth at
https://nrc-publications.canada.ca/eng/copyright
READ THESE TERMS AND CONDITIONS CAREFULLY BEFORE USING THIS WEBSITE.

L'accès à ce site Web et l'utilisation de son contenu sont assujettis aux conditions présentées dans le site
https://publications-cnrc.canada.ca/fra/droits
LISEZ CES CONDITIONS ATTENTIVEMENT AVANT D'UTILISER CE SITE WEB.

Questions? Contact the NRC Publications Archive team at PublicationsArchive-ArchivesPublications@nrc-cnrc.gc.ca. If you wish to email the authors directly, please see the first page of the publication for their contact information.

Vous avez des questions? Nous pouvons vous aider. Pour communiquer directement avec un auteur, consultez la première page de la revue dans laquelle son article a été publié afin de trouver ses coordonnées. Si vous n'arrivez pas à les repérer, communiquez avec nous à PublicationsArchive-ArchivesPublications@nrc-cnrc.gc.ca.

National Research Council Canada | Conseil national de recherches Canada

Canada

NATIONAL RESEARCH COUNCIL CANADA

CONSEIL NATIONAL DE RECHERCHES CANADA

TECHNICAL TRANSLATION 2111

TRADUCTION TECHNIQUE

ANALYZED

Author/Auteur:	Yu.K.Zaretskii and B.D.Chumichev
Title/Titre:	Short-time creep of ice
Reference/Référence:	Kratkovremennaya Polzuchest' L'da, 1982, p. 1-117
Translator/Traducteur:	Tania Thorpe

Ottawa, Canada
K1A 0R6

Preface

Ice is an unusual solid in that it exists normally at a temperature close to melting and so is in a high temperature state. In this state it exhibits under stress deformation behaviour and failure similar to other solids with hexagonal crystalline symmetry. In addition, it is transparent and can have a columnar crystalline structure which is of particular interest in the study of factors controlling crack initiation and propagation.

This translation presents results of Russian investigations of creep and crack formation in ice. It is very relevant to similar work being done at the Division of Building Research, National Research Council of Canada, and to the problem of predicting the forces that ice can exert on structures.

The Division of Building Research expresses its appreciation to Tania Thorpe for the translation of this monograph.

Ottawa

February 1985

L.W. Gold
Acting Director
Division of Building Research

SHORT-TIME CREEP OF ICE

by

Yu.K.Zaretskii and B.D.Chumichev

CONTENTS

	Page
INTRODUCTION	3
CHAPTER 1. STRUCTURAL AND MECHANICAL PROPERTIES OF ICE	11
1.1. Properties and structure of ice	11
1.2. Strength and creep of ice	14
1.3. Brittle structural disturbances and acoustic emission of ice	26
CHAPTER 2. SHORT-TIME CREEP AND FAILURE OF ICE	32
2.1. Mathematical model of phenomenological description of short-time creep of ice	33
2.2. Micromechanism of deformation. Kinetics of accumulation of structural defects in ice	39
2.3. Short-time creep of ice	51
CHAPTER 3. INSTRUMENTS AND METHODS OF EXPERIMENTAL STUDIES	57
3.1. Preparation and testing procedures	58
3.2. Methods of structural-petrographic studies	64
3.3. Acoustic emission method	69

Page

CHAPTER 4. ACCUMULATION OF STRUCTURAL DEFECTS IN ICE DURING SHORT-TIME CREEP 82

4.1. Results of structural-petrographic analyses 82

4.2. Results of acoustic emission studies 96

4.3. Evaluation of the size of microcracks and its relation to structural changes 109

4.4. The process of microfracturing during creep of ice 115

CHAPTER 5. CREEP AND FAILURE OF ICE UNDER STATIC AND CYCLIC LOADS 120

5.1. Deformation and microfracturing 120

5.2. Vibrocreep and vibrostrength of ice 137

5.3. Testing ice under cyclic loads 150

CHAPTER 6. ALGORITHM OF THEORETICAL CALCULATIONS OF SHORT-TIME CREEP OF ICE 159

6.1. Fundamental equations of short-time creep of ice 159

6.2. Algorithm for determining viscoplastic deformations 163

6.3. Results of numerical modelling of uniaxial and triaxial compression of ice under conditions of short-time creep 169

CONCLUSION 177

REFERENCES 180

SHORT-TIME CREEP OF ICE

by

Yu.K.Zaretskii and B.D.Chumichev

AKADEMIYA NAUK SSSR

USSR ACADEMY OF SCIENCES

Siberian Branch

The Red Banner Order Institute of Geocryology

Editor: S.S.Vyalov, Doctor of Technical Sciences

"Nauka" Publishing House, Siberian Branch

Novosibirsk, 1982

Results of theoretical and experimental studies on failure of ice during short-time creep are reported in this work. Deformation and failure of ice under applied load are treated as a stochastic process composed of discrete events of the occurrence and development of microdefects in the crystal structure of ice. Models of ice deformation have been developed in which the magnitude and duration of stresses and the dependence on temperature have been taken into account.

The functional relation between the microprocess of the accumulation of brittle structural defects and the macroprocess of ice deformation has been confirmed.

The possibility of monitoring and predicting the stress strain state of ice masses with the help of acoustic emission records has been demonstrated. It has been established that

the fundamental theoretical propositions are applicable to vibrocreep* and to failure of ice under cyclic loads. The results of dynamic loading experiments confirm that the processes of ice failure during static and dynamic loading are essentially similar, and that the maximum number of structural defects is the proper criterion of failure of ice.

This monograph is intended for specialists dealing with physico-mechanical properties of ice under failure loads.

Fifty-four illustrations, four tables, and eighty-five references.

Novosibirsk, "Nauka", 1982.

* cyclic strain-induced creep. Translator.

INTRODUCTION

Ice is a natural and familiar part of our environment. Yet, owing to its unique properties, ice occupies a singular position in the series of rock-forming minerals and in nature as a whole.

The most important characteristic of ice may well be its being the solid phase of one of the few liquids which expand during freezing. Because of it ice, which in itself precludes life activities of organisms, floats on the surface of its own melt protecting thereby natural bodies of water against freezing and making it possible for water to remain liquid and for organic life to exist under cold climatic conditions.

Ice is the lightest and the lowest-temperature known mineral. Its total bulk on Earth ($\approx$20 million km^3) amounts to a negligibly small fraction of the Earth's volume ($\approx 2 \cdot 10^{-4}$%). Ice is nevertheless one of the most widely distributed solid constituents of the earth's surface. Ice sheets and mountain glaciers occupy close to 11% of land, and floating ice covers constantly or for a significant part of the year close to 12% of the surface of the Ocean of the World. Furthermore, about 10 to 12% of land, from the surface down to the depth of 400 to 600 m, is occupied by permafrost in which ice plays an extremely important rock-forming role. These types of ice and the ice particles disseminated virtually throughout the atmosphere form a specific kind of envelope surrounding the

earth, which may be designated as the cryosphere (Shumskii, 1955, 1969). The cryosphere is situated at the boundary of the lithosphere, hydrosphere and atmosphere. The main properties and distinctive characteristics of the cryosphere are its instability and mobility in time and space owing to the fact that under real conditions ice is always near the phase transition temperature.

Being a powerful natural factor in lithogenesis, as well as in formation of ancient and modern land forms, ice plays an enormous role in the economic activities of man, particularly in engineering. The significance of ice in economic and engineering practices should be assessed from two aspects.

On the one hand natural ice and the ice cover of water bodies are used for roads, crossings and other transport facilities, laying pipelines and supporting drill rigs and other temporary engineering structures. Permafrost is used as a high-bearing capacity foundation material. Ice may be formed in cavities used for storage of oil and gas in rock and to form a protective barrier in the construction of mines or tunnels.

On the other hand the very existence of ice may be extremely undesirable since it is an obstacle to navigation and its effect on dams, bridges, locks, harbours and other hydrotechnical structures, as well as on river banks and walls of water reservoirs, beacon foundations, LEP* and drill-rig supports is enormously detrimental to the economy. Snow and ice

---

* Transliteration. Translator.

avalanches and slides, ice jams and ice dams on rivers and the resultant floods also cause major problems and may even be hazardous. The use of permafrost and ice as a foundation or building material in construction not only involves additional complications and costs during their exploitation, but also the danger of inducing inadmissible deformations or even of causing instability of foundations or of supported structures.

When dealing with ice, be it a question of utilizing or controlling it, all the engineering measures envisaged must be based on information about the chief properties of ice, the amount of which is still inadequate at present.

The behaviour of ice under load is particularly important for practical purposes. In order to use ice as a road-building or construction material it is important to know what loads can be imposed safely on it under given conditions. In the case of ice masses acting on engineering structures, it is necessary to estimate the maximum stresses that can occur during that process. In both cases it is imperative to know the ultimate strength of ice and its deformation behaviour, particularly failure, under the given conditions and loading program.

Ice build-ups against abutments of bridges, moorings, dams or embankments, gates or supports of locks and other structures cause stresses to occur in the region contact of the ice mass with the structure, and deformations to develop simultaneously in ice. This process commonly takes several hours to several

minutes (in the event of a collision between isolated ice fields or ice floes even a few seconds) and ends in an avalanche-like acceleration of deformations and in failure of ice. A similar situation arises during the operation of an ice-breaker in a thick ice-cover that is breaking under the weight of the vessel advancing upon it, as well as during the catastrophic advances of the so-called surging glaciers. This kind of deformation of ice at an increasing rate represents, in fact, failure stretched in time and is referred to as short-time creep. The objective of the present investigation is to study the laws governing short-time creep of ice.

Next to temperature, the fabric of ice, i.e. its textural and structural characteristics, is the most important factor for the assessment of mechanical properties of ice and of the processes occurring in it. The rate, magnitudes and mechanisms of ice deformation under load vary substantially depending on the structural pattern, shape, size and orientation of the ice crystals, as well as on the presence of impurities in ice and on their properties.

On the other hand the direction, time and rate of deformation of an ice body (mass) affect in a definite way the structure of the ice, the development of one or another kind of dynamometamorphic processes, the appearance of characteristic structural features, specific disturbances, qualitative and quantitative changes of structural parameters.

The structure of ice and the processes of its deformation are thus closely interrelated and it is essential to study that relationship.

B.P. Weinberg (1940), P.A. Shumskii (1955, 1969, etc.), B.A. Savel'ev (1963), B.A. Savel'ev, A.E. Gulikov (1964), S.S. Vyalov (1960, 1973, 1976), K.F. Voitkovskii (1960), K.F. Voitkovskii, V.N. Golubev (1972), D. Glen (1955, 1958), L. Gold (1960, 1966, 1972a and b) and other authors have elucidated in their works the fundamentals of the mechanism of ice deformation, determined the general patterns of the behaviour of ice under load, and clarified certain distinctive aspects of the response of ice crystals to the applied force.

Mechanical processes in ice have, however, been so far little studied from the structural viewpoint, particularly experimentally. This may be due to the fact that the numerous investigations into mechanical properties of ice have not always or adequately been combined with structural methods.

It should be noted that the researchers focused for the most part either on determining the conventionally instantaneous strength of ice under different types of stresses (compression, tension, bending, shear, etc.) and on the dependence of that characteristic upon the temperature used in the tests, shape and size of the specimens, their structure and orientation; or on the dependence of the

steady-state (or minimum) creep rate at relatively small stresses upon the above parameters. There are relatively few works [Voitkovskii, Golubev, 1972; Vyalov, 1973; Vyalov et al., 1976; Zaretskii et al., 1974, 1975, 1976, 1979a and b; Korzhavin, Ptukhin, 1966; Lavrov, 1969; and so on] in which failure of ice is treated as a process that occurs in time and is accompanied by internal restructuring of ice and by modification of its mechanical characteristics. Even in the works available the analyses of structural parameters are usually of a qualitative nature.

It is therefore imperative to continue accumulating experimental evidence pertaining to the relationship between the processes of deformation and failure on the one hand and structural metamorphism of ice on the other.

Of considerable interest is the possibility of establishing a link between the structural changes induced in ice by the process of deformation, and the acoustic effects occurring in the course of the deformation.

As is well known [Gold, 1960], the increase of stress in ice above a certain limit results in microfracturing of the ice accompanied by sonic pulses (audible crackling). Yu.K. Zaretskii (1973) and Yu.K. Zaretskii et al. (1975) examined in their works the dependence of the kinetics of the crackling activity that proved to be directly proportional to the number of sonic pulses, the applied stress and time of deformation of ice. The patterns established can be used for

determining the rheological constants of ice from acoustic emission records, which is an important practical result. Structural microscopic studies enabling us to assess "from within" the degree of the structural breakdown of ice, the proportion of brittle and ductile defects, as well as their number and size at different stages of the deformation of ice, will significantly complement these works. Once the relationship has been determined between the stressed state of an ice mass, the magnitude and rate of its deformation, the kinetics of development of structural defects, and, lastly, the acoustic emission in it, the current notions of the mechanism of deformation and failure of ice can be significantly expanded.

In the present work a theoretical analysis of the process of short-time creep in ice (terminating in its failure) is performed on the basis of a variant of the plastic flow theory with the use of the molecular-kinetic theory of failure. A criterion of failure under static and vibrational (cyclic) loads has been formulated. Uniaxial compression tests of polycrystalline columnar-grained ice specimens were carried out at three temperatures with a parallel study of acoustic emissive, mechanical and structural characteristics of ice. A series of vibrocreep tests was performed with cyclic loading of the ice specimens.

The results of the experimental studies are in good agreement with theoretical assumptions.

The authors wish to express their profound appreciation to V.I. Solomatin, Candidate of Geographic Sciences, Associate Professor of Cryolithology at the Moscow State University, and to his colleagues V.G. Khlap and M.V. Kryuchkov for their assistance with structural-petrographic analyses of thin sections of ice. The authors also wish to thank Professor P.A. Shumskii and Professor S.S. Vyalov who examined their data and offered a number of valuable comments.

CHAPTER 1

STRUCTURAL AND MECHANICAL PROPERTIES OF ICE

1.1. Properties and structure of ice

Common ice occurring in nature under the conditions prevalent on the earth's surface is a crystalline substance forming as a result of freezing of water at normal atmospheric temperature and pressure.

Crystals of common ice have a hexagonal symmetry. Moreover, each oxygen atom is located in the centre of the tetrahedron and is bound to the other four oxygen atoms arranged at the vertices of the tetrahedron. The molecular packing within the ice crystals is such that each molecule is bound to three other molecules from the same layer, but only to one molecule from the adjoining layer. Therefore gliding occurs much more easily along the layers (i.e. on basal planes perpendicular to the optic axis of the crystal) than in any other direction.

McConnel and Mügge [Shumskii, 1955] demonstrated experimentally as far back as the end of the XIX century that in the process of deformation an ice single crystal behaves similarly to a set of thin elastic plates (laminae) bonded together with a viscous glue. If the shear plane happens to coincide with the basal plane, there occurs a plastic deformation with a minimum of force; if the shearing force bends the laminae, they undergo an elasticoplastic deformation ending in their fracture, i.e. failure; if the shear plane is perpendicular to the edges of the laminae, the latter undergo a slight elastico-plastic deformation succeeded by failure.

The anisotropy of the mechanical and physical properties of ice on account of the platy (lamellar) structure of its single crystals, and the role of the basal plane as the only plastic slip surface, have been repeatedly studied and have been confirmed by Glen and Perutz (1954), Steinemann (1954), Nakaya (1958), Weertman (1963) and other researchers.

The structure of real crystals differs substantially from the perfect crystal structure because of the presence of microscopic imperfections, i.e. defects therein. Microdefects of the crystal lattice, i.e. dislocations, may be in the form of point defects (omission of atoms in the crystal lattice or inclusion of extra atoms at interstitial sites) or of extended disturbances in the regular lattice pattern designated as line dislocations. In ice crystallizing under real conditions there appear defects in the form of inclusions of various impurities (including dissolved or trapped air). The dislocations may move within the crystal or may agglomerate forming three-dimensional configurations which, in the opinion of S.S.Vyalov [Vyalov et al., 1976], can be treated as ordinary defects. At present there is a fairly large number of works [Weertman, 1963; Webb, Hayes, 1967; Higashi, 1969; and so on] reporting results of theoretical and experimental studies on the occurrence and development of dislocations in ice under the effect of mechanical or thermal factors and on the plastic deformation of ice resulting from the presence and movements of dislocations. These studies were carried out with the help of X-ray crystallography and X-ray diffraction analyses. Fukuda

and Higashi (1973) have demonstrated in particular that dislocations pile up and are arranged in ice parallel to the basal planes. This is an additional factor contributing to the preferred development of plastic deformations in ice single crystals along the basal planes, since it is much easier to shift a dislocation than a perfect crystal lattice.

The anisotropy of mechanical properties of ice single crystals is also characteristic of individual crystals in polycrystalline ice, but the general properties of that type of ice depend to a significant degree on the size, geometry and relative orientation of its constituent crystals.

The structure of natural ice is determined by the conditions under which it forms and by the history of its existence. The main types of natural ice that can be distinguished on the basis of these characteristics are as follows.

1. The atmospheric ice represented by isolated crystals suspended in the air.

2. The land ice in the form of temporary formations (e.g. the snow cover or the ice crust forming as a result of freezing rain), as well as and mainly in the form of long-lasting firn basins, mountain glaciers and continental ice sheets.

3. The ice of streams or bodies of water comprising primarily the ice cover of the seas, rivers and lakes, and, in addition to it, the much less widely distributed frazil and anchor ice.

4. The subsurface (subterranean) ice either formed directly within the ground, or formed on the surface, but subsequently buried in the ground.

The very sketchy differentiation of ice presented above is based entirely on the location of the different types of ice. In addition to it there is a number of detailed classifications of natural ice which take into account its origin and the physical environment in which it forms, as well as the structural characteristics of the different groups, types and other categories of natural ice. The most comprehensive classification of all the types of fresh-water ice has been proposed by P.A. Shumskii (1955; N.V.Cherepanov (1976) developed a structural-genetic classification for the ice of natural fresh- and salt-water bodies, and B.I.Vtyurin [Vyalov et al., 1976] for subterranean ice. In all of these and in many other studies it has been noted that there is a close relationship between the conditions under which the ice forms and occurs and the structure of that ice, which in its turn has a decisive effect on its physical and mechanical properties.

1.2. Strength and creep of ice

Strength is the ability of solids to preserve their structural integrity under the action of external mechanical loads. On the other hand, when applied to rheological bodies, the term "strength" may refer to their resistance to deformation under load.

If failure of a body is treated as a critical event occurring at the time when the effective stress attains a certain critical magnitude, the widely used term "ultimate strength" can be defined as the maximum stress which the given material

sustains prior to failing. The strength of most engineering and building materials has therefore always been determined by means of stress (mainly tensile stress) tests, in which increasingly greater loads are applied until failure occurs. Moreover, it is assumed that if the magnitude of the applied force is smaller than the stress limit, no failure will occur and the specimen will exist for an indefinite length of time.

This approach had also been used for a long time in determining the strength of ice [Weinberg, 1940]. Ice specimens were tested in compression or tensile rupture testing machines to determine their compression, rupture, bending or shear "strength". The factors taken into account in these tests were the temperature, structure and origin of the ice, the presence of air or impurities in it, the direction of the action of the load relative to the structural elements, as well as the size and geometry of the specimens. Survey of the results of these studies [Voitkovskii, 1960; Butyagin, 1966; Savel'ev, 1963; Lavrov, 1969; Bogorodskii et al., 1971] shows that the data available on the magnitudes of the strength of ice under failure loads are highly contradictory. The discrepancies in the values obtained by different authors are ten-fold or greater, which, in addition to the differences in the factors listed above, may be due to variation between the methods employed in the tests.

Brown pointed out as far back as 1926 that the term "compression strength of ice" was meaningless in itself. "The behaviour of ice in compression is different at the same rates of loading at

different temperatures, and at different rates of loading at the same temperature". K.F.Voitkovskii also notes that ultimate strength is a conventional concept with reference to ice, since failure of ice does not correspond to a definite unique maximum value of stress. The maximum stress corresponding to the onset of failure in ice, depends significantly on the loading rate and conditions of deformation, since simultaneously with the increase of stresses there develop creep phenomena in ice.

According to the data of N.A.Tsytovich and M.I.Sumgin [Voitkovskii, 1960], when the rate of application of the load increased in compression tests within the range of (0.3-0.88)·$\cdot 10^5$ Pa/s, the magnitude of the maximum strength of ice decreased from 6 to 2.4($\cdot 10^5$)Pa.

K.N.Korzhavin (1962), F.I.Ptukhin (1962) and V.V.Lavrov (1969) obtained similar data showing that the maximum strength of ice decreases with increasing loading rate (in the event of its rapid rise over the time of 1-2 to $\approx$ 60sec). K.N.Korzhavin and F.I.Ptukhin (1966) believe that the effect of the deformation rate on the strength of ice is qualitatively identical to that of the loading rate, i.e. that an increase in these rates leads to a decrease in the instantaneous strength of ice.

There are, however, experimental data evidencing that at low deformation or loading rates an increase in these rates leads to an increase of the maximum strength of ice. Admittedly, in this case the maximum strength of ice corresponds to the time of transition of the deformation to the stage of tertiary creep

rather than to the time of rupture or fracture of the specimen.

Data of this kind have been obtained by S.S.Vyalov and V.A. Chernigov (1960), E.P.Shusherina and A.E.Gulikov (1964), L.Gold and A.Krausz (1971). It should be noted that the tests described in the above works were run under conditions of creep, i.e. at constant stresses for each given test, all of which caused failure, but over different times indicated by the point of inflection in the creep curve during the accelerating stage. We are therefore no longer dealing here with instantaneous or conventionally instantaneous strength, but with long-time strength defined by the time to failure under the given load.

The experimental works listed above and other similar studies gave rise to a wide-spread belief that the strength of ice initially increases with increasing deformation (or loading) rate, reaches its maximum, and thereafter decreases tending towards the limit at high strain-rates. The maximum strength and the strain-rate associated with it are customarily regarded as the critical values of transition from ductile to brittle failure. Introducing the notion of ultimate failure strain, K.N.Korzhavin and F.I.Ptukhin (1966) explain the experimental data showing that the maximum strength drops off with increasing strain- or loading rate, by analysing a rheological model of ice composed of parallel-connected Hookean and Bingham-Shvedov bodies. According to the tests of K.N.Korzhavin and F.I.Ptukhin, the critical strain-rate $\dot{\varepsilon}^{kp*} \leq 10^{-3} s^{-1}$.

* kp=critical. Translator.

Contrary to this view, Hawkes and Mellor (1972) dispute the fact that the strength decreases at high strain-rates. By using the data from a large number of their own tests over a wide range of strain-rates (in which the maximum strength was determined as the peak in the strain-stress curve), as well as those from the literature, these authors correlate the results of the creep tests with those of the constant strain-rate tests. They obtained one single dependence of compression and tension yield stresses on the strain-rate over the range of 10^{-11} to $10^{-2}sec^{-1}$ for compression and up to $10^{0}s^{-1}$ for tension. In creep tests the strain-rate was assumed to be equal to the steady-state flow (secondary creep) rate. Hawkes and Mellor have demonstrated that combined compression data are described by a smoothly ascending curve over 9 orders of strain-rate magnitudes; moreover, that curve contains no linear sections or sharp transitions, and it gradually flattens out in the region of high strain-rates ($> 10^{-4}s^{-1}$) without, however, showing any tendency of the yield stresses to decrease. The authors point out that initially they also obtained a decrease in strength for high strain-rates, which disappeared, however, as soon as they improved their testing technique. They therefore question the reality of that effect, i.e. of the apparent drop in strength with increasing strain-rates.

The effect of the time factor on the strength of many materials (glasses, polymers, metals, ceramics etc.) has been established experimentally by many investigators over the last 40-50 years in both constant strain-rate and creep tests. The

results of these tests, combined with the molecular-kinetic notions of G.Eyring* and Ya.I.Frenkel, served as a basis for the kinetic concept of strength developed by S.N.Zhurkov and his colleagues (Regel' et al., 1974) since 1952. This concept has evolved from the fact that all bodies, including solids, are systems of particles, in which each individual particle is in vibrational thermal motion, rather than static systems of rigidly bound atoms or molecules (e.g. in a crystal lattice). As a result of this motion the local stresses of interparticle bonds change continuously. It has been demonstrated in theoretical physics that the changes induced in the interparticle bonds by the average level of thermal vibrations are comparable in magnitude to the tensile strength of the bonds, and that the energy fluctuations resulting from the random thermal motion, impart to individual particles a kinetic energy that is many times greater than the energy required to overcome the potential energy barrier and to transform the state of relative "rest" to the state of equilibrium. The kinetic concept of strength proves that the external force itself does not break the interparticle bonds (the strength of which would determine the ultimate strength), but merely activates the process of bond breakup through energy fluctuations increasing thereby the probability of the bonds breaking up and reducing the probability of their fluctuational recovery. The external force thus imparts directivity to the breaking action of the fluctuations and ensures the development of the process of failure.

---

* Transliteration. Translator.

Since in this approach failure is treated as a process of accumulation of disturbances within a body in time, that process can be characterized by the rate at which the process develops or by the time over which it occurs until the body breaks up rather than by some critical stress.

S.N. Zhurkov et al. refer to the time to rupture from the moment of the application of stress as the "longevity" or "durability" of that body, determined experimentally from the results of creep tests. The term adopted for earth materials (including permafrost) and ice is "long-time strength" [Vyalov, 1976; Shusherina, Gulikov, 1964]. The difference in the meaning of these two terms lies in that longevity (or durability) is determined as a rule from tension tests, in which the time at which the specimen fails, regarded as the end of its durability, is clearly fixed. Contrariwise, the tests commonly employed for earth materials and ice are uniaxial tests in which the specimen does not break up as a rule. Long-time strength is therefore defined as the time of the transition of creep to the tertiary stage. From the viewpoint of physics this is a valid approach, since it would indeed be meaningless to talk of strength of a material in the state of tertiary creep. But it increases the difficulty and reduces the accuracy of finding the pertinent time in the creep curve, since transition from one stage of creep to another is a gradual process.

The general dependence of the durability t^* on the stress σ and absolute temperature of the solid (body) T [Regel' et al., 1974] is written in the form

$$t^* = t_o \exp \frac{U_o - \gamma\sigma}{kT} , \qquad (1.1)$$

where t_o, U_o and γ are coefficients characterizing structural and physical properties of the solid, and $\underline{k}$ is Boltsmann's constant.

It should be noted that the temperature forms part of the exponent (1.1). Therefore with a drop in temperature the dependence of t^* on σ becomes extremely sharp, which has also been demonstrated experimentally [Regel' et al., 1974]. Moreover, it creates the illusion that the failure of the body is of a threshold type: a small decrease in stress causes the durability to increase to an enormous value and the solid appears indestructible, while for a small increase in stress the durability drops to a negligibly small value creating the impression of instantaneous failure. In tests with most construction materials (metals, stone, wood) with which the static theory of strength including the notion of instantaneous ultimate strength, has been developed, the normal temperatures (+30 -40°C) are sufficiently low that the resistance to failure of these materials is adequately characterized (in the first approximation) by the conventional instantaneous strength. Ice in its natural state always has, however, a temperature close to the melting point, and the process of its failure can be assessed therefore only by using the kinetic approach.

The process of development of deformations in ice with time is designated as creep. In polycrystalline ice plastic

deformation of individual crystals occurring in the course of their glide along the basal planes, encounters resistance at the grain boundaries on account of changes in their crystallographic orientation. This leads to a nonuniformity of the stressed state throughout the ice mass. The nonuniform internal stresses developed in this manner may increase to the point of generating new types of deformations, including crack formation or breakup of the crystals.

K.F.Voitkovskii (1960) distinguishes three main factors acting during the deformation of ice in time:

-elastic and plastic deformations of individual crystals;

-displacement of crystals in relation to one another, and

-failure of crystals.

Under conditions of a nonuniform stressed state there occur two opposite processes. On the one hand the fragments of the broken-up crystals are stress-free and grow at the expense of stressed crystals, i.e. there occurs recrystallization and structural recovery of undeformed ice, redistribution and evening out of stresses. From the molecular-kinetic viewpoint this process may be regarded as strengthening through compaction of the particles and through "healing" of structural defects. All this naturally causes the strain-rate to drop. The other process taking place at the same time is disturbance of interparticle bonds within the crystals, as well as at their boundaries, and fragmentation of the crystals, i.e. formation and development of structural defects leading to "weakening" of the ice and increase of the strain-rate.

The relation of the intensities of these processes is determined (at a constant temperature) by the magnitude of the effective stress. At small stresses the strengthening prevails or the ice structure is in a mobile equilibrium so that the strain-rate decreases or tends towards a constant magnitude. At great stresses the predominant process is weakening which accounts for the viscous character of creep. In this case the development of structural defects in ice leads to its failure.

It should be noted that the kinetics of accumulation and healing of structural defects leads to volume (cubic) deformation of ice. Moreover, as has been demonstrated in E.P. Shusherina's experiments (1967), strengthening of the ice structure at the stage of transient creep induces a positive dilatancy, i.e. compaction of the ice. Negative dilatancy (decompaction) of ice at the stage of tertiary creep is associated with formation of microcracks and with fragmentation of ice crystals. Imposition of constraints on the cubical expansion makes it difficult for structural defects to develop and alters the mode of deformation of the ice increasing its strength [Goughnour, Andersland, 1968; Frederking, 1972; Jones, 1978].

The stress at which transient or steady-state creep changes creep progressing at an indefinitely increasing rate (i.e. tertiary creep), has been designated by K.F. Voitkovskii (1960) as the long-time creep limit (σ_∞).

The dependence of the steady-state (secondary) creep rate $\dot{\varepsilon}_{min}$ of ice on stress and temperature can be described [Vyalov et al., 1976] on the basis of the Frenkel-Eyring* molecular-kinetic theory of viscous medium, according to which the steady-state creep rate is written as

$$\dot{\varepsilon}_{min} = C \cdot \exp\left(-\frac{U_0}{kT}\right) \cdot \operatorname{sh}\left(\frac{\sigma}{\sigma^*}\right), \qquad (1.2)$$

where U_0 is the activation energy for the undeformed state of the solid, J; k is Boltzmann's constant, j/°k; T is the absolute temperature; σ is the effective stress, Pa; σ^* is a certain constant stress, Pa; and C is the coefficient accounting for the concentration of molecules and frequency of temperature oscillations, s^{-1}.

Taking into account the properties of the hyperbolic sign $\operatorname{sh}X \approx X$ at $X \ll 1$ and $\operatorname{sh}X \approx \frac{1}{2}e^X$ at $X \gg 1$, it may be inferred from (1.2) that at small stresses ($\sigma \ll \sigma^*$) the flow of ice will occur at a constant rate linearly dependent on the stress, while at great stresses ($\sigma \gg \sigma^*$) the dependence of $\dot{\varepsilon}_{min}$ on the stress is described by the exponent. The magnitude σ^* represents the transition from the one type of the dependence of $\dot{\varepsilon}_{min}(\sigma)$ to the other. It is found by plotting the dependence of $\dot{\varepsilon}_{min}(\sigma)$ (the rheological curve) on a semilog scale, where the plot for the $\sigma > \sigma^*$ values becomes linear, whereas that for $\sigma < \sigma^*$ is curvilinear. S.S. Vyalov et al. (1976) believe that the point of inflection in the rheological curve corresponds to the long-time creep limit, i.e. $\sigma^* = \sigma_\infty$.

*Transliteration. Translator.

The dependence of the magnitude or rate of strain on stress, time and temperature has been studied by many researchers within a large range of variations in these parameters. Different investigators proposed for this dependence a number of different empirical equations representing as a rule a combination of exponential functions of one or several of the above parameters. Summing up these proposals, A. Krausz (1968) has found that all the equations can be described by the expression

$$\dot{\varepsilon} = A\sigma^{n}\exp\left(-\frac{CE}{T}\right), \qquad (1.3)$$

where the coefficients A, n, C and E may depend on stress and temperature, as well as on time and magnitude of strain.

S.S. Vyalov et al. (1976) propose to describe the process of creep at a varying rate, i.e. at $\sigma \neq \sigma_{\infty}$, in the form of the empirical dependence

$$\dot{\varepsilon} = \frac{k}{1 + |\theta|}\,\sigma^{n} t^{a-1}, \qquad (1.4)$$

where θ is the temperature, °C; t is the time, and k, n and a are parameters.

When (1.4) is applied to ice or to an ice-rich ground, the parameter a should probably be made dependent on the value of σ. At $\sigma > \sigma_{\infty}$ the parameter a should be > 1, in which case (1.4) will describe tertiary creep, whereas at $\sigma < \sigma_{\infty}$ the value of a < 1, and at $t \longrightarrow \infty$ the strain-rate $\dot{\varepsilon} \longrightarrow 0$ (infinitely attenuating creep).

1.3. Brittle structural disturbances and acoustic emission of ice

As was mentioned earlier, the strength and deformability of ice depend on its structure. When stress is applied to polycrystalline ice with an ordered orientation of crystals, along the optic axes of its crystals (perpendicular to the basal planes), its strength is 1.3-1.5 times greater and the strain-rate 1-2 orders smaller than when stress is imposed along the basal planes [Vyalov, 1960; Korzhavin, 1962; Voitkovskii, 1960; Shil'man, 1948]. The deformability of ice with randomly oriented crystals occupies an intermediate position, but is nevertheless closer to the case of basal slip [Vyalov, 1960].

E.P.Shusherina and A.E.Gulikov (1964) investigated in detail the effect of the grain size of ice on strength and creep in uniaxial compression. They found for three kinds of ice with the grain size roughly in the ratio of 1:100:1000 that with decrease in the grain size the strength of ice increased, while creep (estimated in these tests as the viscosity coefficient) dropped to less than one-tenth.

Many Soviet and foreign investigators established that the structure of ice becomes substantially modified in the process of creep [Steinemann, 1954; Glen, 1955; Gold, 1960, 1966; Vyalov, 1960; Shumskii, 1961; Savel'ev, Gulikov, 1964; Voitkovskii, Golubev, 1972].

Shumskii (1961) distinguishes six principal mechanisms of ice deformation under applied load and differentiates them on the basis of morphological characteristics depending on the magnitude of the effective stress and on the strain-rate (stage of creep).

Having analysed the experimental data and the evidence available in the literature, Yu.K. Zaretskii et al. (1976) propose to divide the structural characteristics of creep of ice into two groups. Formation of slip lines, recrystallization, polygonization and distortion of crystal faces, i.e. relatively slow processes occurring at the molecular level, are associated with the first group of "plastic" mechanisms of deformation. The second group comprises rapid "brittle" processes, primarily the crack formation, local or zonal fragmentation, and formation of cavities. The abrupt displacement of grain faces observed by L. Gold (1966) should probably also be included in this group.

The distinguishing characteristic of brittle structural disturbances in ice is the fact that they excite elastic vibrations in ice, the so-called acoustic emission or emission of stress waves.

The occurrence of wave phenomena in solids during their deformation and failure has been known for a relatively long time. The most representative materials in this respect are wood and tin. The elastic vibrations arising during their deformation have a sufficiently great energy in the audio

frequency range to be perceived by ear without amplification. Similar effects have been discovered in laboratory experiments with various materials as far back as the 1930s [Greshnikov, Drobot, 1976], but the laws governing the relationship between the acoustic noises and the mechanisms of deformation of various materials have been elucidated only over the last thirty years. This has led to practical utilization of acoustic emission phenomena.

The general term "acoustic emission" is used to designate the processes of emission of stress waves from internal sources located within a body of material. Acoustic emission can be induced, for example, by structural elements of a material undergoing a fairly rapid restructuring. Greshnikov and Drobot (1976) list among the sources of acoustic emission the movements of dislocation pileups, twinning of crystals, and phase transformations of the martensitic type in metals, as well as crack formation and propagation.

Dispersion of the wave motion in solids leads to distortion of the shape of the initial mechanical pulse transmitted from the source of emission. Let us assume, for example, that the action of the source is characterized in time by a square shift pulse. The dependence of the phase and group velocity of waves on the frequency distorts the shape of the pulse as it propagates (since it may be represented as the sum of sinusoidal waves with an infinite set of frequencies). As a result of this at the surface reached by the stress wave,

the acoustic emission pulse will no longer be square but will have a form characteristic of damped vibrations. Only some of the parameters of the recorded acoustic signal carry information pertaining to the parameters of the defect in the structure of the material. These are the amplitude and the duration of the pulse, as well as the arrival time of the signal.

Recording of acoustic emission is used largely in nondestructive testing, safety and technical quality assurance of various materials, manufactured goods and engineering structures. Acoustic emission is used effectively for testing production towers in chemical plants, aviation and cosmic equipment, and so on, and for detecting local defects in them [Dunegan, Tatro, 1971].

In the Soviet Union significant achievements in the practical use of acoustic emission phenomena have been attained in the field of predicting coal and gas blowouts and shocks in mines [Shamina, 1956; Vinogradov, 1964; Konstantinova, 1977].

Successful use of the acoustic emission recorded in the ground or directly in the foundation of various structures and in dams has been reported in the literature [Koerner, Lord, 1976].

Brown (1926) was probably the first investigator to report on acoustic emission in ice. Outlining results of determinations of the strength of ice, he refers to the formation of internal cracks in ice and to the attendant

audible "crackling". He qualitatively observed that the intensity of "crackling" depended on the temperature and on the magnitude of the applied stress.

L. Gold made an important contribution with his laboratory experiments on microfracturing during creep of ice and on the relation of that process to the acoustic emission activity [L. Gold, 1960, 1969]. He observed that at the stage of nonlinear (transient) creep the intensity of crack formation decreased as the creep rate approached a constant value. Above a certain stress value, where the creep rate steadily increased, the rate of accumulation of the acoustic emission pulses recorded by piezoelectric crystals, changed accordingly. L. Gold found that for artificial columnar-grained ice the minimum compressive stress above which acoustic emissions could still be recorded with confidence was about 0.6 MPa. As the stresses decreased, isolated pulses were recorded initially, but eventually they disappeared completely.

V.V. Bogorodskii et al. [1968, 1974] investigated theoretically and experimentally the acoustic effects occurring during the deformation and failure of ice under the action of thermal and mechanical factors. They carried out a spectral analysis of the acoustic emission of ice and demonstrated that recording of acoustic emission was a promising method for studying the critical stressed state of the ice cover.

Zaretskii et al, (1975) performed a series of creep tests on specimens of lake ice and recorded the attendant acoustic emission. These investigators observed that the final stage of failure of the ice specimens corresponding to their total loss of shape and structural continuity, occurred in different tests at approximately the same total number of microcracks (acoustic emission pulses). It has been demonstrated in that work that the rheological constants of ice, the long-time creep limit in particular, can be determined from records of the acoustic emission accompanying the deformation of ice under load.

Analysis of records of natural elastic vibrations in the ice cover on the lake Baikal [Berdennikov et al., 1968] has shown that the acoustic method is a promising means of determining the onset of periods of compression in ice and of assessing that process from the amplitudes and frequency of pulse signals.

An interesting study was carried out by Neave and Savage (1970), who recorded the "icequakes" occurring during the formation and development of cracks on an active glacier in Canada. These investigators located with the help of eight pickups (geophones) the sites of the cracks and the direction in which they developed in the surface layers of the glacier. They even succeeded in measuring the velocity of motion of the source of acoustic vibrations, which was close to 30 m/sec.

CHAPTER 2

SHORT-TIME CREEP AND FAILURE OF ICE

Ice behaves under load like an elastico-viscoplastic medium. Moreover, the stress (or the combination of stresses) observed for ice may be below the level at which deformations continue at a decreasing rate. This stress will be referred to as the long-time creep limit of ice [Voitkovskii, 1960] and will be designated by the symbol σ_∞. At stresses $\sigma > \sigma_\infty$. deformations develop in ice at an increasing rate, do not become stabilized, and lead to failure of ice. The time to failure varies and is the shorter, the greater the applied stress, i.e. the greater the σ/σ_∞ ratio. The region of ice deformation at $\sigma/\sigma_\infty > 1$ will be referred to as the short-time creep region.

Microfracturing, increase of the volume of ice (its loosening) in the process of displacement, coalescence of the accumulated microcracks into major fractures, and avalanche-like sudden and violent failure of the material are the phenomena characteristic of short-time creep of ice. Even though each individual act of crack formation is a brittle failure event, the kinetics of accumulation of such structural disturbances in the ice structure is stretched in time and the macroprocess of ice deformation has the appearance of a plastic flow process. The purpose of our investigations was to unify the two aspects of that integral process and to show how creep occurs in ice proceeding from the accumulation of brittle structural failures.

2.1. Mathematical model of phenomenological description of short-time creep of ice

In the phenomenological description of short-time creep of ice use is made of our propositions pertaining to the plastic flow of earth materials [Zaretskii et al., 1979c; Zaretskii, 1980]. These propositions are based on the theory of plastic hardening and on the unified generalized law [Koiter, 1961]. The fundamental equations for ice for the stage of short-time creep must be formulated within the framework of the theory of hardening for viscoplastic media, proceeding from the following assumptions:

a) deformation of ice under conditions of short-time creep is practically irreversible;

b) the magnitude of the irreversible portion of creep deformation depends on the loading program (the sequence in which the loads are applied) and on the nature of the stressed state;

c) under conditions of short-time creep the ice grows looser; the dilatancy of ice occurring as a result of irreversible shear deformations is substantial and depends on the loading path.

The main principle on which all the variants of the plastic flow theory are based is the principle of the mechanical work dissipation maximum or the quasi-thermodynamic postulate of Drucker. A well-known sequel to that principle is the relation defining the plastic strain-rate in the form

$$\dot{e}_{ij}^{(p)} = \dot{h} \frac{\partial \Pi}{\partial \sigma_{ij}}, \tag{2.1}$$

where Π is a function of the stress tensor and possibly of some parameters dependent on the accumulated plastic strains, and $\dot{h}$ is an indeterminate scalar multiplier.

Under the unified flow law the plastic potential is represented in (2.1) by the loading function describing in a mathematical form the boundary between the domains of recoverable and nonrecoverable strains in stress space.

In accordance with (2.1) that boundary must possess the property of normality: the direction of the plastic strain increment vector $\overrightarrow{d\varepsilon}^{(p)}$ is normal to the regular load surface and is independent of the direction of the additional load vector $\overrightarrow{d\sigma}$; only the magnitude of the $/\overrightarrow{d\varepsilon}^{(p)}/$ vector modulus depends on the direction of the $\overrightarrow{d\sigma}$ vector (fig. 2.1a).

Under the unified generalized flow law the constitutive relations of the theory are written in the form

$$\dot{\varepsilon}_{ij}^{(p)} = \sum_r \dot{h}^{(r)} \frac{\partial \Pi^{(r)}}{\partial \sigma_{ij}}, \tag{2.2}$$

where $\Pi^{(r)}$ are the components of the plastic potential associated with the load surface.

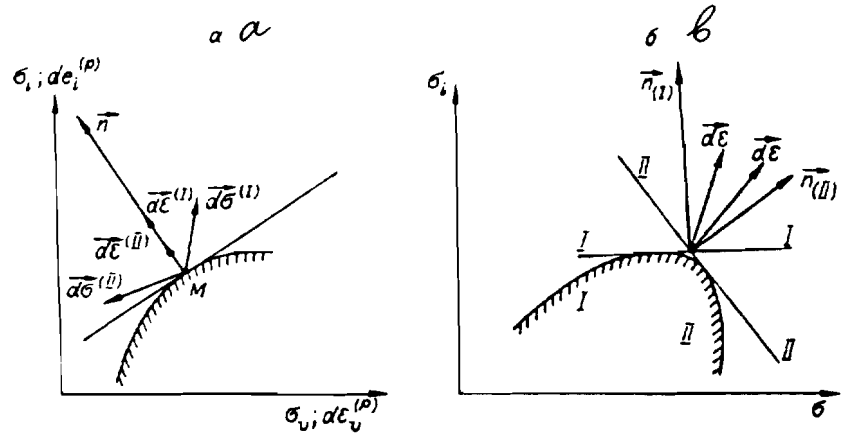

Fig. 2.1

Properties of the load surface under the unified law
a - in the smooth segment; b - at a singular point

***

The loading condition is formulated as

$$\dot{h}^{(r)} > 0; \quad \text{at}$$

$$\Pi^{(r)} = 0 \quad d'\Pi^{(r)} \equiv \frac{\partial \Pi^{(r)}}{\partial \sigma_{ij}} d\sigma_{ij} > 0, \tag{2.3a}$$

and the unloading or neutral loading condition as

$$\dot{h}^{(r)} = 0; \quad \text{at}$$

$$\Pi^{(r)} \leqslant 0 \quad d'\Pi^{(r)} \equiv \frac{\partial \Pi^{(r)}}{\partial \sigma_{ij}} d\sigma_{ij} \leqslant 0. \tag{2.3b}$$

At singular points of the load surface (fig. 2.1b) the direction of the plastic strain increment vector depends on the direction of the additional load vector, but lies within the plastic angle determined by the positions of the normal to the corresponding segments of the load surface at the given singular point. In other words, according to the unified generalized flow law (2.2), the plastic strain increment vector is composed of the constituents of $d\varepsilon_{ij}^{(p)} = \sum_r d\varepsilon_{ij(r)}^{(p)}$, each of which is normal to the corresponding regular portion of the loading surface ($\Pi^{(r)}=0$).

The load function is another concept introduced for viscoelastic-viscoplastic solids [Naghdi, Murch, 1963]. Moreover, for these media the load function depends on the strain rate dependence of the viscosity parameters. In this case the new value of the load function $\Pi+\dot{\Pi}dt$ at $\Pi<0$ gives a smaller value of the function at the next time than its last value, and the medium changes from the viscoplastic to the viscoelastic state. The process of unloading is therefore associated with the value of $\dot{\Pi}<0$, and the inequality $\dot{\Pi}\geq 0$

indicates that an active loading process is taking place in the medium.

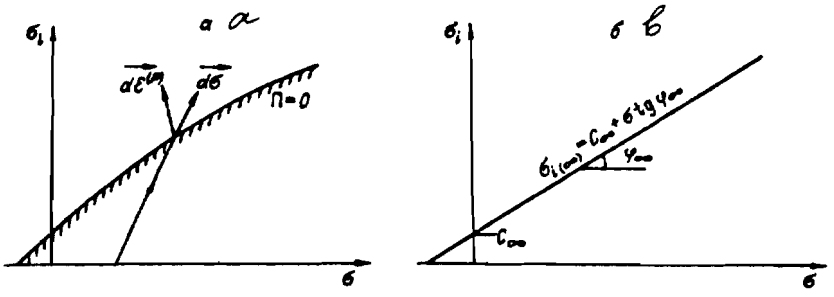

Fig. 2.2

Loading surface trace in the stress plane:

a - in a general form; b - after Mises-Schleicher

***

Analysing short-time creep of ice and keeping in mind that at stresses $\sigma > \sigma_\infty$ dilatancy volume strains predominate, the load surface is assumed to be an open surface. In the plane of the stress tensor invariants $\sigma_i \div \sigma$, where σ_i is the second invariant of the stress deviator

$$\sigma = \frac{1}{\sqrt{6}} \sqrt{(\sigma_1 - \sigma_2)^2 + (\sigma_1 - \sigma_3)^2 + (\sigma_2 - \sigma_3)}$$ and σ is the first invariant of the stress tensor $\sigma = 1/3(\sigma_1 + \sigma_2 + \sigma_3)$, the load surface trace is represented by a line that does not intersect the σ axis at $\sigma \longrightarrow \infty$ (fig. 2.2a). Viscoplastic yield under conditions of a composite stressed state is designated by $\sigma_{i(\infty)}$ and is taken in the form proposed by Mises-Schleicher (fig. 2.2b):

$$\sigma_{i(\infty)} = c_\infty + \sigma \cdot tg\phi_\infty \,, \qquad (2.4)$$

where c_∞ and $tg\phi_\infty$ are the coupling and the internal friction angle in the octahedral plane.

The invariants of stresses σ_i and σ are thus arguments of the loading function $\Pi = 0$.

In order to develop a concrete mathematical model for short-time creep of ice it is necessary to determine the form of the function $\Pi(\sigma_i, \sigma)$. Our fundamental hypothesis postulates that the loading function depends directly on the number of brittle structural disturbances accumulated in ice, designated by N.

As may be seen from the experimental data in section 5.1, there are two characteristic values of the number of brittle structural disturbances accumulated in ice (fig. 2.3):

a) N^*, the critical number of defects corresponding to the initiation of tertiary creep in ice (or the minimum strain-rate; and

b) N^{**}, the maximum number of defects corresponding to the time of failure of ice.

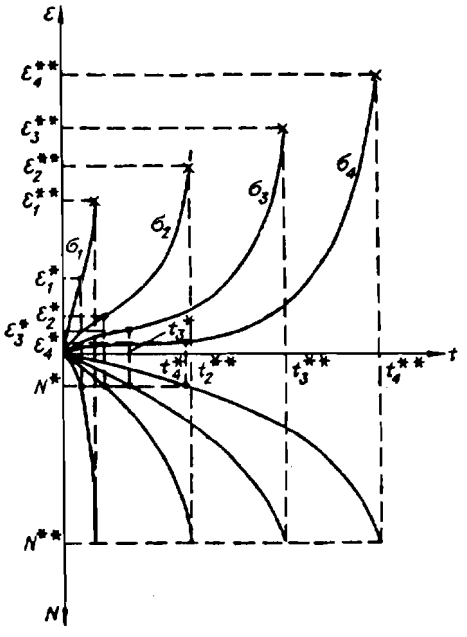

Fig. 2.3

Development of creep deformations and accumulation of defects in time under failure loads ($\sigma_1 > \sigma_2 > \sigma_3 > \sigma_\infty$)

In constructing the loading function Π it is assumed that the tertiary plastic flow rate corresponds to the condition that the number of accumulated plastic defects N is greater than the critical value N^*. The fundamental assumption regarding the loading function is derived from the analysis of the graphical plots in fig. 5.9a at $N \geq N^*$ and is formulated in the following manner:

$$\Pi = \ln\frac{N}{N^*} - m \cdot \ln\frac{\dot{e}_i^*}{\dot{e}_i^{**}} , \qquad (2.5)$$

where $N = N(\sigma_i, \sigma, t, T)$; $N^* = (\sigma, T)$; $\dot{e}_i^{(p)}$ is the plastic strain rate in shear; $e_i^{(p)}$ is the amount of plastic shear strain equal to

$$e_i^{(p)} = \sqrt{2/3}\sqrt{\left[\varepsilon_1^{(p)} - \varepsilon_2^{(p)}\right]^2 + \left[\varepsilon_2^{(p)} - \varepsilon_3^{(p)}\right]^2 + \left[\varepsilon_1^{(p)} - \varepsilon_3^{(p)}\right]^2}; \text{ and}$$

$\dot{e}_i^*$ is the minimum rate of strain of ice at $N=N^*$ (see fig. 5.9a) dependent on the average stress.

The components of the plastic strain-rate for ice are determined on the basis of (2.1) and (2.5) in the form

$$\dot{e}_{ij}^{(p)} = \dot{h}\frac{\partial \Pi}{\partial \sigma_{ij}} = \dot{h}\left[\frac{1}{N}\frac{\partial N}{\partial \sigma_{ij}} - \frac{1}{N^*}\frac{\partial N^*}{\partial \sigma_{ij}}\right], \qquad (2.6)$$

where $\frac{\partial \Pi}{\partial \sigma_{ij}} = \frac{\partial \Pi}{\partial \sigma_i}\cdot\frac{S_{ij}}{2\sigma_i} + \delta_{ij}\frac{1}{3}\frac{\partial \Pi}{\partial \sigma}$; $S_{ij} = \sigma_{ij} - \sigma_{ij}\sigma$; δ_{ij} is the Kronecker symbol $\left(\delta_{ij} = \begin{cases} 0\,(i \neq j) \\ 1\,(i = j) \end{cases}\right)$.

The plastic strain rate in shear

$$\dot{e}_i^{(p)} = \sqrt{\frac{2}{3}}\sqrt{\left(\dot{e}_1^{(p)} - \dot{e}_2^{(p)}\right)^2 + \left(\dot{e}_2^{(p)} - \dot{e}_3^{(p)}\right)^2 + \left(\dot{e}_1^{(p)} - \dot{e}_3^{(p)}\right)^2},$$

and the plastic volume strain-rate

$$\dot{e}_v^{(p)} = \dot{e}_1^{(p)} + \dot{e}_2^{(p)} + \dot{e}_3^{(p)}.$$

In conformity with relations (2.6), $e_i^{(p)}$ and $\dot{\varepsilon}_\nu^{(p)}$ are expressed through

$$\left.\begin{aligned} \dot{e}_i^{(p)} &= \dot{h}\left(\frac{1}{N}\frac{\partial N}{\partial \sigma_i}\cdot\frac{1}{N}\frac{\partial N}{\partial \sigma_i}\right)^{\frac{1}{2}}; \\ \dot{\varepsilon}_v^{(p)} &= \dot{h}\left(\frac{1}{N}\frac{\partial N}{\partial \sigma} - \frac{1}{N^*}\frac{\partial N^*}{\partial \sigma}\right). \end{aligned}\right\} \tag{2.7}$$

from which it follows that the volume strain-rate is directly related to the shear strain-rate

$$\dot{\varepsilon}_v^{(p)} = \frac{\left(\frac{1}{N}\frac{\partial N}{\partial \sigma} - \frac{1}{N^*}\frac{\partial N^*}{\partial \sigma}\right)}{\left(\frac{1}{N}\frac{\partial N}{\partial \sigma_i}\cdot\frac{1}{N}\frac{\partial N}{\partial \sigma_i}\right)^{\frac{1}{2}}}\cdot\dot{e}_i^{(p)}. \tag{2.8}$$

These general correlations between the components of the strain-rate tensor on the one hand and those of the stress tensor on the other should be examined together with the equations of motion for ice

$$\sum_{j=1}^{3}\frac{\partial \sigma_{ij}}{\partial x_j} = \delta_{i3}\rho g + \rho \ddot{U}_i \tag{2.9}$$

where $\ddot{U}_i$ are components of the acceleration vector; ρ is the density of ice; $\delta_{i3} = \begin{cases} 1\,(i=3); \\ 0\,(i\neq 3), \end{cases}$ and g is the acceleration due to gravity directed along the x_3 axis. In solving problems related to the action of ice on structures, movement of ice masses and other processes, it is advisable to add to the above appropriately formulated boundary and initial conditions, as well as, if necessary, equations of thermodynamics and mass balance [Shumskii, 1969].

2.2. Micromechanism of deformation. Kinetics of accumulation of structural defects in ice

The fundamental coupling equations for ice depend on the formulation of the load function. According to our hypothesis

the load function is related to the number of brittle structural disturbances accumulated in the process of creep (2.5). The kinetics of development of these structural defects during short-time creep is examined below.

Deformation and failure of ice under load are processes substantially modifying the structure of ice. Beside the temperature, the structure of ice is the most important factor determining its rheological properties. The strength and flow of ice depend in many ways on the form, size and orientation of its crystals. On the other hand the magnitude and direction of the effective stress, the path and program of loading, and the time and rate of deformation of an ice body (mass) are reflected in a definite way in the internal structure of the ice. As has been demonstrated in the review article by P.A. Shumskii (1955) and in later publications [Voitkovskii, 1960; Savel'ev, Gulikov, 1964; Gold, 1972; and so on], during creep of polycrystalline ice under load there occur processes such as the growth and degradation of crystals, gliding on basal planes and changes in the orientation of the optic axes, relative displacement of the crystals, their fragmentation, etc. The intensity of these phenomena depends on the magnitude of the effective stress, as well as on the initial structure of ice.

Studies by L. Gold (1972), V.V. Bogorodskii et al. (1968) and B.K. Zaretskii et al. (1975) have shown that above a certain stress there arise microcracks in ice and that their

formation is accompanied by acoustic vibrations (audible crackling) which can be recorded instrumentally. Studies on kinetics of the development of microcracks during the deformation of ice under load make it possible to describe the process of its creep and its long-time strength.

In the present work parallel experimental studies were carried out on mechanical, structural and acoustic processes during creep of ice under load.

A detailed structural-petrographic description of a series of variously deformed specimens has shown that under a constant load the structure of ice alters substantially with development of deformation in time. By analysing thin sections we have succeeded in identifying a number of structural formations related genetically to creep of ice. The results obtained are in good agreement with the classification system proposed by P.A. Shumskii (1961). There may be distinguished two groups of morphologically different structural changes resulting from the action of different mechanisms of structural modifications. The first group comprises distortions of grain faces, displacements of grain faces, development of slip lines, and recrystallization.

The structural phenomena belonging to the first group arise in our opinion as a result of relatively slow processes of displacement of the material that occur at the molecular level under the action of small local stresses and are plastic in character.

The second group comprises brittle processes, which develop very rapidly, within fractions of a second. These processes include polygonization, formation of linear cracks, local and zonal fragmentation, formation of cavities and mylonitization.

The processes listed for the two groups are arranged in the order of increasing deformation. It should, however, be emphasized that it does not mean that we are dealing with a succession of processes replacing one another (since several processes, both plastic and brittle, have been observed to occur simultaneously), but merely indicates their relative significance at different stages of deformation.

As has been established by L. Gold (1972a and b) and confirmed by our own observations, acoustic effects are associated only with the structural phenomena referred to in the second group. It has also been established experimentally [Zaretskii et al., 1975] that the curves showing the time dependence of the number of acoustic pulses are similar to those showing the time dependence of the deformation of ice specimens under load, and that the two dependences can be described by the same equations. This close analogy between the time dependence of deformation and the total number of acoustic pulses suggests that for the stresses applied in our experiments, the main factor determining the rate of deformation of the specimens was the occurrence of brittle disturbances. In other words the macroprocess of viscoplastic flow is composed of elementary events of brittle failure of the structural elements of ice.

This assertion does not rule out the action of plastic deformation mechanisms, but merely relegates them to secondary phenomena under conditions of short-time creep, i.e. at relatively great loads. Plastic mechanisms are evidently active under any loads; moreover, they play an increasingly greater role as the load decreases, and below a certain magnitude of the load (about $5\text{-}6 \cdot 10^5$ Pa) plastic structural phenomena fully control the development of deformation at all stages. This is also supported by the fact that at stresses below the aforementioned limit significant acoustic pulses have not been detected.

Modification of the ice structure in time under the action of applied stresses determines the process of creep and failure of ice. The structural changes will be associated not with disturbances of isolated molecular bonds, but with the breakdown of a whole complex of bonds leading to the formation of a defect corresponding to a structural disturbance of the order of 10^{-2} cm.

The occurrence and development of such structural defects are a stochastic process.

The state at which a unit volume of ice has n structural defects will be designated as E_n. If at any time the system is in the E_n state, the probability that the transition $E_n \longrightarrow E_{n+1}$ will occur over time $(t, t+\Delta t)$ is $\mu n^+ \Delta t$. Let the probability of the transition $E_n \longrightarrow E_{n-1}$, during which a defect is healed, be equal to $\mu n^- \Delta t$. The probability that more than one change will occur over time $(t, t+\Delta t)$ has a higher order of triviality than Δt.

The probability that at time $\underline{t}$ the system is in the state E_n, i.e. that the structure of ice has $\underline{n}$ defects per unit volume, will be designated by $P_n(t)$.

In the theory of stochastic processes there has been developed a system of differential equations for determining the probability $P_n(t)$:

$$\left.\begin{aligned} P_n'(t) &= -\left(\mu_n^{(+)} + \mu_n^{(-)}\right)P_n(t) - \mu_{n-1}^{(-)}P_{n-1}(t) + \mu_{n+1}^{(+)}P_{n+1}(t); \\ P_0'(t) &= -\mu_0^{(-)}P_0(t) + \mu_1^{(+)}P_1(t). \end{aligned}\right\} \quad (a)$$

If at t=0 the system was in the state E_k, then the initial conditions should also be met:

$$P_k(0) = 1 \text{ and } P_n(0) = 0 \text{ at } n \neq k. \quad (b)$$

In the theory of stochastic processes it has been demonstrated that if the coefficients of the system (a) are bounded or increase sufficiently slowly, that system has one single solution satisfying the condition of regularity:

$$\sum_n P_n(t) = 1. \quad (c)$$

For our problem it suffices to determine the mathematical expectation M(t) of the distribution of probability $\{P_n(t)\}$, which would also give us the variation of the number of structural defects in time:

$$N(t) \equiv M(t) = \sum_{n=1}^{\infty} nP_n(t). \quad (2.10)$$

Prior to determining definitively the number of structural defects N we wish to make the following comment.

As was mentioned earlier, $\mu_n^{(+)} \cdot \Delta t$ stands for the probability of structural damage to ice over time Δt in the presence of $\underline{n}$ defects. Let $\mu^{(+)} \cdot \Delta t$ be the probability of damage to the ideal structure (or the probability of

occurrence of an isolated defect) under the combined stresses applied to ice. Then in the presence of n defects the probability of the appearance of a new defect will be n times greater. Each defect present at time t will act as a sort of "embryo" (nucleus) of a new defect and at time $t+\Delta t$ it will either heal with the probability $\mu^{(-)}\cdot\Delta t$ or engender a new defect with the probability $\mu^{(+)}\cdot\Delta t$.

Consequently $\mu_n^{(+)} = n\mu^{(+)}$ and $\mu_n^{(-)} = n\mu^{(-)}$. Taking into account the aforegoing, it is not difficult to work out a differential equation for the mathematical expectation of the number of defects M(t). To do so the expressions adopted for the coefficients $\mu n^{(+)}$ and $\mu n^{(-)}$ are substituted into the system of equations (a), the equations are multiplied by n and added up as n = 1, 2, 3, ... as a result of which we shall obtain

$$M'(t) = (\mu^{(+)} - \mu^{(-)})M(t). \qquad (2.11)$$

If the initial number of structural defects per unit volume of ice is $M(0) \equiv N_o$, then on the basis of (2.11) the mathematical expectation of the number of defects at time t will be

$$M(t) \equiv N(t) = N_0 \cdot \exp\left[\int_0^t (\mu^{(+)} - \mu^{(-)})\, dt\right]. \qquad (2.12)$$

The kinetics of formation of structural defects in ice characterizing the development of deformations and failure, is thus determined by exponential growth if $\mu^{(+)} > \mu^{(-)}$, or by exponential decrease if $\mu^{(+)} < \mu^{(-)}$. The probability of occurrence of an isolated defect $\mu^{(+)}$ depends apparently on the acting combination of stresses and time. The process examined is therefore a nonuniform Markov (Markoff) process.

We shall make a few assumptions regarding the probabilities $\mu^{(+)}$ and $\mu^{(-)}$ that are substantiated farther on by experimental data.

The probability of annihilation (healing) of a defect $\mu^{(-)}$ does not depend on the applied shear stress (shear stress intensity). It is obvious that the higher the temperature of the ice, the more intensive the processes of annihilation of the defects, i.e. that the probability $\mu^{(-)}$ increases with the rise of the absolute temperature T. It is equally obvious that the greater the mean hydrostatic pressure in the given element of the ice volume $\sigma = 1/3(\sigma_1+\sigma_2+\sigma_3)$, the greater the probability of annihilation of the defects. It may be assumed that the probability $\mu^{(-)}$ is proportional to the value of the long-time creep limit of ice $\sigma_{i(\infty)} = C_\infty+\sigma tg\phi_\infty$.

The probability of healing $\mu^{(-)}$ can therefore be represented in the first approximation in the form

$$\mu^{(-)} = (T)\cdot\dot{\psi}(t)\cdot\sigma_{i\infty}. \qquad (2.13)$$

Function (T) within the narrow temperature range $250°K < T < 270K$ may be assumed to be linear: $\kappa(T) = \kappa_o\cdot T+\kappa_1$. Function $\dot{\psi}(t)$ defining the nonuniformity of the stochastic process of the annihilation of structural defects, must satisfy the condition $\int_0^\infty \dot{\psi}(t)dt \longrightarrow \infty$ and is determined experimentally. In our investigations that function was chosen in the form

$$\dot{\psi}(t) = \delta_1 \frac{1}{t^{1-\delta_1}}, \text{ i.e. } \psi(t) = \int_0^t \dot{\psi}(\tau)\,d\tau = t^{\delta_1}. \qquad (2.14)$$

As will be shown experimentally, under these conditions the value of the index δ_1 for ice can be assumed to be equal to $\frac{1}{3}$.

The probability of occurrence of a single defect $\mu^{(+)}$, unlike the probability of its healing, should probably depend to a significant degree on the intensity of shear stresses δ_i. Let us make a simplifying assumption. From now on it will be assumed that the probability of formation of a defect is as many times greater than the probability of its healing as the applied stress is greater than some stress $\delta_{(i\infty)}$ characteristic of ice, which we identify with the long-time creep limit for ice, i.e.

$$\frac{\mu^{(+)}}{\mu^{(-)}} = \frac{\sigma_i}{\sigma_{i(\infty)}} . \qquad (2.15)$$

Kinetics of development of structural defects in ice is thus predicted by the following analytical expression:

$$N(t) = N_0 \exp\left\{\int_0^t \varkappa[T(\tau)]\cdot(\sigma_i - \sigma_{i(\infty)})\cdot\dot{\psi}(\tau)\,d\tau\right\}. \qquad (2.16)$$

During creep, i.e., at $\sigma_i(t) = \sigma_1 = \text{const.}$, and under isothermal conditions $T(t) = T = \text{const.}$, and assuming that the $\omega(t)$ characteristic is in the form of (2.14), we get

$$N_t = N_0 \exp\left[(\varkappa_0 T + \varkappa_1)\cdot\sigma_{i(\infty)}\left(\frac{\sigma_i}{\sigma_{i(\infty)}} - 1\right)\sqrt[3]{t}\right]. \qquad (2.17)$$

Here, as in (2.12), N_o is the specific number of structural defects in ice at the initial time t = 0 (preceding the application of the load); and the parameters κ_o and κ_1 possess dimensionality:

$$\kappa_o \left[\frac{1}{\text{degrees}\cdot\text{sec}^{1/3}\cdot\text{Pa}}\right]; \quad \kappa_1 \left[\frac{1}{\text{sec}^{1/3}\cdot\text{Pa}}\right] .$$

The relation obtained (2.17) can be verified directly from experimental data. To do so the time dependence of the number of cracks that form in ice is observed for different

stresses and temperatures. If equation (2.17) is valid, the experimental data for each temperature should fall on a series of lines

$$\ln N_t = \ln N_o + \text{tg } a \; 3\sqrt{t} \qquad (2.18)$$

with the pole corresponding to the value of $\ln N_o$, where N_o is the specific number of the crystal lattice defects at the initial time that act as nuclei of future microcracks.

Stress $\sigma_{i(\infty)}$ is treated as the limit above which the flow rate will increase continuously leading ultimately to failure of ice. It now becomes clear that $\sigma_{i(\infty)}$ has the meaning of the stress above which structural defects develop progressively, i.e. that $\sigma_{i(\infty)}$ is the stress at which the probability of formation of a defect becomes equal to the probability of its healing.

The intensity of the development of microcracks in an ice specimen during its deformation under load and the total crack count indicate the degree of destruction of the specimen and may serve as criteria of its strength.

Results of short-time creep tests of ice in uniaxial compression with simultaneous recording of acoustic emissions at different loads are reported in chapter 4. Each recorded pulse corresponds to the formation of a microfracture. The data obtained on the number of acoustic pulses per unit volume of the specimen N_t over time $\underline{t}$ and their dependence on the applied stress σ_1 are consistent with dependence (2.17) presented earlier.

It has thus been confirmed by the experimental verification that the kinetics of structural disturbances at $\sigma_i > \sigma_{i(\infty)}$ obeys, at least in uniaxial compression, dependence (2.17).

Investigation into kinetics of the development of structural processes in ice during deformation in time permits us to formulate the criterion of ice failure under conditions of short-time creep, i.e. when $\sigma > \sigma_{i(\infty)}$. To substantiate this criterion a parallel investigation on structural changes in ice in the process of creep was undertaken in conjunction with the study on acoustic emission (see chapter 4).

It has been established on the basis of a structural-petrographic analysis and acoustic emission records that during short-time creep the principal mechanism controlling the development of deformations in time is the process of formation and accumulation of brittle disturbances (micro- and macrocracks, cavities, etc.).

As was mentioned earlier, failure of ice during creep can be defined either as the time of transition to tertiary creep or as the time when the ice specimen or ice mass breaks up into fragments (total failure). Analysis of experimental data shows that for each of these states there is a definite characteristic number of brittle structural defects (see fig. 2.3), and that both of them (the critical N^* and the maximum number of accumulated defects, N^{**}) depend on the long-time creep limit $\sigma_{i(\infty)}$:

$$N^{*} = N_{o} \exp\left[\kappa^{*} \cdot \sigma_{i(\infty)}\right], \tag{2.19}$$

$$N^{**} = N_{o} \exp\left[\kappa^{**} \cdot \sigma_{i(\infty)}\right]. \tag{2.19a}$$

Within a limited range of temperatures functions κ^{*} and κ^{**} depend on it linearly. The dimensionality of the parameters κ^{*} and κ^{**} is [1/Pa].

The creep strains of ice corresponding to the criteria of failure depend on the applied stress (see fig. 2.3).

The time of transition to the stage of tertiary creep $t = t^{*}$ corresponding to a definite number of accumulated brittle disturbances $N = N^{*}$, and the effective stress σ_{i} are linked by a dependence that may be written on the basis of (2.16) and (2.19) in the form

$$\int_{0}^{t^{*}} (\varkappa_{0} T + \varkappa_{1}) \left(\frac{\sigma_{i}}{\sigma_{i(\infty)}} - 1 \right) \cdot \sigma_{i(\infty)} \cdot \dot{\psi}(\tau)\, d\tau = \varkappa^{*} \sigma_{i(\infty)}. \tag{2.20}$$

Under conditions of creep, where stress and temperature do not vary in time, the condition for transition to the tertiary stage of creep is determined from (2.20) in the following closed form:

$$\sigma^{*}_{i(t)} = \sigma_{i(\infty)} \left[1 + \left(\frac{\varkappa^{*}}{\varkappa_{0} T + \varkappa_{1}} \right) \frac{1}{\psi(t^{*})} \right];$$

or

$$\psi(t^{*}) = (t^{*})^{\delta_{1}} = \left(\frac{\varkappa^{*}}{\varkappa_{0} T + \varkappa_{1}} \right) \frac{\sigma_{i(\infty)}}{\sigma^{*}_{i(t)} - \sigma_{i(\infty)}}. \tag{2.20a}$$

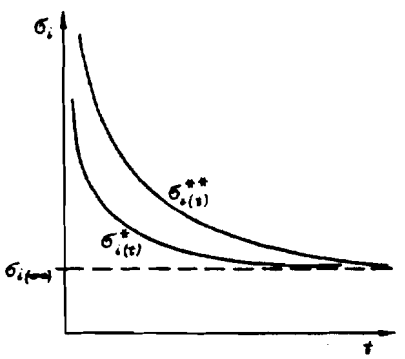

Fig. 2.4

Long-time strength of ice curves

$\sigma^{*}_{i(t)}$ - for the time of initiation of accelerating creep;

$\sigma^{**}_{i(t)}$ - for the time of total failure

***

Failure of ice near time t** occurs in an avalanche-like fashion, and the creep curve (fig. 2.3) asymptotically tends towards the vertical. The number of defects N tends then towards their maximum number N**. The condition of long-time strength for time t** written analogously to expression (2.20a), but with κ^{**} substituted for κ^{*}, is known from the literature as the Bairstow condition of long-time strength. It is substantiated experimentally for ice in chapter 5.

Both conditions of strength can be represented in the "failure stress-time to failure" coordinates in the form of two long-time strength curves with their common asymptote representing the long-time creep limit (fig. 2.4).

2.3. Short-time creep of ice

The relations (2.6), (2.7) and (2.8) presented above and the proposed dependence of the number of defects on time, stress and temperature (2.16), (2.17) and (2.19) can be used to write fundamental relations for ice under conditions of short-time creep.

Proceeding from the basic assumption (2.5), the load function Π can be rewritten in the form

$$\Pi = \int_0^t \varkappa(T)\cdot(\sigma_i - \sigma_{i(\infty)})\cdot\dot{\psi}(\tau)\,d\tau - \varkappa^{*}\sigma_{i(\infty)} - m\cdot\ln\frac{\dot{e}_i^{(p)}}{\dot{e}_i^{*}}. \tag{2.21}$$

Under creep conditions, at σ_i = const and σ = const, the load function assumes on the basis of (2.21) and (2.20a) the form

$$\Pi = \varkappa(T)\cdot\psi(t)\cdot(\sigma_i - \sigma_{i(t)}^{*}) - m\cdot\ln\frac{\dot{e}_i^{(p)}}{\dot{e}_i^{*}}, \tag{2.21a}$$

where the long-time strength of ice $\sigma^*_{i(t)}$ is given by expression (2.20a). The load surface trace $\Pi = 0$ in plane $\sigma_i \div \sigma$ represents a series of lines

$$\sigma_i = \sigma_{i(\infty)}\left(1 + \frac{\varkappa^*}{\varkappa(T)\cdot\psi(t)}\right) + \frac{m\cdot\ln\dfrac{\dot{e}_i^{(p)}}{\dot{e}_i^*}}{\varkappa(T)\cdot\psi(t)}. \tag{2.22}$$

The components of the strain-rate are expressed in the form

$$\dot{e}_{ij}^{(p)} = \dot{h}\left\{\int_0^t \varkappa(T)\frac{S_{ij}}{2\sigma_i}\dot{\psi}(\tau)\,d\tau - \delta_{ij}\frac{\operatorname{tg}\varphi_\infty}{3}\left[\int_0^t \varkappa(T)\dot{\psi}(\tau)\,d\tau + \varkappa^*\right]\right\}, \tag{2.23}$$

and the strain-rate tensor invariants derived from it are equal to

$$\left.\begin{aligned} \dot{e}_i^{(p)} &= \dot{h}\int_0^t \varkappa(T)\cdot\dot{\psi}(\tau)\,d\tau; \\ \dot{e}_v^{(p)} &= -\dot{h}\operatorname{tg}\varphi_\infty\left[\int_0^t \varkappa(T)\dot{\psi}(\tau)\,d\tau + \varkappa^*\right]. \end{aligned}\right\} \tag{2.24}$$

The undetermined factor $\dot{h}$ is found from the load condition: $\Pi = 0$; $d'\Pi > 0$, where $d'\Pi$ is the total differential of the load function equal to

$$d'\Pi = \frac{\partial\Pi}{\partial\sigma_{ij}}d\sigma_{ij} = \frac{\partial\Pi}{\partial\sigma_i}d\sigma_i + \frac{\partial\Pi}{\partial\sigma}d\sigma.$$

It should also be taken into account that the stress point is at each time on the load surface, i.e. that the condition $\Pi = 0$ must be met at each time. Consequently,

$$m\cdot\ln\left[\frac{\dot{h}\int_0^t \varkappa(T)\dot{\psi}(\tau)\,d\tau}{\dot{e}_i^*}\right] = \int_0^t \varkappa(T)\cdot(\sigma_i - \sigma_{i(\infty)})\dot{\psi}(\tau)\,d\tau - \varkappa^*\sigma_{i(\infty)}. \tag{2.25}$$

To close the model, it is necessary to formulate the dependence for the minimum plastic strain-rate $\dot{e}_1^*$. To do so

let us introduce an additional hypothesis that has been justified experimentally. Let us assume that

$$\dot{e}_i^* = \frac{1}{\eta_o}\,\dot{\psi}\,(t^*). \qquad (2.26)$$

The results of the experiments performed show that the function $\dot{\psi}(t) = \frac{1}{3t^{2/3}}$, in view of which condition (2.26) can be written in the form

$$3\eta_0 \cdot t^{*2/3} \cdot \dot{e}_i^* = 1 \quad \text{or} \quad \dot{e}_i^* = \frac{1}{3\eta_0 \cdot t^{*2/3}}. \qquad (2.27)$$

It follows from the graphical plot in fig. 5.7a that the points of the minima of the strain-rate time-functions in the logarithmic scale lie on the line with a 2/3 slope* and with parameters $3\eta_o = 1.6 \cdot 10^5 s^{1/3}$.

It should be noted that Yu.K. Zaretskii and S.S. Vyalov also provide in their work (1971) a theoretical substantiation for the condition of the onset of tertiary creep, which states that the product of the initial tertiary creep rate and of a certain function from the time of initiation of that process is a constant.

The assumptions leading to the formulation of the load surface (2.21) and (2.27) are thus sufficient for describing short-time creep of ice under conditions, where $\sigma_i \geq \sigma_{i(\infty)}$ for any complex loading path and under any testing conditions.

---

* The Russian term for "gradient" and "slope" is the same. Translator.

The relation between the volume strain-rate and shear strain-rate is defined on the basis of (2.8) and (2.24) by the dependence

$$\frac{\dot{e}_v^{(p)}}{\dot{e}_i^{(p)}} = -\operatorname{tg}\varphi_\infty\left[1+\frac{\varkappa^*}{\int_0^t \varkappa(T)\cdot\dot{\psi}(\tau)\,d\tau}\right]. \tag{2.28}$$

From relations (2.24) and (2.28) it follows that volume deformation of ice under conditions of short-time creep has the character of decompaction (dilatancy).

Under conditions of creep (2.28) becomes simplified

$$\frac{\dot{e}_v^{(p)}}{\dot{e}_i^{(p)}} = -\operatorname{tg}\varphi_\infty\left(1+\frac{\varkappa^*}{\varkappa(T)\,\psi(t)}\right) = -\operatorname{tg}\varphi_\infty\frac{\sigma^*_{i(t)}}{\sigma_{i(\infty)}}, \tag{2.29}$$

and is defined by the ratio of the long-time strength $\sigma^*_{i(t)}$ to the long-time creep limit $\sigma_{i(\infty)}$.

Let us now examine the fundamental relations for creep under conditions of uniaxial compression. In this case the long-time creep limit of ice in compression $\sigma_{i(\infty)}$ is a constant and, on the basis of the Mises-Schleicher condition (2.4), is equal to

$$\sigma_{1(\infty)} = \frac{\sqrt{3}\cdot c_\infty}{1-\frac{1}{\sqrt{3}}\operatorname{tg}\varphi_\infty}.$$

The invariants that are arguments of the load function, are $\sigma_i = \frac{1}{\sqrt{3}}\sigma_1$; and $\sigma = \frac{1}{3}\sigma_1$.

It may thus be seen that the kinetics of development of structural defects in ice during uniaxial creep is still predicted by relation (2.17):

$$N = N_0 \exp\left[\bar{\varkappa}(T)\left(\frac{\sigma_1}{\sigma_{1(\infty)}} - 1\right)\sqrt[3]{t}\right]. \tag{2.17a}$$

where $$\bar{\varkappa}(T) = \varkappa(T)\cdot\sigma_{i(\infty)} = \frac{(\varkappa_0 T + \varkappa_1)\cdot\sigma_{1(\infty)}}{\sqrt{3}}.$$

During uniaxial creep of a cylindrical ice specimen the intensity of shear strains $e_i^{(p)} = \frac{2}{\sqrt{3}}\left(\varepsilon_i^{(p)} + \varepsilon_3^{(p)}\right)$, bearing in mind that in this case $\varepsilon_3^{(p)} < 0$; $\varepsilon_i^{(p)} > 0$. Dilatancy volume strain $\left(-\varepsilon_v^{(p)}\right)$ is determined as the sum $-\varepsilon_v^{(p)} = \varepsilon_1^{(p)} - 2\varepsilon_3^{(p)}$, from which the axial strain may be expressed as

$$\varepsilon_1^{(p)} = \frac{\sqrt{3}\varepsilon_i^{(p)} - \varepsilon_v^{(p)}}{3}.$$

Proceeding from the relation (2.29) obtained earlier, we ultimately find

$$\dot{\varepsilon}_1^{(p)} = -\dot{\varepsilon}_v^{(p)}\left[\frac{1}{3} + \frac{\sqrt{3}}{3\left(1 + \frac{\varkappa^*}{\varkappa(T)\,\psi(t)}\right)\operatorname{tg}\varphi_\infty}\right], \tag{2.30}$$

where $\dot{\varepsilon}_v^{(p)}$ is the dilatancy volume strain-rate of ice.

In further account ε and σ will designate axial strain and stress, respectively, unless stated otherwise.

It may be assumed that volume strain of ice during short-time creep is determined directly by the development of brittle structural disturbances and can therefore be represented as the product of independent stochastic variables: the number of defects by the size of a single defect. More precisely, volume strain is proportional to the product of the mathematical expectation of the characteristic

size of a single defect and of the expectation value of the number of accumulated defects:

$$\varepsilon_v^{(p)} = - qM(\Sigma) \cdot M(N-N_o), \qquad (2.31)$$

where Σ is the characteristic size of a single structural defect, $N-N_o$ is the number of the newly accumulated structural defects in ice, and q is the coefficient of proportionality.

Experimental studies should be conducted in the following direction:

1. To determine during uniaxial creep of ice at various temperatures the number of brittle structural disturbances in ice at stresses $\sigma > \sigma_\infty$, and to ascertain the validity of formula (2.17).
2. To ascertain on the basis of studies on the size of defects the validity of the assumption that the dilatancy volume strain of ice depends on the size of the accumulated structural defects [formula (2.31)].
3. To determine experimentally that the condition N=N** can be used as the criterion of failure for ice.
4. To ascertain the validity of the proposition regarding the load function (2.21) for predicting viscoplastic deformations of ice.

CHAPTER 3

INSTRUMENTS AND METHODS OF EXPERIMENTAL STUDIES

In conformity with the objectives defined in chapter 2, the problems formulated for this stage of experimental research were as follows:

1. To test a series of identical ice specimens with an identical structure under conditions of uniaxial creep for several temperatures and under a series of loads ($\sigma > \sigma_\infty$) at each given temperature so that the creep time (time to failure) would be a few minutes to several hours.
2. To measure the intensity of accumulation of brittle structural disturbances in ice during creep and to determine the relationship of that process with parameters of the external factors, i.e. effective stress and temperature.
3. To investigate the dependence of dynamometamorphism of the initial ice structure on the size and duration of the load. To determine the form of the dependence of the total strain of ice on the total surface of the microdefects forming in the process of tertiary creep.
4. To determine the criterion of failure for ice during short-time creep and the dependence of that criterion on the load and temperature parameters.

To arrive at an integrated solution to the above problems, the acoustic emissions were used as a measure of the number and size of brittle structural microdefects formed in ice during creep, in combination with structural-petrographic techniques for assessing the degree of dynamometamorphism of ice at different stages of creep.

3.1. Preparation and testing procedures

The ice used in the experiments was prepared artificially in a special tray with thermally insulated walls and bottom. The tray measured 80 × 80 cm in plane and 20 cm in depth. The tray was placed in the cold chamber at -10°C. The ice was prepared from distilled water deaerated in a vacuum pump. After the total volume of water cooled down to 0°C and a 2 to 5 mm layer of ice formed at its surface, the ice was removed and further freezing was initiated by seeding the water surface with ice crystals sifted through a screen with 1 mm meshes. As a result of this a protocrystallization layer several millimetres in thickness formed at the water surface and, as the crystallization front moved downwards, there gradually developed a layer of orthotropically accreting crystals. The ice specimens were prepared from the orthotropically crystalled ice.

As has been pointed out by B.A. Savel'ev (1963), the potential energy of ice molecules is the lowest in the direction of basal planes, which accounts for the highest growth rate of crystals in that direction. Therefore the crystals growing in the direction of basal planes are in an advantageous position relative to the crystals developing in other crystallographic directions. The latter crystals, therefore, fairly rapidly become forced out and there arises a columnar-grained structure of ice with prismatic crystals, the long axes of which are parallel to their basal planes. Moreover, the optic axes of these crystals are parallel to the freezing surface.

During the unilateral freezing of water as a result of the so-called geometric selection [Shumskii, 1955] the crystals decrease in number, but increase in size. This phenomenon was also observed in our experiments, but at the depth of 1-2 to 6-7cm the increase in the size of the crystals was negligible and could be disregarded. The cross-sectional area of the crystals was 0.5-1.2cm^2, and the area of their longitudinal section at the depth of about 5cm was 2.5-4.0cm^2.

Therefore the specimens prepared from an ice layer taken from a definite depth from the surface generally have standard structural characteristics, even though variations in their structural details cannot be ruled out. These were the considerations borne in mind in preparing the ice specimens, structural parameters of which had to be as close as possible in all the experiments.

To prepare the specimens the ice blocks were sawn into 60 × 60 × 150mm prisms, from which cylindrical specimens measuring 50.5mm in diameter (with an area of 20cm^2) and 100±0.5mm in height were turned on a lathe. The butt ends of the cylinders were polished on a warm plate with the help of a special plastic foam collar ensuring that the butts of the cylinder were perpendicular to its generatrix. The test specimens were cut in such a way that the prismatic (columnar) ice crystals were perpendicular to the longitudinal axis of the cylinders.

The ice specimens were tested under conditions of uniaxial stress and isothermal creep, i.e., at constant values of compressive stress and temperature for each test.

To determine the effect of the characteristics of ice that were under study, the tests were run at three different temperatures: -4, -8.5 and -13°C. The temperature of the specimen was monitored by means of a mercury thermometer graduated in 0.1°C. The thermometer was secured right next to the specimen tested. The specimens were stored in kerosene (to prevent sublimation) and were maintained at the temperature of the experiment for at least twenty-four hours before being tested. In the course of the test the temperature of the specimens was maintained constant with an accuracy of +0.3°C.

A special uniaxial compression apparatus (see fig.3.1) was used to apply loads to the specimens and to measure their deformations. The specimen (with the butt ends coated with cool grease) was placed between two polished steel platens; the upper one of which was furnished with a ball joint to prevent angular deflection. The loading rod with a guide bar provided for translational displacements of the die during the deformation of the specimen. A block diagram of the monitoring and measuring instruments employed in the tests is shown in fig. 3.2.

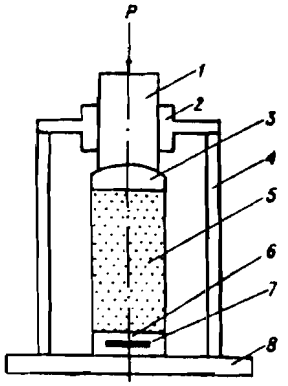

Fig.3.1

Diagram of the uniaxial compression apparatus

1-Die; 2-Guide bar; 3-Upper platen; 4-Stand; 5-Specimen; 6-Lower platen; 7-Piezoelectric transducer; 8-Base

***

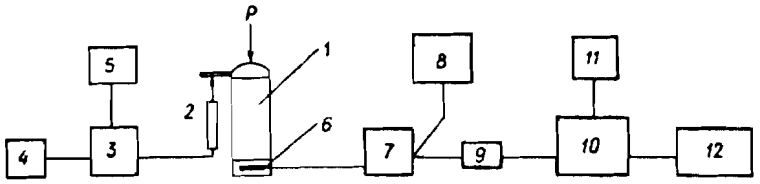

Fig.3.2

Block diagram of the monitoring and measuring instrumentation 1-Specimen; 2-Displacement gauge DP*2; 3-Amplifier VI*6-5Ma*; 4-Power source; 5-Digital voltmeter Shch*-1413; 6-Piezoelectric transducer; 7-Measurement amplifier U*4-12; 8-Storage oscillograph S*1-37; 9-Pulse normalizer; 10-Pulse analyser AI*-128-2; 11-Digital printer B*3-15; 12-Electron-counting frequency meter Ch*3-33

---

* Transliteration. Translator.

Axial deformation of the specimen was determined from the displacement of the upper platen by the inductive displacement gauge (2) of the type DP-2 combined with the measuring equipment VI6-5MA (3), (4) and with the digital voltmeter Shch-1413 (5). The accuracy of the measurements was 0.01mm. A dial gauge was mounted parallel to the DP-2 gauge and was used for measuring the conventional instantaneous deformation of the specimen and for monitoring the creep strain.

The radial deformation of the specimen was used to monitor the change in the cross-sectional area of the specimen during creep and was measured by a dial gauge graduated in 0.01mm. The measurements took into account the ellipsoid cross-sectional shape of the specimen that developed during axial compression.

Compressive load was applied to the ice specimens with a lever-type press with the uniaxial compression device mounted in it. The loading was done with weights, in one single operation, smoothly, over time $\approx$ 0.5-1 sec. Two series of specimens were tested at each given temperature. The first series consisted of four specimens, each of which was subjected to a different constant load and to a maximum axial deformation of 10%.

In the second series five identical specimens were tested under one of the loads used for the first series, but were subjected to varying degrees of deformation. The tests were discontinued when the axial deformation attained 1, 2, 4, 6 or

8% of the initial height of the specimen.

It should be noted that in selecting the loads for the temperatures of -4 and -8.5°C, we were guided by the conventionally instantaneous strength of ice determined at these temperatures for analogous specimens. The loads were specified for the creep tests as fractions of the values of the conventionally instantaneous strength σ_0 (e.g. $\sigma_1=0.5\,\sigma_0$; $\sigma_2=0.7\sigma_0$; and so on). However, it was found in the course of the tests that the creep strain-rate was defined not by the ratio of the effective stress to the conventionally instantaneous strength, but by the absolute value of the stress. Therefore the values of the loads chosen for the temperature of -13°C, were not fractions, but integers unrelated to the instantaneous strength.

The loads set at different temperatures were as follows ($\cdot 10^5$Pa):

$\theta = -4°C$ $\quad \sigma_1 = 20{,}25;\ \sigma_2 = 16{,}0;\ \underline{\sigma_3 = 11{,}4};\ \sigma_4 = 9{,}1,$

$\theta = -8{,}5°C$ $\quad \sigma_1 = 20{,}4;\ \underline{\sigma_2 = 16{,}3};\ \sigma_3 = 14{,}2;\ \sigma_4 = 12{,}3,$

$\theta = -13°C$ $\quad \sigma_1 = 24{,}0;\ \underline{\sigma_2 = 20{,}0};\ \sigma_3 = 16{,}0;\ \sigma_4 = 14{,}0.$

Underlined are the values of the loads at which the second series of tests was performed.

Readouts of the test time from the stopwatch began simultaneously with the application of the load to the specimen. The readings were taken from the gauges immediately after the loading; the first readout after the zero deformation reading, within 1.0-1.5 sec. from the beginning of the test, was regarded

as the "instantaneous" deformation ε_0. After that two more readings were taken from the axial deformation indicator 15 and 30 seconds from the beginning of the test. After 1 minute the readouts from the digital voltmeter 5 were taken (see the block diagram of the monitoring and measuring equipment in fig. 3.2). In tests lasting 1 hour or less the readings were taken every minute, and in longer tests at least every five minutes.

To maintain a constant stress in the specimen, additional load was applied to it after every 1-3% increase in its cross-sectional area (depending on the stress) by suspending appropriate weights on the lever-type press.

Once the axial deformation attained the value chosen for the given test, the load was removed and the specimen was subjected to crystallo-optic investigations.

3.2. Methods of structural-petrographic studies

Structural-petrographic studies of the ice specimens were carried out according to standard methods [Savel'ev, 1963] with certain supplementary procedures that were required owing to the specific nature of our investigations.

Preliminary investigations have shown that ice specimens with an initially uniform structure deformed in different ways under applied load. The degree of deformation varied significantly at different points of the specimen. The most intensive deformation processes occurred once in the upper, once in the middle, once in the bottom part of the specimen. It was therefore imperative to characterize the structure of the specimen as fully as possible

throughout its bulk in order to minimize the effect of the differences in the location of the maximum deformation zone on the results, primarily on the quantitative structural indices pertaining to the specimen as a whole. Therefore the system chosen for the preparation of thin sections was such that the sections were cut from five characteristic planes of the specimen. As is shown in fig.3.3, the plane of the sections a_1 and a_2 was perpendicular to the long axes of the columnar ice crystals, along the longitudinal axis of the cylindrical specimen, and the planes of the sections c_1, c_2 and c_3 along the long axes of the crystals, parallel to the butt ends of the specimen.

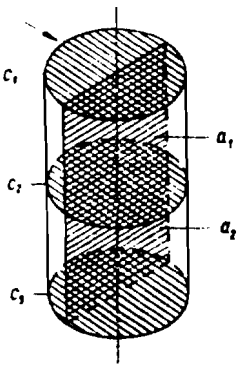

Fig. 3.3

Diagram of the preparation of thin sections from the specimen

***

The thin sections were first photographed using Polaroid film, which allowed us to establish the structure of the sections as a whole. After that the sections were examined, described and photographed with an MPS*-2 microscope at different magnifications depending on the size of the structural elements. The MPS-2 microscope provides for a

* Transliteration. Translator.

rapid resetting of magnification so that not only the minute structural formation itself, but also its relation to the other structural elements that are of a different size, can be readily observed. These data formed the basis for the determination of the petrographic deformation patterns and internal mechanisms controlling plastic and brittle movements in ice.

All the quantitative structural indices were determined from the photographs of thin sections.

$S_{cp*}(cm^2)$, the average area of the crystals within each thin section, was determined from the expression

$$S_{cp}=\frac{S_{ш*}\cdot 1.5616}{n(M\cdot Y)^2}\quad , \qquad (3.1)$$

where $S_ш$ is the total area of the section, n is the number of crystals in the section, 1.5616 is the coefficient of areal distortion, and MY is the magnification scale.

The average length of the crystal boundaries is

$$l_{cp}=\frac{l_ш\cdot 1{,}25}{n\cdot MY}\ см, \qquad (3.2)$$

where $l_ш$ is the length of the crystal boundaries in the section and 1.25 is the coefficient of linear distortion.

At first the area of each crystal in the section was

---

* Transliteration.

cp=average, mean;

ш=thin section.

Translator.

determined directly from the millimetre grid if the crystal form was irregular, or by calculating the area of the figure (square, rectangle, hexagon, trapezoid, etc.) corresponding to the shape of the crystal by using the method of standard areas [Shumskii, 1955]. These initial data were used for plotting histograms of the areas of the crystals in different sections or planes, as well as, after separating ice grains of different sizes, for constructing diagrams of the relative content of grains of different sizes at different stages of deformation.

The average dimensions of the crystals varied to a greater or lesser degree throughout the specimen. Therefore their values are somewhat scattered for the planes a_1, a_2 and c_1, c_2 and c_3. Graphical plots of the dependence of S on ε were constructed by taking into account the range of variations in the size of the crystals in each of the planes (a and c). Approximating curves of the areal measurements of the crystals were plotted on these graphs for each plane and amount of deformation. This method of obtaining approximate values of the areas makes it possible to eliminate the discrepancies in structural indices (in the graphs the curves depicting the dependence of S on ε do not always correspond to the average values of the area in different planes) that are due to the inevitable differences in the initial structure of individual specimens or to subjective errors in the count taken from the photographs of the sections because of the imperfection of the photographs (when small adjoining crystals have a similar orientation, the boundaries

between them cannot always be accurately identified), as well as to the fact that exact determination of the number and size of submicroscopic crystal fragments and of the nuclei of new crystals is often impossible, particularly at the stage of advanced recrystallization.

Mean values of the area of the averaged crystal in planes "a" and "c", respectively, were determined for a number of selected values of strain from the approximating curves. Assuming that the form of the averaged crystal in our specimens was a prism with the base in plane "c" and with the altitude in plane "a", the mean volume $V_{cp}(cm^3)$ of individual crystals in the specimen is calculated from the expression $V_{cp}=S_c \cdot \sqrt{S_a}$, where S_a is the average area of a crystal in plane "a" and S_c is its average area in plane "c".

The quantity characterizing the number of crystals per unit volume $\underline{d}$ is determined from the expression $d=1/V_{cp}$. The same assumption pertaining to the form of the crystals was used to determine the surface area of the averaged crystal P_{cm2} from the expression $P=2S_a+4S_c$ using the values obtained for S_a and S_c. The specific surface, i.e. the surface of the crystals present in a unit volume of the specimen, proved to be a convenient indice. Designating that quantity as $f(cm^2/cm^3)$, we obtain $f=P \cdot d$.

The values of the indices pertaining to the number and size of the crystals were subsequently processed graphically to illustrate the changes occurring in them with deformation.

3.3. Acoustic emission method

The acoustic vibrations occurring during the formation of microcracks in the specimens, were recorded using the monitoring and measuring instruments (see fig.3.2).

The primary converter of the mechanical elastic vibrations of the acoustic emission into electrical signals was a piezoelectric transducer (6) made of lead zirconate-titanate ceramic and built into the lower platen of the uniaxial compression machine. The acoustic emission pulses converted by the transducer into electric signals, were transmitted to the measurement amplifier U*4-12 with a band width of 0-30kHz. The signals were transmitted through the pulse normalizer 9, acting as a matching attachment, to the multi-channel pulse height analyser AI*-128-2 (10) and were recorded separately in 128 channels of the storage unit with the channel numbers proportional to the amplitude of the signals. An electronic digital frequency meter Ch*3-33 (12) was connected to the output of the pulse analyser. The frequency meter operated in the continuous count mode and was used for counting the total number of pulses transmitted to the analyser. A S*1-37 storage oscillograph was connected to the output of the U*4-12 amplifier for visual monitoring and photographing (8).

---

* Transliteration. Translator.

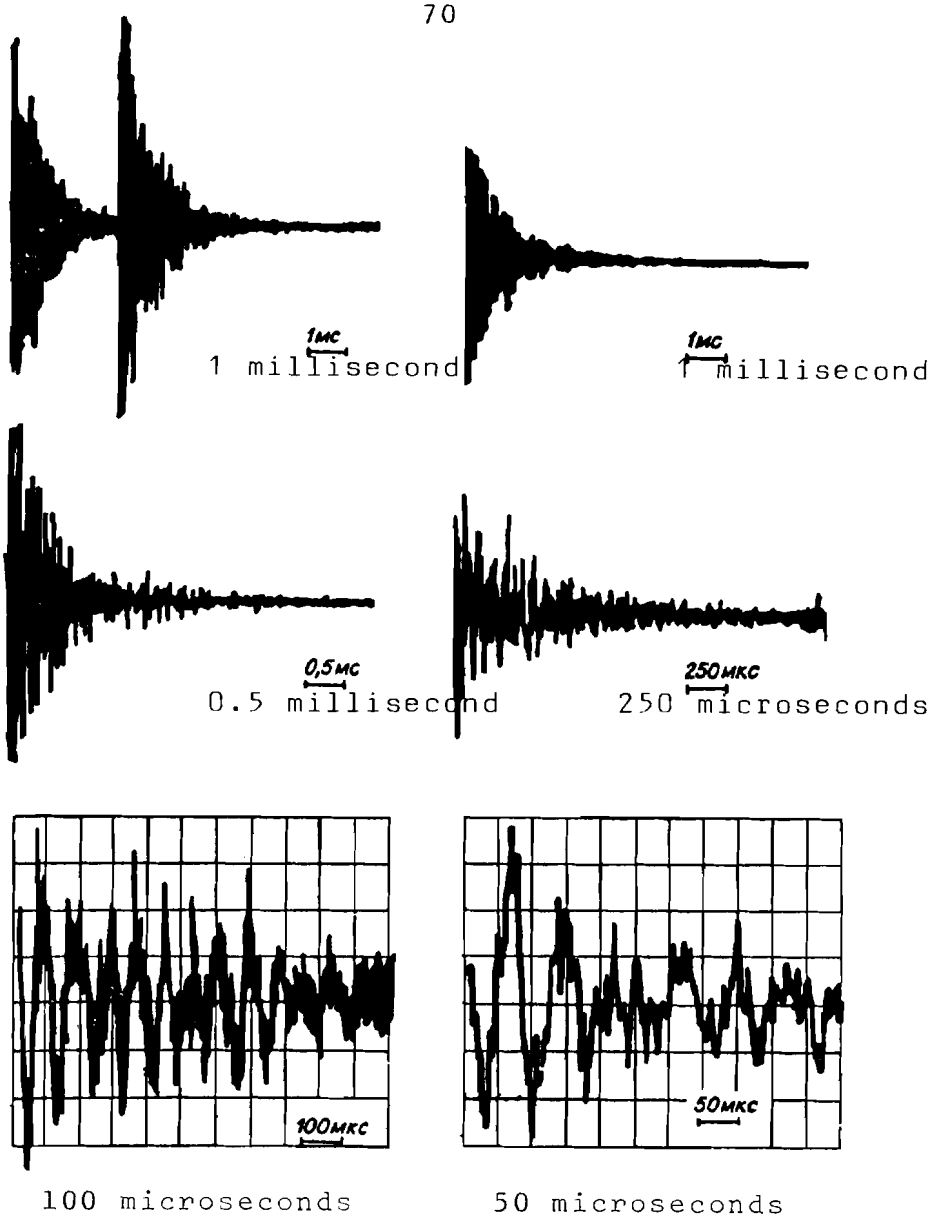

Fig. 3.4

Oscillograms of the acoustic pulses generated during the formation of microcracks in ice. Vertical scale 0.01 V/div

***

The design and operation of the pulse normalizer (9) should be discussed in greater detail, since that instrument was built especially for our experiments.

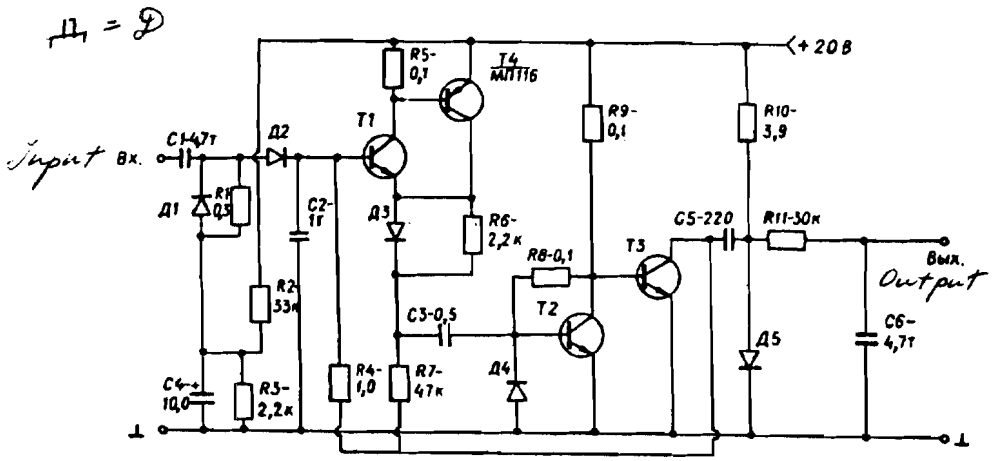

Fig. 3.5

Diagram of the pulse normalizer

***

The need for the matching attachment in front of the pulse analyser is dictated by the fact that the electric pulse corresponding to a single acoustic emission is a complex double-polarity signal with a total duration of the damped amplitude of 2-10 milliseconds or even longer (see oscillograms in fig.3.4). On the other hand the design of the pulse analyser AI*-128-2 assumes transmission to its input of a single-polarity signal with the duration of the leading edge < 1 microsecond and that of the trailing edge > 1 microsecond.

The pulse normalizer generates short pulses suitable for recording by the pulse analyser AI-128. The amplitude of these pulses is proportional to the maximum amplitude of the oscillations transmitted to the input of the normalizer from the output of the amplifier. A diagram of the normalizer is shown in

fig.3.5 and its operation is explained by the voltage curves in fig.3.6, where the input pulse is stretched in time for a greater clarity of representation.

At the time of negative input voltage half-waves the capacitor C1 is charged through the diode D1, and at the time of positive half-waves its charge is transmitted through D2 to C2, at which the voltage increases in steps to the level equal to the maximum of the amplitude U_{input}. When the amplitude U_{input} begins to decrease, U_{c2} remains at the maximum level attained. The U_{c2} voltage charges the C3 capacitor through the combined emitter-coupler T1-T4 and R6. When C3 discharges, the current flows through the base of T2, that transistor is saturated, and T3 is off. During that time the voltage from the emitter-coupler is transmitted to the collector of T3 through R7 and charges C5 to the voltage $U_{c5}=U_{c2}$. Having reached the maximum level U_{c2}, the charge of C3 remains over the access time t_o: if U_{c2} does not increase further during that time, the current of the charging decreases to the point where T2 closes and T3 opens. At that moment U_{c5} drops sharply and the negative recharge pulse C5 proceeds to the output through R11.

After that C3 becomes discharged through T3 that is now open, and through R7, while C2 becomes discharged through R4. During the discharging of C2 and C3 the circuit does not react to weak signals with smaller amplitudes than the voltage remaining in the capacitors, which results in the loss of the weak signals that rapidly succeed the strong ones. An example of such a signal is shown in the curve labled U_{Bx}*. The

* $U_{Bx}=U_{input}$. Translator.

discharge time constant depends mainly on C3. It has been established experimentally that C3=0.5 microfarad adequately protects the circuit against spurious counts; at the capacity given above t_0=1.2 milliseconds and the discharge time constant is 25 milliseconds. Control tests have shown that the acoustic pulses succeed one another as a rule at intervals greater than 100 milliseconds whatever the rate at which they accumulate. The cases similar to that shown in fig.3.4a, where the intervals between the pulses are 3 milliseconds, amount to less than 1% of the total number of pulses.

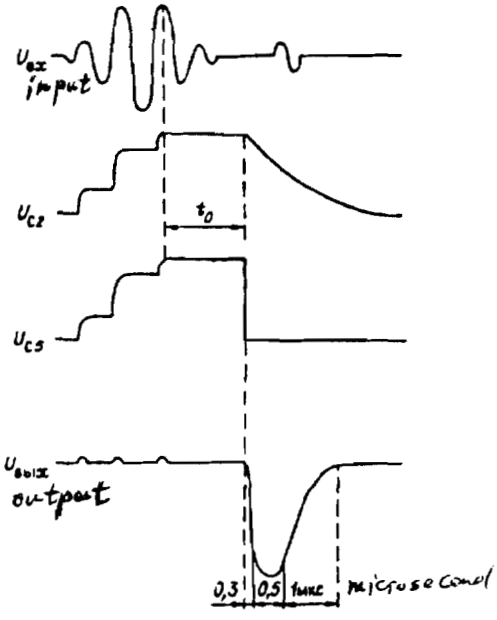

Fig.3.6

Voltage curves

In the output voltage, in addition to the negative pulse, there form small positive pulses as U_{c5} increases in steps. These positive pulses are not recorded by AI-128 and do not affect the results.

To reduce the nonlinearity of the conversion of the amplitude of the input signal to the amplitude of the output signal, forward bias is applied through R2 to the diodes D1 and D2, and D5 is biased by the current through R10. However, a normalizer with such a simple circuit cannot ensure a perfect linearity of conversion, and to obtain accurate measurements it is necessary to calibrate the equipment so as to match the numbers of the AI-128 channels to the known amplitudes of the U_{input} signal.

The total number of acoustic pulses was recorded continuously throughout the test by the digital display of the frequency meter (12). The readings of the meter were taken at the same times as the deformation readings.

At the instant when the load was applied the initial reading produced by the noise during the loading was recorded by the display of the frequency meter. Before the first minute readout that figure was "erased" and was disregarded from there on. That operation introduced no errors into the pulse count, since it was observed that the first microfracture (clearly observable visually in the form of planes reflecting light in the optically transparent specimen) and the attendant acoustic pulses appeared not immediately after the load was applied, but after a delay of 3-4 to 10-20 minutes, depending on the load.

The amplitude of the pulses was recorded periodically (6 to 15 times) throughout the test with the help of the AI-128 analyser. To ensure statistical uniformity of random pulse samples, the pulses were introduced into the analyser in roughly equal batches of about 100 each. Recording of the first batch was usually initiated during the 2nd or 3rd minute of the test by pressing the "start" button of the analyser. Once 100 pulses accumulated in the display of the meter, the "stop" button was pressed to disconnect the storage unit from the amplifier, the analyser was switched over to the "output" mode, and the accumulated information was outputted to the digital printer (11, fig. 3.2), where the number of the pulses transmitted to individual channels was recorded for each channel number. After that the "memory" (storage) of the analyser was "erased", the analyser was switched over to the operating mode and was ready to record the next batch of pulses. The switching over of the analyser and the withdrawal of the information take 1.0-1.5 minute, which makes it possible to obtain samples succeeding one another fairly closely.

As was mentioned earlier, the pulse normalizer with a simple circuit did not ensure a perfectly linear conversion. To determine the degree of nonlinearity of the measuring system it was calibrated according to two schemes.

When the first scheme was employed, square pulses with a duration of 10 microseconds and specified amplitude of 0.4 to 12V were transmitted to the input of the normalizer from the

G*5-15 pulse generator. The pulse frequency was arbitrary ranging from a few (if the generator was actuated manually) to 40Hz.

When the second calibration scheme was used, mechanical vibrations simulating acoustic emission pulses were transmitted to the piezoelectric transducer. To obtain simulated pulses, an emitting piezoelectric transducer was used that was similar in design to the sensing piezoelectric transducer. The emitting and receiving transducers were tightly (with lubrication) pressed together through a thin plexiglass plate providing electrical insulation between the casings of the transducers. After that short square electric pulses were transmitted to the emitter from the G5-15 generator with a frequency of 10Hz. The pulses excited mechanical vibrations in the piezocell of the emitter similar to the acoustic emission accompanying microfracturing. The pulse converted once again to an electric signal by the sensing transducer, travelled after that along the measuring channel "amplifier-normalizer-analyser-counter" identical to that used in the tests with ice. The amplitude of the test pulse from the generator was selected in such a way that the amplitude of the signal obtained, the signal monitored from the screen of the oscillograph, was equal to the specified value in volts. In the process of this the number of the analyser's channel, in which the signal of the given amplitude was recorded, was fixed.

The results of the calibration according to the two schemes proved to be very close and were used to construct a graphical plot reflecting the relationship between the amplitude of the

signal and the number of the corresponding channel in the analyser (fig. 3.7). As may be seen from the plot, up to about 7V the conversion coefficient is markedly nonlinear. To eliminate the effect of that nonlinearity on the results of the measurements, the processing of the digital printer's tapes (carrying the information on the amplitude distribution of the pulses in the batches of samples) began with "correction for nonlinearity", i.e. with substitution for the AI channel numbers read from the corresponding channels from the linear dependence in the graphical plot from fig. 3.7.

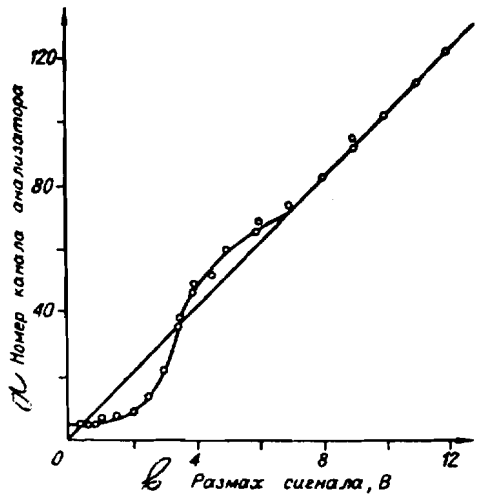

Fig. 3.7

Calibration graph of the acoustic channel

a - Number of the analyser's channel;

b - Amplitude of the signal

***

After each sample batch of pulses was corrected for nonlinearity, the mean value of the pulse amplitude was determined as the mathematical expectation of that amplitude.

Fig.3.8 shows the amplitude distribution plot for a sample batch of pulses from one of the tests. If A_i is the pulse amplitude (channel number AI-128) and n_i is the number of pulses of the given amplitude (the pulses allocated to the "i" channel of the analyser), then the mathematical expectation of the pulse amplitude M(A) is the sum

$$M(A) = \Sigma P_i \cdot A_i, \qquad (3.3)$$

where $P_i = n_i / \Sigma n_i$ is the relative frequency or the probability of the appearance of pulses with the given amplitude.

With 6 to 15 sample batches of pulses for each test at our disposal, we obtained from calculations the same number of M(A) values for definite time intervals. However, so far it is impossible to use these M(A) values for further processsing and computation, since they were obtained without taking into account the changes in the attenuation of the pulses in the process of creep and accumulation of defects.

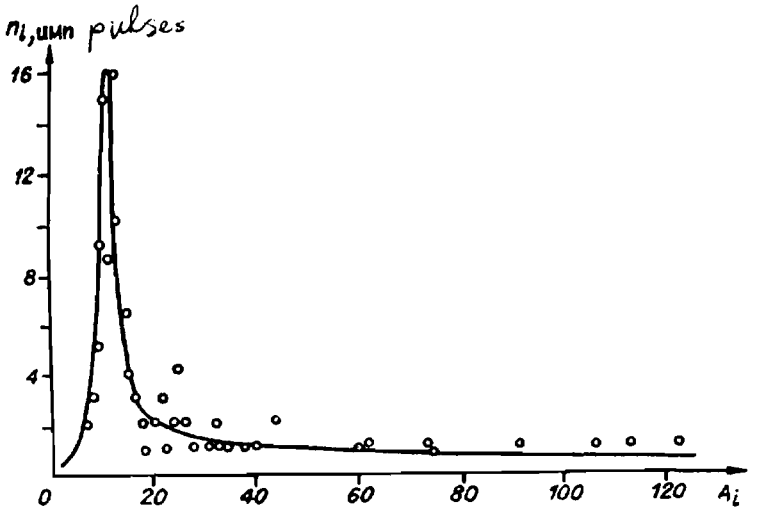

Fig. 3.8

Amplitude distribution of acoustic pulses

***

V.V.Bogorodskii et al. have shown in their work (1971) that the loss of acoustic energy in the structure of polycrystalline ice is due to a number of factors and mechanisms. Moreover, theoretical analysis of the attenuation of elastic vibrations in a real solid is extremely complicated and the attenuation must therefore be estimated experimentally.

A special test was performed to obtain the attenuation coefficient of pulses under conditions of our experiments. The technique employed in that test was the same as in all the creep tests (see section 3.1) except for the fact that an emitter-piezoelectric transducer was mounted in the upper platen of the uniaxial compression apparatus. In the course of the test constant-amplitude pulses were transmitted to that transducer from the G5-15 generator with a frequency of 10Hz, and the amplitude of the pulses which passed through the specimen, was recorded from the lower transducer with the help of the oscillograph.

TABLE 3.1

The values of the attenuation coefficient for the pulse count intervals

N, 1/cm³ *	K_s	N, 1/cm³	K_s	N, 1/cm³	K_s
0—0,05	1,0	5,10—6,20	1,8	13,80—15,05	2,6
0,05—0,35	1,1	6,20—7,07	1,9	15,05—16,38	2,7
0,35—0,62	1,2	7,07—8,06	2,0	16,38—17,85	2,8
0,82—1,55	1,3	8,06—9,12	2,1	17,85—19,50	2,9
1,55—2,40	1,4	9,12—10,20	2,2	19,50—21,50	3,0
2,40—3,30	1,5	10,20—11,38	2,3	21,50—23,88	3,1
3,30—4,20	1,6	11,38—12,58	2,4	23,88—26,75	3,2
4,20—5,10	1,7	12,58—13.00	2,5		

*· cm^3.

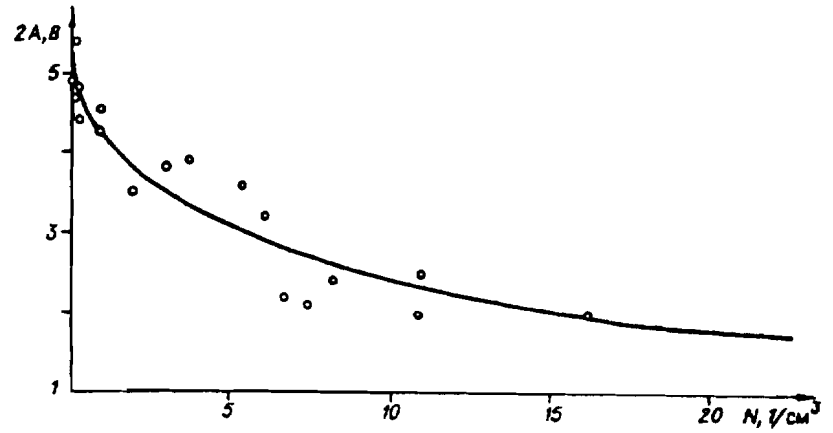

Fig. 3.9

The amplitude of the signals passing through the specimen as a function of the number of microcracks

***

The dependence of the amplitude of the pulses that traversed the specimen on the test time and deformation was derived from the results of the test. However, it was impossible to determine in that test the number of cracks at different stages of creep, which appears to be precisely the quantity controlling the attenuation of elastic vibrations in ice with a given initial structure and at a constant temperature. The information on the number of cracks was taken from the results of the creep test with recording of acoustic emission that was run at the same temperature and load as the experiment described above. It should be noted that

a) the creep curves $\varepsilon = f(t)$ for the two experiments were

practically coincident, and b) it has been established experimentally that in such cases the acoustic emission intensity curves also coincide.

Fig.3.9 shows the changes in the amplitude of the acoustic oscillations traversing the specimen with the accumulation of microcracks in it. The envelope curve is plotted through the experimental points according to the method of least squares. The attenuation coefficient K_3 is determined for any value of N by dividing the initial ordinate (at N=0) by the corresponding running ordinate (table 3.1).

The final expectation value of the amplitude of the acoustic emission pulse was determined by multiplying the M(A) value obtained earlier by the attenuation coefficient calculated for the same N as M(A).

CHAPTER 4

ACCUMULATION OF STRUCTURAL DEFECTS IN ICE DURING SHORT-TIME CREEP

4.1. Results of structural-petrographic analyses

Visual observations on the state of the specimens in the process of creep show that at the initial stages of deformation under load, while the ice is still transparent, the cracks in the specimen are clearly observable as surfaces reflecting light. It has been established that each microcrack formed (and observed) corresponds to an acoustic emission pulse recorded. Sometimes it is even possible to hear the crackling accompanying the formation of a crack.

It has been noted that all the isolated cracks observed were in the first approximation in the form of markedly stretched rectangles; moreover, the direction of the long side of the rectangles invariably coincided with the long direction of the columnar crystals. The fact that the predominant direction of the cracks persisted even at later stages of deformation (when visual observations were no longer possible because the specimen grew cloudy on account of the multitude of cracks therein) was corroborated by the fact that the transverse expansion of the specimens during uniaxial compression developed unevenly, practically only in the direction perpendicular to the long axes of the crystals, and that no expansion of the specimen occurred in the long direction of the crystals.

The unilateral expansion of columnar-grained ice specimens was also noted earlier [Gold, 1966; Frederking, 1972;

Zaretskii et al., 1975]. In the same works it was observed that cracks propagated parallel to the long axes of the crystals. When the transverse expansion of the specimens in the direction perpendicular to their crystal axes was restrained, the strength of the specimens increased significantly, but when the deformation along the crystal axes was constrained, it remained virtually unchanged [Frederking, 1972].

Having observed the transformation of the cross-section of the specimen from circular to ellipsoid, Yu.K.Zaretskii et al. (1975) concluded that microcracks formed predominantly (or even exclusively) at crystal boundaries. Moreover, it was assumed that the crystals themselves remained practically unchanged.

The investigations by L.Gold (1972), K.F.Voitkovskii, V.N. Golubev (1972) and our own experiments have shown, however, that in the process of deformation of ice there develop intercrystalline (crystal-boundary) cracks, as well as intracrystalline cracks and that the size and shape of the crystals undergo significant changes.

Detailed crystallo-optic observations on the microstructure of thin sections cut from specimens deformed to varying degrees have shown that in the process of creep under failure loads there develop in ice all the types of structural transformations: those designated earlier as "plastic", as well as "brittle" ones. The main structural phenomena are described here in brief for the different stages of deformation at which they were observed.

As was mentioned earlier, the tests were carried out at the following loads: at $\theta = -4°C$ $\sigma = 11.4 \cdot 10^5$ Pa; at $\theta = -8.5°C$ $\sigma = 16.3 \cdot 10^5$ Pa; and at $\theta = -13°C$ $\sigma = 20 \cdot 10^5$ Pa. Each series corresponding to a given temperature (and load) consisted of six tests in which the maximum axial deformation amounted to 1, 2, 4, 6, 8 and 10%.

Deformation 0.01. Regular, virtually undisturbed structure was observed at all the three temperatures in the a and c planes. Small notches in crystal faces, minor cleavages in isolated crystals, and sparse short cracks confined mainly to crystal faces and stretched in the long direction of the grains were observed. Weakly developed slip zones in a number of crystals and incipient fragmentation at the contact of several crystals were also observed.

Deformation 0.02. The characteristic feature at $\theta = -4°C$ was the presence of minor structural disturbances, such as undulate and clearer (thicker) faces of crystals, short sparse cracks, here and there recrystallization with incipient fragmentation along the serrated faces of crystals, and nucleation of crystals. At lower temperatures the structural disturbances developed to a somewhat greater degree. Slip zones within the crystals, twinning and dislocation blocks occurred on a larger scale. There evolved chains of vesicular cracks and microcavities, as well as isolated zones of fragmentation composed of small crystals. Many cracks were parallel to or gently inclined towards the faces of the crystals.

Deformation 0.04. In plane a at θ=-4°C most of the crystal faces were finely undulate or serrated and displayed clearer zones. There were observed series of brittle cleavages without significant displacement of parts of the crystals, but with a change in orientation. Isolated loci of fine (up to 1.2mm) fragmentation were particularly clearly observable against the general background in the central part of the rectangular crystals perpendicular to their long axes. Slip zones in isolated crystals and flexure zones of recrystallization were confined to the same loci of thin sections. A portion of the section consisted of equisize isometric idiomorphic crystals, sometimes with finely undulate faces and clearer areas in them, but more often with microcrystals along the faces. Only one of the crystals displayed in its face a fairly large step-like fracture forming variously coloured rectangular blocks. Slip zones were developed throughout the section area, particularly in the aforementioned crystal and in the crystals adjacent to it. In the other half of the section the deformations were localized.

At θ=-8.5°C there appeared distinctive features against the general background of the structural disturbances characteristic of θ=-4°C. First of all the slip and crush zones were less well defined over the area of the section. Secondly there appeared cigar-shaped cavities (measuring 1 to 10mm). These cavities were parallel to one another, but perpendicular to the long sides of the rectangular sections. In some cases these voids cut

across several crystals, but in others they ran along the faces of the crystals or occurred within the crystals.

At θ=-13°C the structural disturbances were more intensively and more extensively developed than at any of the other temperatures. Sloping planes of fragmentation blocks conjugated with slip or twinning zones were observed. Warping and serration, fine cracks and microcrystals predominated along some of the faces near the crush zones. There formed locales with lath-like crystals.

The features characteristic of plane c at the three temperatures were complete dynamometamorphism of some of the single columnar crystals and stability of others. Alongside extreme degrees of deformation the sections contained crystals at different stages of dynamometamorphism. Small-scale fractures of crystal faces with the cracks running along the faces or bending at an angle to them, were a characteristic sight. The crack density and cracking pattern varied depending on the colour, i.e. on the orientation of the optic axes of the crystals.

At θ=-13°C there was practically no dynamometamorphism, although the crystals were broken up by a system of microcracks. The crystals were perceptibly displaced along transverse cracks. A characteristic feature was fragmentation along some of the faces and at the wedging-out edges. Development of blocks within the crystals predominated. A closely spaced system of cracks was observed and it consisted of major cracks running

parallel to the crystal faces, and of subordinate (secondary) cracks perpendicular to them. Microcavities were also present.

Deformation 0.06. The structure observed in plane a at $\theta = -4°C$ was inequisize with lath-shaped elements in some parts of the section. Disturbances of the kind of strongly undulate or fractured crystal faces with interpenetration of the crystals, slip zones, twinning and formation of blocks were extensively developed throughout the section area. Isolated crush zones were present with area up to $1.5 cm^2$.

The lath-like structure was more extensively developed at $\theta = -8.4°C$ and $\theta = -13°C$ than at $\theta = -4°C$. As may be seen from plane c , fragmentation occurred at the boundaries of some large crystals, while others remained close to their initial form. In the specimen as a whole the zones of recrystallization expanded relative to the 1,2 and 4% deformations. Recrystallization occurred not only locally and along the faces of the relatively well-preserved crystals (as was the case in plane a), but began to spread all over some of the crystals or left their fragments intact. The zones of recrystallization attained 1cm in width. Their trend generally coincided with the orientation of the long axes of the crystals, which was due to the fact that the process developed only in some, i.e. in the most strongly stressed crystals. Fragmentation of these crystals relieved the stress, as a result of which the other crystals remained completely or partly unaffected by recrystallization.

Deformation 0.08. For plane a at the three temperatures there were observed nonuniformly distributed lath-like crystals. This feature was more pronounced at low temperatures. Extensively developed elongated cavities had an identical orientation perpendicular to the long sides of the rectangular sections, but were distributed nonuniformly over the section area. The cavities were located on the crystal faces and occurred mainly in the crush zones or in the loci adjoining these zones. Slip zones, less often block formation, twinning and vesicular cracks were widely developed in the crystals.

In plane c the zones of recrystallization continued to expand and in some of the crystals they attained 2cm in width. A characteristic feature was the presence of a system of cracks composed of microvesicles and/or microcavities, which in some cases broke up the columnar crystals into a semblance of rectangular blocks, but in others cut across 2-3 crystals. Elongated cavities oriented for the most part parallel to the long axes of the crystals, were present.

At $\theta = -13^{\circ}C$ there were fewer voids in plane c and they were mainly drop-shaped. Chains of vesicles (vesicular cracks) and strings of microcavities were randomly oriented.

Summing up the evidence pertaining to the 8% stage of deformation, it can be stated that intensive dynamometamorphism and fragmentation processes continued in the ice and that formation of cavities became the leading process among the brittle deformations. Lath-like crystals developed most prominently at low temperatures ($-8.5^{\circ}C$ and $-13^{\circ}C$).

Deformation 0.1. The feature characteristic of plane a was a lath-like texture that was relatively uniform in character throughout the specimen. Some of the crystals were still fairly large, which was compensated by extremely intensive fragmentation in isolated zones and loci. At this stage of deformation there were observed all the forms of dynamometamorphism, but it was obvious that the leading processes were recrystallization and fragmentation. At $\theta = -8.5°C$ the specimen displayed an interstitial lath texture. The grains persisted in part, but were bordered to a greater or lesser degree by laths of small fragmented crystals. The large grains were relatively isometric, equisize, subhedral or panidiomorphic. In some of the grains the slip zones were linear changing partly to cleavages. Serrated crystal faces were here particularly clearly observable. In other cases there was observed formation of blocks, i.e. fractured rectangular lines within the crystals, constituent parts of which did not alter their orientation. Oval cavities (0.1 × 2-5mm) were present.

At $\theta = -13°C$ there was observed a nonuniformly disturbed lath texture, where the crushed zones (the laths) framing the large crystals, were composed of microcrystals that were much smaller than those observed at $\theta = -8.5$ or $\theta = -4°C$.

Otherwise the disturbances were the same: fractures of crystal faces, slip zones, block formation with uneven attenuation, vesicular cracks, and cavities measuring up to 5 × 10mm. Plane c exhibits no radical changes relative to deformation 0.08. The maximum stage of deformation in the

experimental studies performed was thus marked by a continued development of all the types of disturbances, but progressive processes of recrystallization and fragmentation, crack formation and development of cavities became here particularly important.

As was mentioned earlier, it was visually observed that deformation and crack formation were distributed nonuniformly throughout the specimen. Examination of individual thin sections revealed the same lack of uniformity: alongside the zones of deep recrystallization and fragmentation there occurred isolated crystals or groups of crystals affected but little by the processes of dynamometamorphism, with their size and internal structure virtually intact. This was probably due to the fact that the crystals were variously oriented relative to the direction of the effective stress and progressing deformation and resisted failure in different ways owing to the mechanical anisotropy of ice single crystals in different crystallographic directions.

Deformations appeared to develop nonuniformly at different points of polycrystalline ice specimens on account of the local redistribution of stresses induced by the anisotropy of the ice crystals. The deformation affected first of all the least stable crystals and zones in the specimen. These were small grains at the junctions of three or four large crystals, and wedge-shaped zones of orthotropically growing crystals in the form of stretched triangles with slender, fairly unstable ends.

Deformation began in these loci with migration of crystal faces. It was observed in the tabular specimens, tested with the help of a special device directly under a microscope according to the method of V.I.Solomatin [Solomatin et al., 1978], that at this stage the faces of small crystals became distorted and displaced. Moreover, these crystal faces acquired an undulate shape and their microdisplacements (fractions of a millimetre) occurred at a perceptible velocity. These processes resulted in degradation of the small crystals and in growth of the large neighbouring crystals. This was followed by the development of serration in the faces of the large crystals near their contact with the small crystals undergoing degradation. The serration of crystal faces was a consequence of the motion of dislocations in the crystal lattices at these loci. In the course of this dislocation motion, there occurred polygonization processes with formation of microfragments acting as nuclei, from which new crystal developed.

The glide zones that appear in large crystals during the next stage, and the twinning of these crystals develop from the faces at which the polygonization and recrystallization occur. These processes occur on basal planes and may therefore differ in direction even in neighbouring crystals.

Once a certain level of strain has been reached, the deformation enters the region associated with rupture, and the intracrystalline translational movements and twinning give way to brittle processes of dislocation induced crack formation.

Studies by M.V. Klassen-Nekhlyudova (1960) on metals have shown that during deformation there appears a so-called substructure in the structure of single crystals and polycrystalline aggregates, i.e. a microblock structure. The crystal lattice is rearranged into a multitude of micro units. This process precedes directly the formation of cracks.

It should be stressed once again that in polycrystalline ice, owing to the anisotropy of ice crystals, the deviations in their orientation from a strictly ordered pattern lead to a parallel development of various brittle and plastic processes in diversely oriented crystals. This also contributes to the overlapping of the regions in which they occur.

From structural-petrographic observations there may be distinguished cracks forming subparallel to the faces (as a rule these cracks occur before all the other fractures), and intra- or transcrystalline cracks cutting across the faces. Within the crystal there also form echelon-like fractures. Having attained a certain density, the cracks produce a "macroblock" structure, and independent development of these blocks, i.e. their degradation or growth and changes in their orientation, determine the development of this stage of dynamometamorphism.

These are the most general patterns of the development of dynamometamorphic processes under the conditions of our

experiment. The main outcome of these processes is the decrease in the size of the averaged crystal in the specimen. The modification of the petrographic structure in the range of 0 to 0.1 strain is generally the same for all the temperatures and loads. Moreover, the development of the lath texture has been observed in all the cases. In other words plastic and brittle recrystallization processes begin at the crystal faces and gradually spread into the inner parts of the crystals. This feature of the process also accounts for the change of the cross-section of the specimen from circular to ellipsoid with the long axis of the ellipsoid oriented transversely to the long axes of the crystals.

At the same time there have also been observed temperature- and load-related differences in the structural modifications. Whereas high temperatures and relatively smaller loads are favourable for the formation of fairly wide crushed zones with large zones of recrystallization, with large fragmented blocks and individual grains, at low temperatures and great stresses there form narrower crushed zones of recrystallization, with submicroscopic crystalline individual grains. In this case the other parts of the crystals are considerably less affected by both plastic and brittle deformation.

The degree of dynamometamorphism of the ice structure in the process of creep was quantitatively assessed on the basis

of the grain count from thin sections according to the method described in section 3.2. The range of scatter of the experimental data on account of the initial structural heterogeneity of the ice specimens and the nonuniform fragmentation of these specimens throughout their bulk, as well as because of errors in the calculations and measurements of structural elements from microphotographs of thin sections, is shown by vertical lines in fig. 4.1. The average curves were plotted through the experimental points using the method of least squares. The points marked by "x" in the graphical plots were subsequently used for calculating the volume and the surface of the averaged crystal at different stages of deformation.

The graphical plots in fig. 4.1 illustrate the process of fragmentation of the crystals as observed in thin sections, which is particularly intensive in plane c. The trend towards the stabilization of that process is also distinctly observable: the size of the crystals tends towards a constant minimum value. Moreover, that minimum value decreases somewhat with decreasing temperature.

K.F. Voitkovskii and V.N. Golubev (1972) investigated for a large range of loads the changes occurring in the process of deformation in the structure of finely crystalline ice ($V<1$ mm^3) with randomly oriented optic crystal axes. As a result of these studies it has been established that for an effective stress exceeding a definite value characteristic

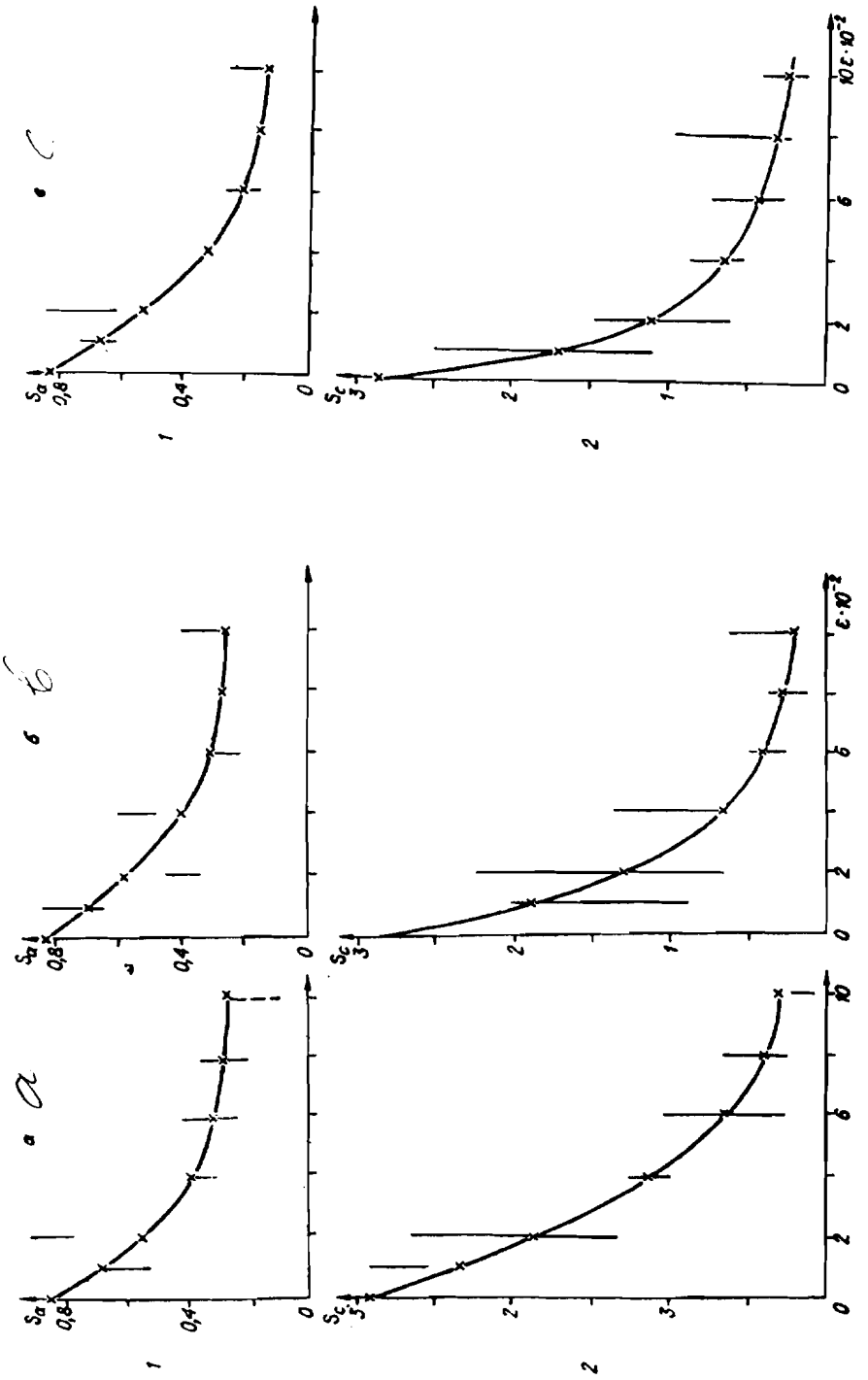

Fig. 4.1

The average area of crystals in thin sections as a function of deformation

a---θ=-4°C; σ=11.4·10^{5}Pa; b---θ=-8.5°C; σ=16.3·10^{5}Pa;

c---θ=-13°C; σ=20·10^{5}Pa; 1-for the sections in plane a;

2-for the sections in plane c

***

of the given type of ice, the recrystallization is unidirectional in character: i.e. fragmentation of the crystals begins immediately after the application of the load and attenuates with increasing deformation. These authors have also shown that at stresses below that level, i.e. stresses inducing only transient or steady-state creep, over time of tens or hundreds of hours, there can be distinguished two other recrystallization states: crystal growth and structural stabilization.

Of course in our experiments these two stages were not identified, since the stresses used in our tests were much greater than the required stress level and induced in all the cases tertiary creep that lasted from several minutes to several hours.

4.2. Results of acoustic emission studies

By continuously recording acoustic emission in the process of creep the number of acoustic emission pulses N (per 1 cm^3 of the volume of the specimen) can be determined as a function of time t(c) for all the loads and temperatures. The graphical plots showing that dependence (fig. 4.2) resemble creep curves except for the transient creep region.

A similar type of dependence N(t) on time was obtained by L. Gold from the records of acoustic emission obtained with the help of a piezoelectric crystal [Gold, 1960] and from the visual count of cracks in the specimen [Gold, 1972b], as well as by A.M. Fish [Zaretskii et al., 1975].

It follows from equation (2.17) that the experimental data for each temperature should lie along a series of lines in the coordinates $\ln N \div 3\sqrt{t}$. In fig.4.3 the experimental data are plotted in these coordinates. The points were taken from the graphical plots in fig.4.2 and the value of t(c) was determined for a number of selected values of N.

As may be seen from fig.4.3, the points fit well to the lines $\ln N_t = \ln N_o + \text{tga } 3\sqrt{t}$; moreover, the point on the Y-axis acting as a sort of a pole at which all the straight lines converge, corresponds to the value of $\ln N_o$, where N_o is the number of the crystal lattice defects at time t=0 acting as "nuclei" of future cracks.

According to equation (2.17), the gradient of each of the straight lines in fig.4.3 should be equal to $\text{tg } a = \bar{\kappa}(T)\left(\frac{\sigma}{\sigma_\infty} - 1\right)$, which is verified by plotting these gradients against the load. Fig.4.4 shows data for all the loads at the three temperatures investigated. As may be seen from that plot, the dependence of the gradient (tga) on stress σ for each temperature is well approximated by a straight line.

It was established that when these straight lines were extrapolated in the direction of decreasing σ, they crossed the X-axis at the point corresponding, according to equation (2.17), to the long-time creep limit σ_∞.

We used equation (2.17) to process the data obtained by L.Gold (1972b) from the visual count of cracks per cross-sectional unit area (crack density) of a columnar-grained ice specimen for a large range of temperatures and stresses. From this it was established that his results also

became linear in both $\ln N \div 3\sqrt{t}$ (fig.4.5) and tg a-σ coordinates (fig.4.6) and that σ_∞ was also close to $5 \cdot 10^5$Pa for all the temperatures.

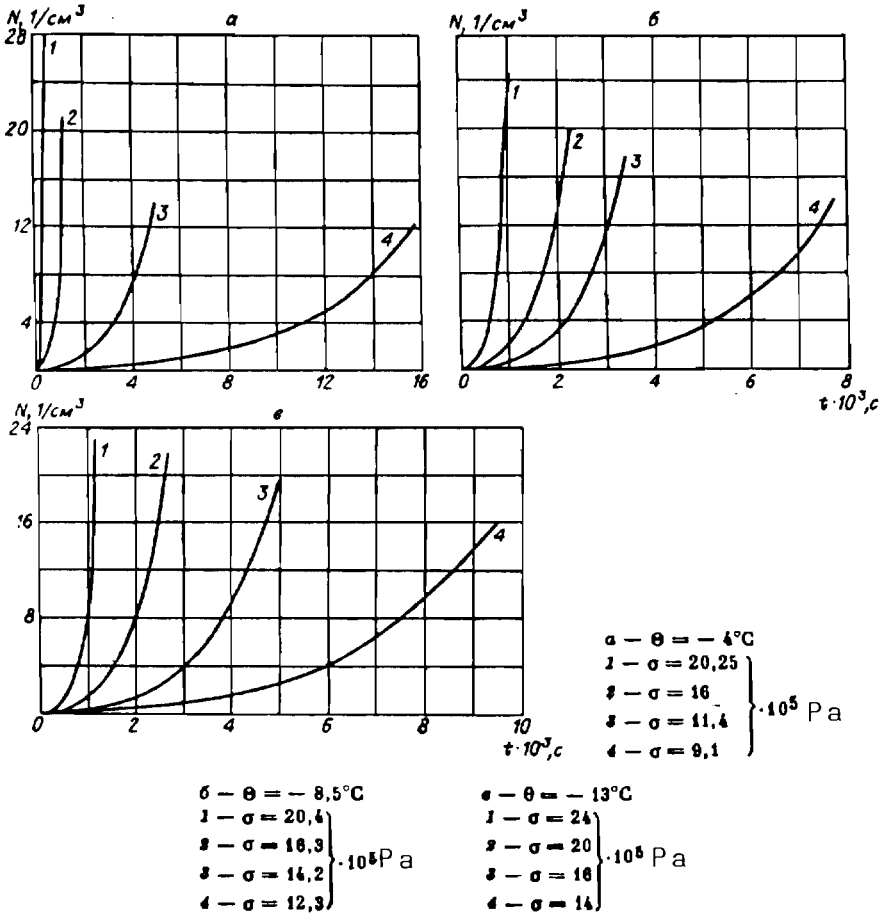

Fig.4.2

Pulse count as a function of time

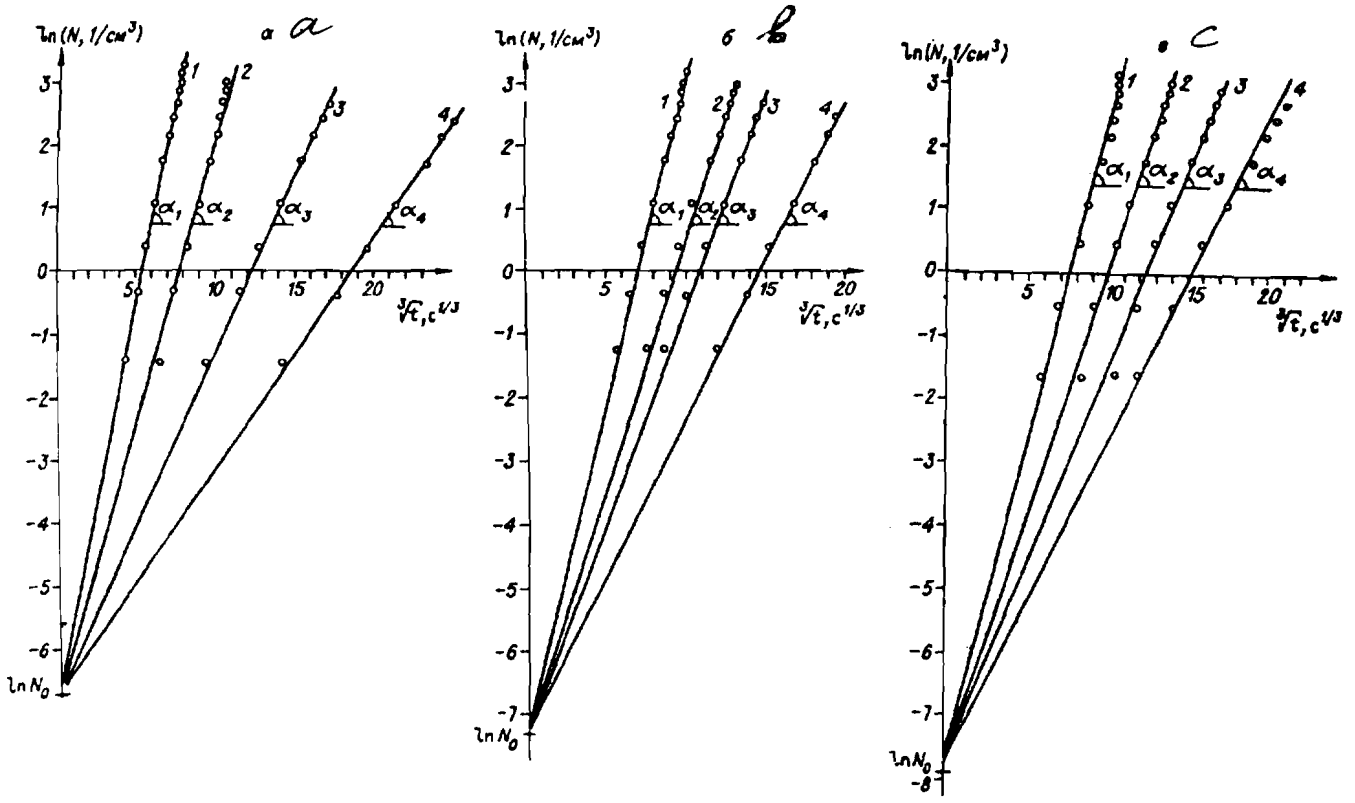

Fig. 4.3

Number of pulses as a function of time

[verification of equation (2.17)]

Same notation as in Fig. 4.2

Yu.K.Zaretskii et al.(1975) report results of their short-time creep tests on columnar-grained lake ice under uniaxial compression with simultaneous recording of acoustic emission at a temperature of -4°C and under various loads. Processing the data from these tests (fig. 4.7) shows that their results are also described by dependence (2.17). The deviation of one of the straight lines from the common pole appears to indicate that the initial state of that specimen differed somehow from that of the others. On the other hand the tangent of the angle of inclination of that line fits into the general dependence (4.4), which, as may be seen from the graphical plot, is in good agreement with our data for the same temperature. This coincidence can be easily explained, since the structure and size of the ice crystals were very close in the two cases.

It may thus be concluded from the experimental data that within the temperature range investigated the creep limit σ_∞ is independent of temperature and is a constant for ice with given initial structure.

Long-time creep limit of ice σ_∞ was defined earlier as the stress above which the flow rate of ice will increase steadily eventually leading to its failure. It is now becoming clear that it is the stress at which the probability of formation of a defect becomes equal to the probability of its healing, i.e. that σ_∞ has the meaning of the stress above which progressive accumulation of structural defects occurs. This is supported by the experiments of L.Gold mentioned earlier [Gold, 1960, 1966, 1972a and b] in which the cracking activity

and acoustic pulses were absent at stresses below a certain level. That level evidently corresponds to the creep limit σ_∞.

In one of his works (1972a) L.Gold uses the following expression corresponding to the Griffith criterion, for determining the minimum stress required for a crack to form as a result of the pileup of dislocations:

$$\tau_e = \sqrt{\frac{\pi\gamma E}{4(1-\nu^2)l}}, \qquad (4.1)$$

where τ_e is the effective stress, l is the length of the crack, E is Young's modulus, v is Poisson's ratio, and γ is the surface energy of the ice.

Assuming that the minimum crack length is equal to the average ice-grain diameter, L.Gold obtained $\tau_e = 4.9 \cdot 10^5$ Pa in accordance with equation (4.1). The magnitude τ_e corresponds in meaning to the creep limit σ_∞ regarded as the minimum stress initiating brittle disturbances and tertiary creep. It may thus be seen that the numerical value of σ_∞ obtained by L.Gold for an ice with a similar structure is very close to the value presented above.

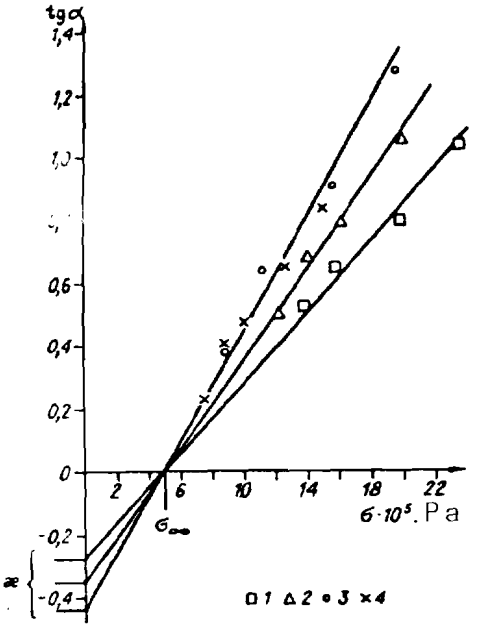

Fig.4.4

Gradient tg a as a function of stress

1 - θ=-13°C; 2 -θ=-8.5°C; 3 - θ=-4°C; 4 - θ=-4°C; (according to the data of A.M.Fish [Zaretskii, Fish et al., 1975])

Expression (4.1) can be used to explain why σ_∞ does not depend on temperature. As is well known [Bogorodskii et al., 1971], Poisson's ratio for ice is virtually independent of temperature and Young's modulus increases linearly with decreasing temperature for both single crystals and polycrystalline ice, which should cause σ_∞ to rise. The change in Young's modulus within the temperature range investigated (-4°C to -13°C) is, however, small. For example, according to the data of V.V.Bogorodskii [Bogorodskii et al., 1971], the increment of E within that range is 8% or less, and according to the data of M.I.Serikov (1959), it does not exceed 2%. I.G. Petrov (1976) generally believes that "no general dependence of the modulus of elasticity on temperature...has been found".

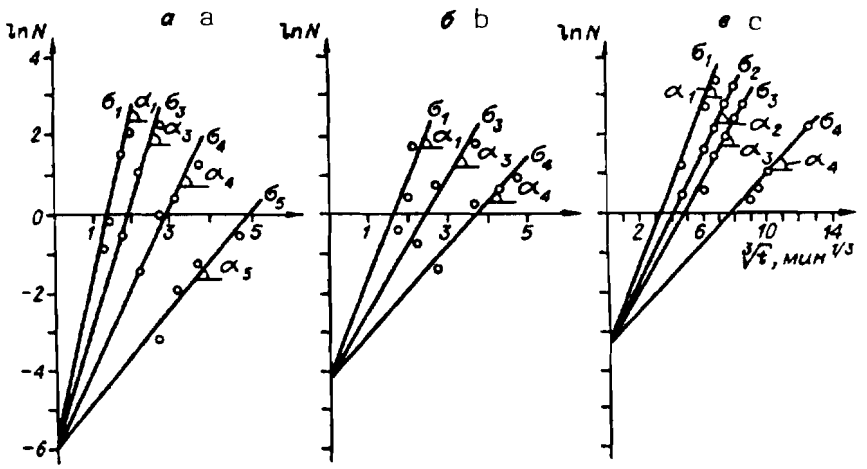

Fig. 4.5

Number of microcracks as a function of time [according to the data of L.Gold (1972b)]

a $\alpha - \theta = -4{,}8$°C
b $\delta - \theta = -9{,}5$°C
c $\varepsilon - \theta = -31$°C

$\sigma_1 = 20$
$\sigma_2 = 18$
$\sigma_3 = 16$
$\sigma_4 = 12$
$\sigma_5 = 8$
$\cdot 10^5$ Pa

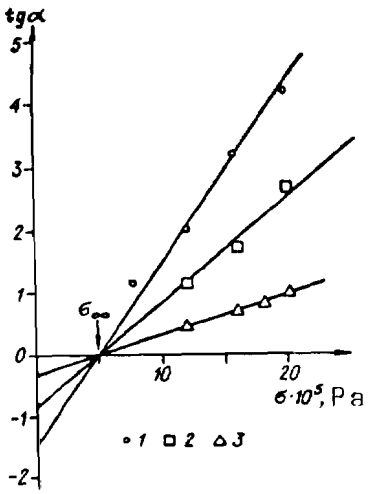

Fig. 4.6

Gradient as a function of stress (according to the data of L.Gold [Gold, 1972b])
1 - θ=-4.8°C; 2 - θ=-9.5°C; 3 - θ=-31°C.

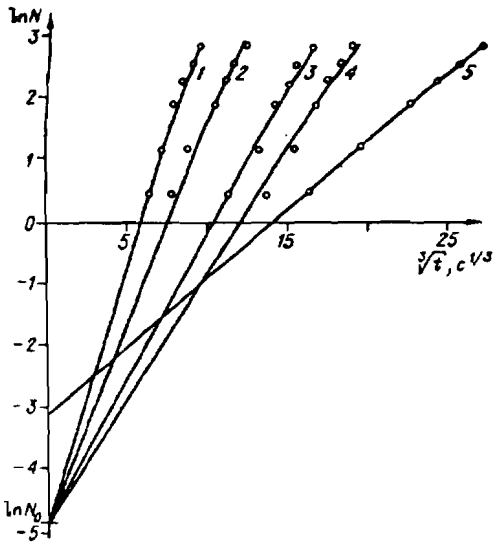

Fig. 4.7

Number of pulses as a function of time [verification of equation (2.17) on the basis of A.M.Fish's data (Zaretskii, Fish et al.,1975] at σ equal to: 1---15.3kG/cm^2; 2---12.75; 3---10.2; 4---8.9; 5---7.65 kG/cm^2. θ=-4°C.

***

***

As concerns the magnitude of the surface energy of ice, according to the measurements of Ketcham and Hobbs (1969) its temperature gradient is 0.1-0.35erg/cm^2 X degrees, which corresponds to a 1-3% variation of γ at temperatures ranging from -4°C to -13°C.

If we take into account that in (4.1) both E and γ appear under the square root sign, the effect of their change on the value of σ_∞ will decrease further and probably won't exceed the maximum scatter of the experimental data.

The segments intercepted by the straight lines in fig.4.4 on the Y-axis are the values of the function $\bar{\kappa}(T)$ for the corresponding temperatures θ ($\theta^\circ C = 273 - T^\circ K$). The linearity of the function $\bar{\kappa}(T)$ assumed by us for (2.17), is corroborated within the temperature range examined by the graphical plot in fig.4.8, from which it follows that

$$\bar{\kappa}(T) = 0.273 + 0.017(T-260),\ s^{-1/3} \qquad (4.2)$$

We shall treat the deformation of ice as a thermally activated process that initiates the development of structural defects on account of the activation energy imparted to them, as was done in S.S.Vyalov's work (1976). The initial number of structural defects N_0, i.e. the number of the elements activated initially, is then assumed to be subject to Boltzmann's distribution law

$$N_0 = C \cdot \exp\left(-\frac{U_0}{RT}\right), \qquad (4.3)$$

where C is a constant, U_0 is the creep activation energy, cal/mole, R is the universal gas constant (2cal/mole·dg.), and T is the absolute temperature, $^\circ K$.

The activation energy U_0 can be determined for ice on the basis of (4.3) by using the values of $\ln N_0$ derived from fig.4.3a for $\theta = -4^\circ$, those from fig.4.3b for $\theta = -8.5^\circ$, and those from fig.4.3c for $\theta = -13^\circ C$. The values of $\ln N_0$ are plotted (fig.4.9)

as a function of the reciprocal value of the absolute temperature 1/T. The gradient of the line obtained is equal to U_o/R, whence $U_o \approx 17.5$ kcal/mole.

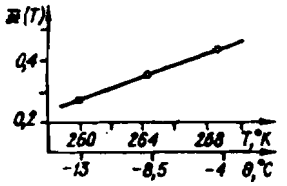

Fig. 4.8

Verification of the linearity of the function $\bar{K}(T)$.

***

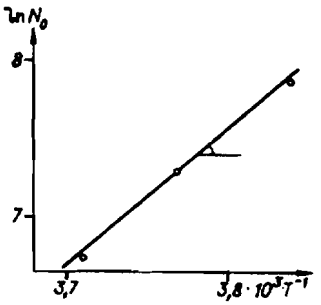

Fig. 4.9

Determination of the activation energy (negative logarithms of N_o).

***

For the purpose of verification the activation energy of ice is determined directly from the results of the creep tests. We shall proceed from a well-known proposition applied by many investigators [Vyalov et al., 1976]. That proposition postulates that the "secondary" creep rate or, in the absence of the steady-state creep segment, the minimum creep rate is described by the equation based on the Frenkel-Eyring molecular-kinetic theory

$$\dot{\varepsilon}^* = F \cdot \exp\left(-\frac{U_o}{RT}\right), \qquad (4.4)$$

where F is a certain function of stress and of the initial structure of ice.

It follows from equation (4.4) that once the rates $\dot{\varepsilon}^*$ are determined at two temperatures for the same ice and at identical stresses, the activation energy can be found from the expression

$$U_0 = \ln \frac{\dot{\varepsilon}_1^*}{\dot{\varepsilon}_2^*} \cdot \frac{R}{(1/T_2) - (1/T_1)}. \tag{4.5}$$

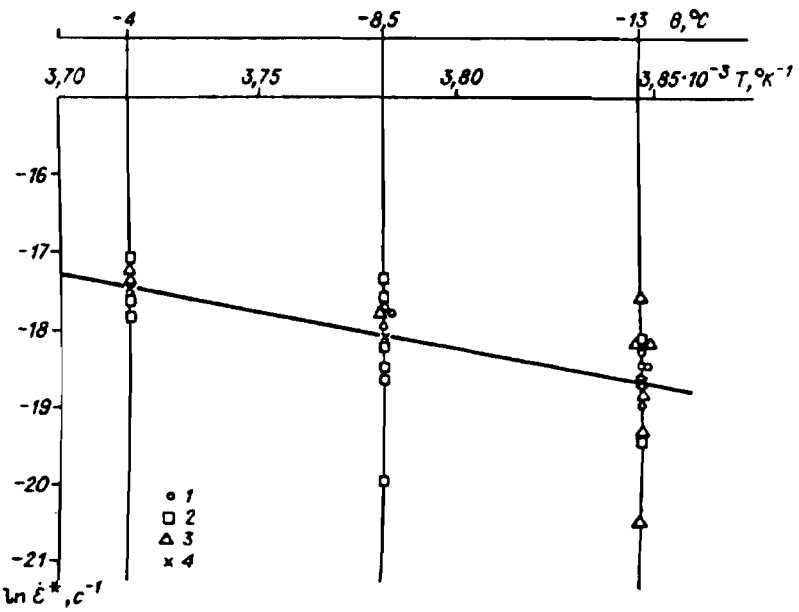

Fig. 4.10

The minimum creep rate as a function of temperature (determination of activation energy)

1--- σ=14
2--- σ=16 $\cdot 10^5$Pa
3--- σ=20
4---average for all the σ

***

To determine the minimum creep rate the initial segments (up to 15 minutes) of the experimental creep curves were plotted on a large scale. A segment uniting 3-4 points that fitted into a straight line, was sought for each of the plots. If all the points preceding these points in time were below that line and all the subsequent points were above it, then the tangent of its angle of inclination to the time axis was precisely the value of the minimum creep rate obtained in the given test.

The values of $\dot{\varepsilon}^*$ for the parallel tests vary rather widely, sometimes by more than an order of magnitude. In some of the tests it was necessary to determine two or even three rates instead of one, while in others it was generally impossible to find $\dot{\varepsilon}^*$, since creep for these underwent a brief stabilization, during which $\dot{\varepsilon}^*=0$ and expression (4.5) lost its meaning.

When the experimental points were plotted in a graph with coordinates $\ln \dot{\varepsilon}^* \div \frac{1}{T}$, it became clear that the dependence on the load cannot be determined from these data (see fig.4.10); the values of $\ln \dot{\varepsilon}^*$ for each temperature were therefore averaged for all the loads and the values obtained were as follows:

at $\Theta = -4°C$ $\quad \ln \dot{\varepsilon}^* = -17{,}422;$
at $\Theta = -8{,}5°C$ $\quad \ln \dot{\varepsilon}^* = -18{,}08;$
at $\Theta = -13°C$ $\quad \ln \dot{\varepsilon}^* = -18{,}618.$

The average values listed above readily fit into a straight line (fig.4.10), which gives a value for the activation energy U_o=18.5 kcal/mole that is fairly close to the value determined from the count of initial defects.

TABLE 4.1

Creep activation energy of polycrystalline ice

U_o, kcal/mole	Type of ice* and kind of test	References
14.3(G)	T_1; σ=const., small stresses	Butkovich and Landauer, 1960
11.4	T_1; σ=const., small stresses	Dillon H. and Andersland U., 1967
19.9-28.4	T_1; σ=const., great stresses	Same as above
32.3(G)	T_1; $\dot{\varepsilon}$=const., great stresses	Glen, 1955
16.1(G)	T_1; σ=const.	Jellinek and Brill**, 1956
14.1(G)	T_1	Jellinek, 1962
12.0(G)	S_1; σ=const., small stresses	Bromer** and Kingeri**, 1968
16.1(G)	S_2; $\dot{\varepsilon}$=const	Muguruma, 1969
21.0(G)	S_2; σ=const., $-5 > \theta > -15$°C	Gold, 1972a
10.7-17.8	T_1; σ=const., small stresses	Mellor and Smith, 1967
14.3(W)	S_2; σ=const., $\dot{\varepsilon}$=const.	Ramseier** and Dikins, 1972
14.3(W)	T_1; σ=const., $\dot{\varepsilon}$=const.	Same as above
18.6(W)	σ=const.	Barnes, Tabor and Walker, 1971
20(W)	σ=const.	Steinemann, 1958
12(W)	Friction	Bowden and Tabor, 1964
16.4(W)	T_1; σ=const.	Mellor and Testa, 1969
15.5(W)	S_2; σ=const.	Gold, 1973

* The type of ice according to the genetic classification of Michel and Ramseier [Gold, 1972b]: T_1-ice prepared from snow and water(snow ice); random orientation of optic crystal axes; S_1- columnar-grained ice, optic axes perpendicular to the long direction of the crystals, and randomly oriented in the horizontal plane; (G)-after Gold (1972b); (W)- after Weertman (1973).

** Transliteration. Translator.

Table 4.1 also shows data on the activation energies obtained by different researchers from creep tests for polycrystalline ice. As may be seen from the table, these data are in good agreement with our results.

4.3. Evaluation of the size of microcracks and its relation to structural changes

The amplitude of a single acoustic pulse recorded in the process of ice deformation characterizes the energy dissipated in the form of oscillations during the formation of a single defect. At constant stress and temperature this energy is probably determined only by the size of the cracks. Consequently the amplitude of the acoustic signal is proportional to the area of the new surface arising as a result of the formation of a microcrack.

V.A.Greshnikov and Yu.B.Drobot (1976) have demonstrated that if the microrupture (microfracture) formed in a material is regarded as an approximation of a spherical cavity on the surface of which the stresses dynamically drop from the initial level to zero, then the amplitude of the acoustic emission signal is proportional to the square of the radius of that cavity, i.e. to its surface area.

Since crack formation is a stochastic process, the magnitude of the surface area of a single microcrack should be interpreted as the mathematical expectation of that magnitude $M(\Sigma)$.

In accordance with the method outlined in section 3.3, the experimentally determined correction for the absorption of the pulse by the previously formed cracks was applied to the observations for each test, depending on its duration. From this, there were obtained six to fifteen expected values of the acoustic pulse amplitude M(A). Since that magnitude was obtained in conventional units, it will be identified with the mathematical expectation of the surface of a microcrack $M(\Sigma)$ assuming that, all the other conditions being equal, the amplitude of the acoustic pulse is determined only by the surface area of the defect generating that pulse.

As may be seen from the results of the experiments, the statistical mean of the surface area of a single microcrack $M(\Sigma)$ increases in the course of each test with increasing strain and increasing number of microfractures. Appropriately constructed plots show that the load and the temperature are independent variables in the dependence of $M(\Sigma)$ on the test time, which greatly complicates the processing of experimental data. The dependence of $M(\Sigma)$ on strain proved to be the same for all the stresses and temperatures, but had a nonlinear character, while the dependence of the magnitude of $M(\Sigma)$ on the number of accumulated defects $(N-N_0)$ was the same for all the stresses and temperatures investigated and was described by extremely simple relations (fig. 4.11).

$$\left.\begin{aligned} M(\Sigma) &= 0 && \text{at } N = N_0, \\ M(\Sigma) &= M(\Sigma_0) + B(N - N_0) && \text{at } N > N_0, \end{aligned}\right\} \tag{4.6}$$

where B is the proportionality factor, $M(\Sigma_0)$ is the mathematical expectation of the surface area of a single crack formed in ice under applied load $\sigma=\sigma_\infty$.

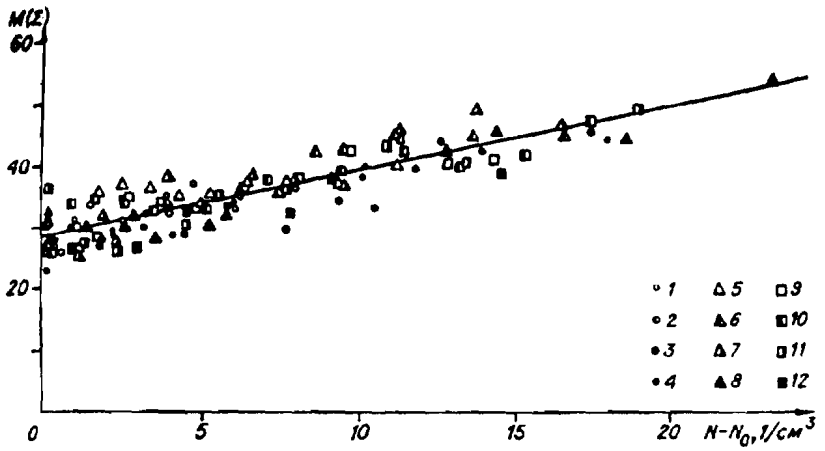

Fig. 4.11

Statistical mean of the size of a defect as a function of the number of defects

θ = −4°C	θ = −8,5°C	θ = −13°C
1 — σ = 9,1	5 — σ = 12,3	9 — σ = 14
2 — σ = 11,4	6 — σ = 14,2	10 — σ = 16
3 — σ = 16	7 — σ = 16,3	11 — σ = 20
4 — σ = 20,25	8 — σ = 20,4	12 — σ = 24
·10⁵Pa	·10⁵Pa	·10⁵Pa

***

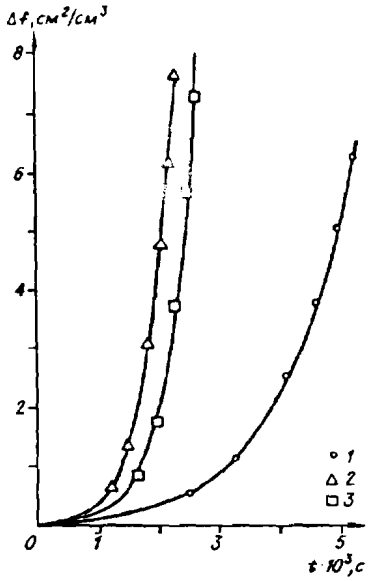

Fig. 4.12

Growth of the new surface of crystals in time during creep

1 - θ=-4°C; σ=11.4·10⁵Pa;
2 - θ=-8.5°C; σ=16.3·10⁵Pa;
3 - θ=-13°C; σ=20·10⁵Pa.

***

The dependence of the size of microcracks on their number presented above was derived from analyses of a vast amount of experimental evidence, taking into account the attenuation of the sonic disturbances in ice. That dependence shows that at $\sigma > \sigma_\infty$ the rate of growth of the total surface of microdefects increases in time in a manner similar to the rate of tertiary creep (fig. 4.12). Our earlier conclusion [Zaretskii et al., 1979a] that for a given rate of formation the new surface is constant, was drawn from a preliminary analysis of the amplitudes of acoustic pulses which did not take into account the attenuation of the acoustic emissions in ice.

The methods and results of the structural-petrographic studies on structural changes in ice specimens at different stages of deformation are discussed in sections 3.2 and 4.1. The range of scatter of the experimental data and the approximating curves reflecting the dependence of the area of the crystals in thin sections on the amount of deformation are plotted in fig.4.1. Averaged volumes of the crystals for all the stages of deformation were calculated from the values of $S(cm^2)$ derived from these curves, proceeding from the assumption that ice crystals have the form of regular tetrahedral prisms. The reciprocal of the calculated value of the volumes represent the specific number of crystals (per unit volume of the specimen -d, $(1/cm^3)$). The increment in that amount Δd, from which the initial value (for the initial structure of ice) is subtracted, characterizes the degree of shattering (fragmentation) of the crystals in the process of creep and microfracturing.

The experiments in which the kinetics of crack formation is determined with the help of acoustic emission records, allow us to find the number of pulses N for a given amount of strain at corresponding values of temperature $\theta(^{o}C)$ and stress σ. The dependence of the number of pulses N on the specific number of crystals Δd can be easily plotted on the basis of these data (fig. 4.13a). As may be seen from the graphical plots, the dependence $N(\Delta d)$ is described by the same curve for all the temperatures and stresses investigated.

Another important parameter characterizing the structural changes in ice resulting from the accumulation of defects during creep, is the specific surface of the crystals (per unit volume of the specimen $f(cm^2/cm^3)$). The quantity $\underline{f}$ or rather $\Delta f = f - f_o$ is the newly formed surface (where f_o is the surface of the crystals in the initial structure of ice prior to deformation) resulting directly from the action of brittle deformation mechanisms, since each fracture or void formed leads to the formation of a new surface. From this viewpoint it is interesting to examine the dependence of the two parameters, both of which are related to brittle structural modifications in ice: the number of acoustic pulses and the total area of the new surface Δf (fig.4.13b). As may be seen from the graphical plots, the dependence $N(\Delta f)$ is also common for all the stresses and temperatures.

The results of the structural-petrographic analyses thus support the conclusion drawn earlier (4.6) on the basis of acoustic measurements that the surface area of a single defect

is directly proportional to the number of these defects, since the plot in fig. 4.13b shows that the surface of a single defect is equal to the total surface formed in the process of microfracturing divided by the number of the defects developed during that time.

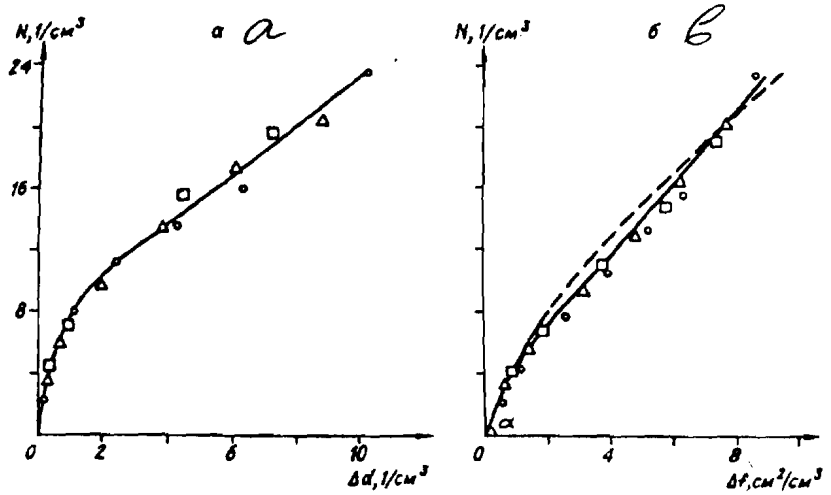

Fig. 4.13

The dependence between the number of pulses N and structural parameters; a - the number of crystals and b - the surface of the crystals. Same notation as in fig. 4.12

***

The dependences $N(\Delta d)$ and $N(\Delta f)$ (see fig. 4.13) are nonlinear in their initial segments, but become directly proportional with the growth of the arguments. Strictly speaking it follows from the dependences $M(\Sigma)=\frac{\Delta f}{N}$ and $M(\Sigma)=M(\Sigma_0)+BN$ that $\Delta f=M(\Sigma_0)\cdot N+BN^2$, which means that the plot $N(\Delta f)$ is nonlinear throughout its extension. Calculations show, however, that within the actual range of variations of the argument (dashed line in fig. 4.13b) the nonlinearity is

rather small and that for $N>5cm^{-3}$ the experimental points are well approximated by a straight line. The tangents of the angles of inclination of the resultant straight lines to the X-axis correspond to the constant rate of accumulation of acoustic pulses, i.e. to the minimum number of pulses required for a new crystal (fig. 4.13a) or a new unit surface (fig. 4.13b) to form. In other words the number of the pulses generated during the formation of a new crystal or of a new unit surface initially decreases, but with the development of the deformation it tends towards some constant value independent of the degree of further deformation. Moreover, that value is equally independent of the temperature of ice and of the effective stress (at least within a certain range of their variations).

The size of the smallest possible defect $M(\Sigma_0)$ can be defined as the minimum surface increment rate during the formation of a single defect (see fig. 4.13b). The cotangent of the largest angle of inclination of the curve to the X-axis characterizes the minimum surface of a single defect. Assuming that the initial segment of the plot is linear, we find $M(\Sigma_0) = 0.2$ cm. The coefficient B in equation (4.6) varies proportionally to the changes of $M(\Sigma_0)$ during the transition from conventional to dimensional units.

4.4 The process of microfracturing during creep of ice

Unstressed ice, like any real crystalline solid, contains a certain initial number of crystal lattice defects which act as "nuclei" of future cracks. The number of these initial defects was designated earlier by N_0. A single

crystal contains point defects or linear pileups of dislocations in their crystal lattice, and polycrystalline solids have defects associated with grain faces in addition to the above.

In a solid under applied load the defects are the sites of stress concentrations and simultaneously the weak points of the crystal lattice. Therefore these are precisely the locations where the stress exceeds the ultimate strength and where the structural continuity of the material becomes disrupted by the formation of a crack. The fracture runs across the weakest section, i.e. in the direction of the next closest defect, which arrests its further development for a certain time until a new stress concentration arises that is sufficient to cause further growth of the crack. The fracture thus develops in stages, with interruptions, which is consistent with visual observations on cracks during creep. The developing fracture generates new acoustic pulses when it passes in stages through the intracrystalline defects, as well as when it crosses crystal boundaries.

Our experiments show that at the initial stages of deformation there develop predominantly intracrystalline cracks. Their number is relatively small, as is also the number of crystal boundaries. Therefore at the initial stage of creep the cracks formed "engulf" (absorb) the initial defects. Moreover, the number of defects per unit volume decreases (since one single defect, i.e. crack, replaces two defects present initially). Therefore the

number of the pulses generated during the formation of a new unit surface or of a new crystal, also declines, which explains the damped character of the initial segments of the curves in fig. 4.13.

Moreover, this process is not entirely straightforward. The development of the cracks leads to the fragmentation of the crystals, i.e. to an increase in the number of the faces which themselves are defects. Transcrystalline cracks cutting across the crystal faces, increase in number, as a result of which the number of the pulses also rises. The effective stress may also induce new dislocations of the crystal lattice. The number of defects per unit volume of the specimen thus increases causing the number of the pulses generated within that volume also to rise.

Eventually the two opposite processes balance each other, attaining a dynamic equilibrium in the specimen: the number of the defects "absorbed" by the cracks is compensated by the newly formed defects so that their number per unit of the new surface (or new crystal) remains roughly constant, as is evident from the constant angle of inclination in fig. 4.13.

In addition to the accumulation of cracks the process of creep appears to be accompanied by the opposite phenomenon, i.e. by their healing. The probability of the latter is always nonzero, but healing of the existing defects appears to play a significant role only under stresses that are smaller than the creep limit. This is supported by the data from the experiments of V.I.Solomatin et al. (1979) in which direct observations were carried out on the structure of ice in the process of creep.

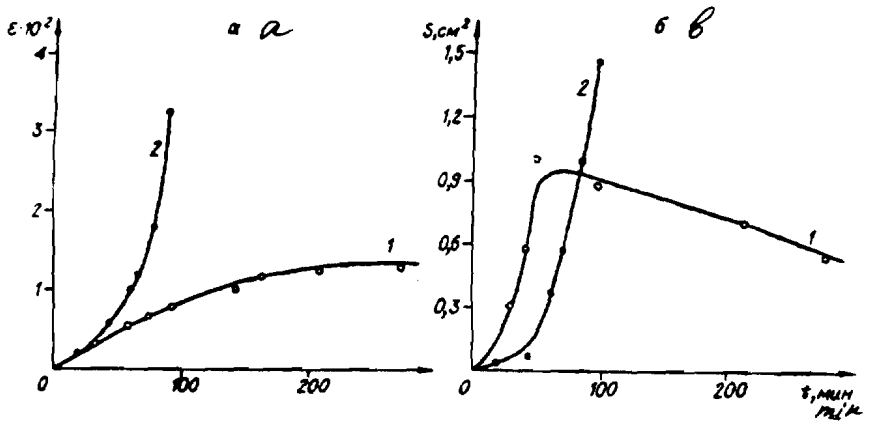

Fig. 4.14

Data from direct observations on the structure of ice during creep

a - creep curves; b - development of the total area of cracks.

1 ---σ=6.4 X 10^5Pa; ϑ=-1.8°C; 2 ---σ=10.2·10^5Pa; ϑ=-4.2°C.

***

Tabular ice specimens were subjected to uniaxial compression under a constant load and, using a microscope, the development of disturbances in the crystals were simultaneously observed and photographed. Fig. 4.14 shows results of two tests in which creep strains were recorded and the total area of the cracks was calculated from the photographs taken at different times during the tests.

As may be seen from the graphical plots in Fig. 4.14, in the test the creep curve of which has a damped character, cracks accumulated during the initial stage with the largest creep rate. This may be explained by the presence of local overstresses in the crystals owing to the differences in their orientation relative to the action of the load. Later, as the internal stresses were evened out, the growth

of the crack surface went through a maximum and began to decrease. Moreover, the authors noted that some of the cracks became almost completely annihilated (healed).

In test 2 (curve 2, fig. 4.14) during tertiary creep the cracks steadily increased in number and size, which suggests that in this case plastic mechanisms of dynamometamorphism had no opportunity to manifest themselves and played a subordinate role.

CHAPTER 5

CREEP AND FAILURE OF ICE UNDER STATIC AND CYCLIC LOADS

5.1. Deformation and microfracturing

Let us examine the relationship between the macroprocess of deformation of ice under load and the micro-events of the formation and development of structural defects in that ice.

L.Gold has demonstrated experimentally [Gold, 1966, 1972a and b] that short-time creep strain of ice ε is closely related to the number of brittle structural disturbances N. The dependence of the total strain on the number of structural defects has been experimentally established for soils (earth materials) by Yu.K.Zaretskii (1970, 1973), Yu.K. Zaretskii and S.S.Vyalov (1971) and experimentally confirned by S.S.Vyalov et al. (1973) for soils and by Yu.K.Zaretskii, A.M.Fish et al. (1975) for ice. K.F.Voitkovskii and V.N. Golubev (1972), who carried out crystallo-optic studies on the structure of ice during creep, established that at $\sigma > \sigma_\infty$ there is a functional relationship between the volume of the ice crystals and the magnitude of the short-time creep strain. On the other hand there is a functional relation between the volume and surface area of the crystals forming during tertiary creep, and the number of the acoustic pulses generated in the specimen during that process (see chapter 4).

These facts suggest (see chapter 2) that at $\sigma > \sigma_\infty$ the plastic volume strain of ice is proportional to the total surface formed in the process of microfracturing (2.31).

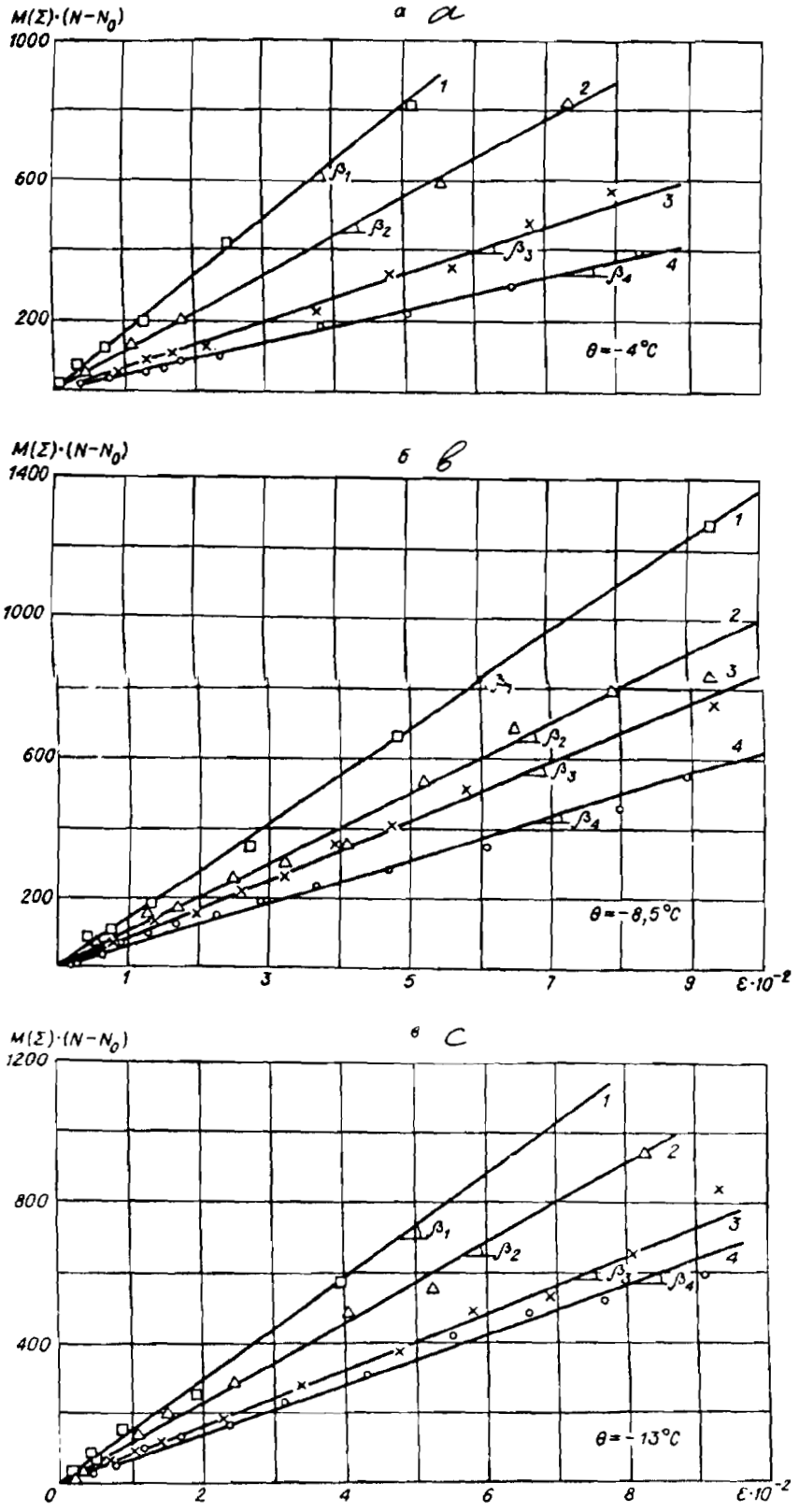

Fig. 5.1

Total surface of the defects as a function of strain (same notation for curves 1-4 as for a-c in fig. 4.2)

***

It has already been demonstrated (section 4.3) that the newly formed surface Δf is equal to the product of the number of the defects (i.e. cracks) formed $N=N_o$ and of the statistical mean of the surface of a single brittle disturbance $M(\Sigma)$. This suggests that the experiments should focus on the relationship between the kinetics of accumulation of brittle structural defects and their size on the one hand, and volume strain on the other. However, it is practically impossible to measure volume strain in uniaxial compression tests because of the strong distortion of the initially cylindrical specimens in the process of creep. It is therefore advisable to proceed instead with the axial plastic strain by using relation (2.30). It follows from that relation that the axial strain-rate $\dot{\varepsilon}_1^{(p)}$ is proportional to the volume strain-rate $\dot{\varepsilon}_v^{(p)}$. Moreover, at a constant temperature the proportionality factor corresponding to the expression enclosed in square brackets in equation (2.30) depends only on creep time. The empirical parameters κ^*, $\kappa(T)$ and $\psi(t)$ determined from the tests, permit us to work out the relationship between the axial and volume strain-rates at any time, enabling us to substitute in equation (2.31) the axial plastic strain ε for the volume plastic strain.

It is thus assumed that the strain of ice

$$\varepsilon = q\, M(\Sigma) \cdot (N-N_o), \tag{5.1}$$

where q is the proportionality factor.

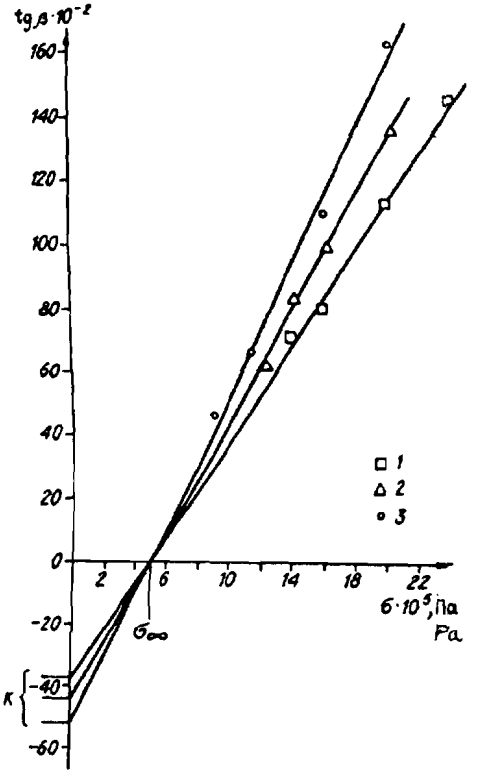

Fig. 5.2

The slope $tg\beta(cm^{-1})$ as a function of the stress σ (Pa). Same notation as in fig. 4.4

The magnitude $M(\Sigma)$ is determined from the records of acoustic emission during creep in conventional units as the mathematical expectation of the acoustic pulse amplitude, and from the results of crystallo-optic measurements in dimensional units.

To verify the validity of equation (5.1), all the experimental data are plotted in graphs with coordinates $M(\Sigma)\cdot(N-N_o) \div \varepsilon$ (figs 5.1a, b and c). It can be easily seen that for each temperature the plot consists of a series of straight lines corresponding to equation (5.1), and that the slope of these lines $tg\beta$ is a function of the effective stress σ. To determine the shape of that function, all the data for all the stresses and temperatures investigated are plotted on a graph with coordinates $tg\beta - \sigma$ (fig. 5.2).

It can be seen that the three tgβ (σ) lines corresponding to different temperatures, cross at the same point on the X-axis and that the segment intercepted by them on the σ-axis and equal to $\sigma_\infty = 5.10^5$Pa, coincides in value with that of σ_∞ derived by the analysis of the data on the number of acoustic pulses according to equation (2.17). In other words by estimating the statistical mean of the size of a brittle defect we were able to obtain by independent means the same creep limit σ_∞ and to confirm that it is invariant relative to temperature within the range investigated.

It follows from the graphical plot in fig. 5.2 that q in equation (5.1) is described by the expression

$$\frac{1}{q} = tg\beta = K(T)\left(\frac{\sigma}{\sigma_\infty} - 1\right), \qquad (5.2)$$

where K(T) is a function of the absolute temperature T, °K.

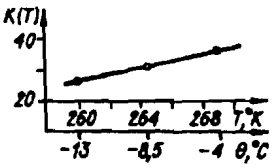

Fig. 5.3

Verification of linearity of the K(T) function

***

The segments intercepted by the straight lines on the Y-axis represent the values of the K(T) function for the corresponding temperatures. Within the temperature range

examined the function K(T) is linear (fig. 5.3) and is given by the equation

$$K(T)=26.5 + 1.156\ (T-260)\ cm^{-1}. \qquad (5.3)$$

Additional verification of whether the total surface of the defects is directly proportional to the creep strain at $\sigma > \sigma_\infty$, can be carried out on the basis of the data obtained from crystallo-optic studies on the magnitude of the increment in the new surface Δf resulting from the fragmentation of the crystals. Indeed, the points plotted in the coordinates $\Delta f - \varepsilon$ are well approximated by straight lines (fig. 5.4a). For the sake of comparison three plots from fig. 5.1 constructed for the same stresses and temperatures, are inserted in fig. 5.4b. The similarity of the results obtained by acoustic and crystallo-optic methods is obvious.

Having confirmed the validity of the experimental equation (5.1), and by taking into account equations (2.17) and (5.2), it is possible to write a general equation for the strain of ice during short-time creep ($\sigma > \sigma_\infty$) under uniaxial compression and isothermal conditions:

$$\varepsilon = \frac{M(\Sigma_0) + B(N-N_0)}{K(T)\left(\frac{\sigma}{\sigma_\infty} - 1\right)} \cdot (N-N_0), \qquad (5.4)$$

where $N-N_0=N_0\left\{\exp\left[\bar{K}(T)\left(\frac{\sigma}{\sigma_\infty} - 1\right)\cdot 3\sqrt{t}\right]-1\right\}$.

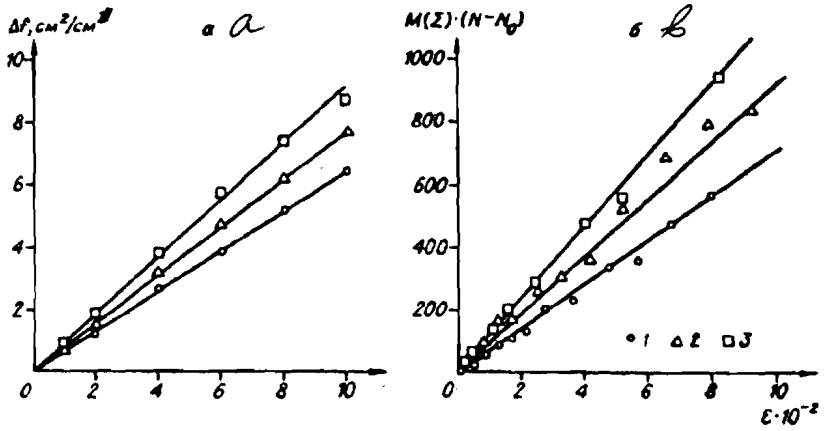

Fig. 5.4

Dependence of the new surface of the crystals (a) and of the total surface of the defects (b) on strain. Same notation as in fig. 4.12

***

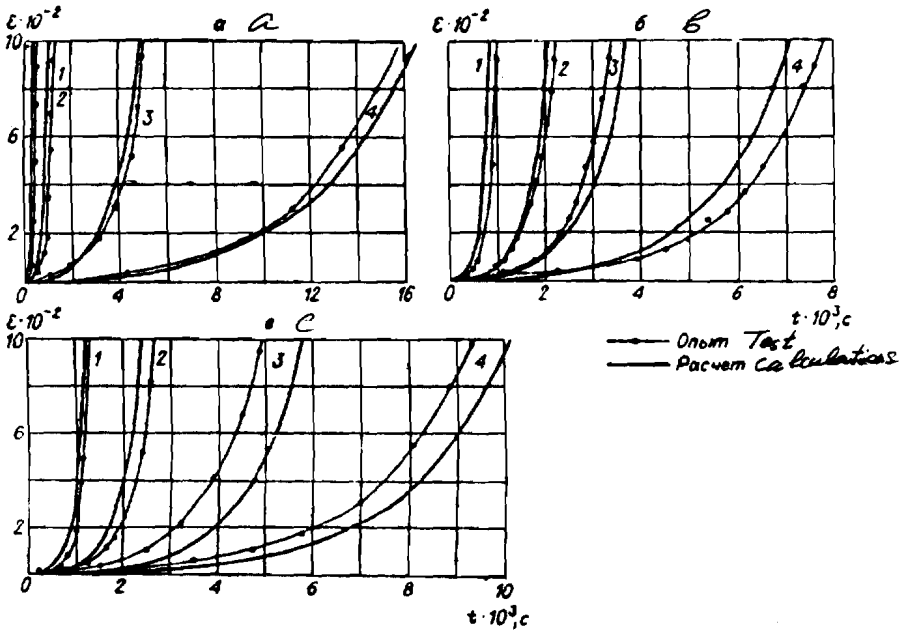

Fig. 5.5

Development of strain in time (creep curve). Same notation as in fig. 4.2

***

The notations, dimensionality and experimentally determined numerical values of the parameters, functions and constants forming part of equation (5.4), are as follows: ε and $\dot{\varepsilon}$, s^{-1}, are the axial strain and strain-rate; N, cm^{-3} is the number of the brittle defects forming in the crystal structure of ice during creep and recorded in the form of acoustic emission pulses; N_o, cm^{-3}, is the initial number of the defects ("nuclei") present in the given ice at the given temperature prior to the application of the load ($InN_o = 25.765 - 8769/T$); σ, Pa, is the effective stress; σ_∞, Pa, is the creep limit of the ice, i.e. the stress characteristic of the given ice, below which there develop only plastic deformations at a decreasing or constant rate, but above which the deformations are of a progressive nature and there accumulate brittle defects leading to failure ($\sigma_\infty \approx 5 \times 10^5$Pa); $M(\Sigma_o)$, cm^2, is the mathematical expectation (statistical mean) of the surface area of the minimum brittle defect forming in ice under the applied stress $\sigma \to \sigma_\infty$ [$M(\Sigma_o) \approx$ $\approx 0.2cm^2$)]; t, sec, is the time; B, cm^5, is the proportionality factor ($B=0.00754cm^5$); $K(T), cm^{-1} = 26.5+1.156\ (T-260)$; $\bar{\kappa}(T)$, $sec^{1/3} = 0.273+0.017\ (T-260)$; and T, °K, is the absolute temperature ($T \leq 273$).

Fig. 5.5 shows the creep curves obtained in our experiments for ice at all the temperatures and loads, and the calculated creep curves constructed on the basis of equation (5.4) with the values of σ and T equal to their experimental values. K(T), $\bar{\kappa}(T)$ and N_o were calculated by using the expressions provided for them earlier. Creep limit σ_∞ was assumed to be equal to $5 \cdot 10^5$Pa.

In assessing the discrepancies between the experimental and calculated creep curves it should be kept in mind that creep of ice is generally a process that is difficult to reproduce, as parallel experiments yield significant inconsistencies even if great care is taken to accurately reproduce conditions of the tests. Figure 5.6 shows, for example, creep curves for eight ice specimens tested at identical temperatures and loads. As may be seen from the graphical plot, the experimental curves have a large scatter. On the other hand the average behaviour is fairly well given by the curve plotted from the calculations according to equation (5.4). Given the significant variations in the creep curves, the agreement of the calculated curves with the experimental curves (see fig. 5.5) can be rated as good.

It should also be noted that in equation (5.4) the creep strain (ε) refers to "pure" creep of ice without the contribution of the initial conventionally instantaneous deformations. This explains why the experimental plots of the total strain are located in all the initial segments of the curves above the calculated plots. The same plots (see fig. 5.5) show, however, that the error resulting from the omission of the conventionally instantaneous strain amounts to only a small portion of the plastic creep strain developed in time.

Substituting into equation (5.4) the empirical constants and functions obtained, we can calculate the increase of

strain in time for any temperature and load, and the creep curve can be constructed the same way as during the verification of formula (5.4). However, calculations with the help of that formula are fairly cumbersome and laborious, in view of which there has been written a BESM*-6 computer program for calculating creep curves.

The use of a computer for calculations enabled us to obtain data not only on the number of the accumulated defects and on the magnitude of deformation in time for any specified load ($\sigma > \sigma_\infty$) and temperature, but also on the dependence of the strain-rate on time and number of defects, which is practically impossible by manual calculations. The program provides for computation of strain-rates by determining the gradient of the creep-time curve.

Calculated dependences of the strain-rate $\dot{\varepsilon}(\text{sec}^{-1})$ on the time, total strain and number of accumulated acoustic pulses are presented in figs. 5.7a, 5.8a and 5.9a for the same temperature, respectively, as an example. As may be seen from these plots, during the deformation of ice under the loads $\sigma > \sigma_\infty$ the so-called secondary, i.e. steady-state stage of creep is practically absent. The decrease in the creep rate goes through the minimum and is succeeded directly by an increase in that rate.

Rectilinear segments were also absent from the creep curves for the clay tests carried out by G.I.Ter-Stepanyan (1976), who

---

* Transliteration. Translator.

believes that "the notion of a rectilinear segment . . . is a result of the scale effect", i.e. is due to the excessively small scale on which the creep curves are plotted. This investigator distinguishes only two stages of creep: the phase of mobilization, i.e. transient creep, and the phase of failure, i.e. tertiary creep.

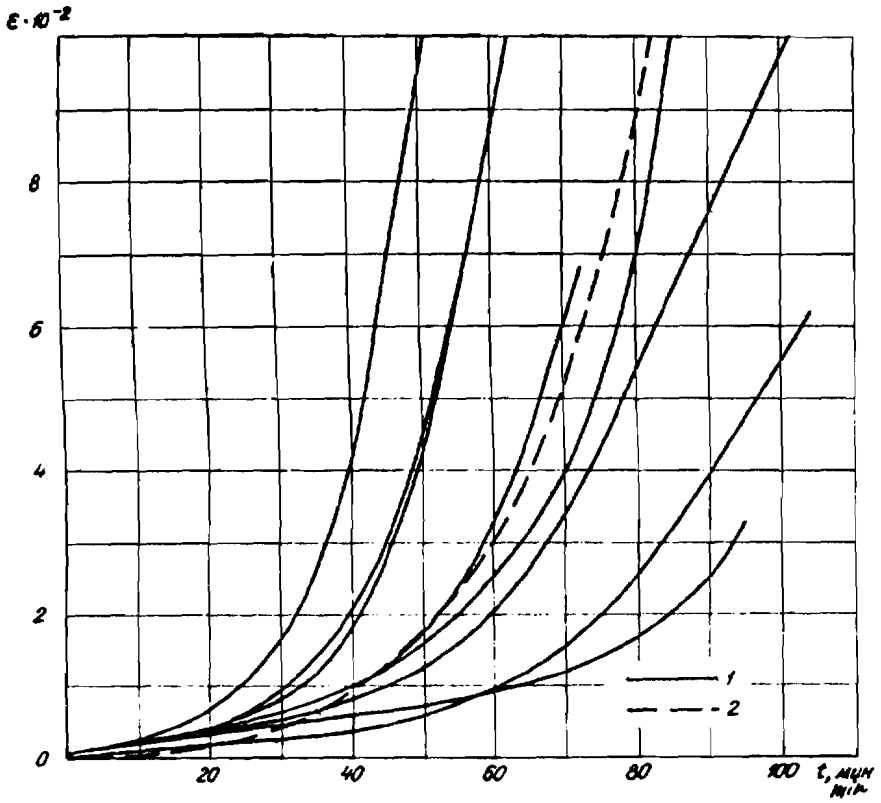

Fig. 5.6

Creep-rates in eight parallel tests

θ=-4°C; σ=11.4•10^{5}Pa. 1 - Experimental; 2 - Calculated from equation (5.4)

***

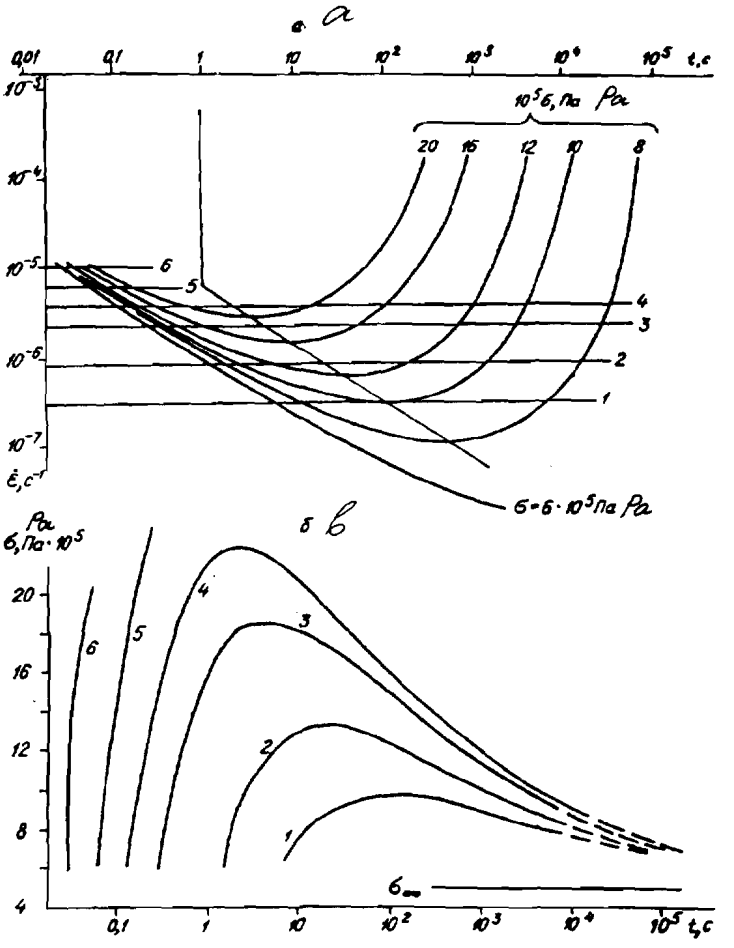

Fig. 5.7

Strain-rate variations (a) in time at σ =const, and stress variations (b) in time at $\dot{\varepsilon}$ =const(θ=-4°C). Strain-rate $\dot{\varepsilon}\,10^5$, sec^{-1}: 1 - 0.30; 2 - 0.83; 3 - 2.26; 4 - 3.73; 5 - 6.14; and 6 - 10.13

***

Examination of the minimum creep-rate values shows that at different loads the minimum rates are attained over different times and at different values of deformation (see figs 5.7a and 5.8a). On the other hand it follows from fig.5.9a that the minimum creep-rate coincides for all the loads with the same number of acoustic pulses. The same results have been obtained for other temperatures.

Selecting arbitrarily the creep-rate $\dot{\varepsilon}(sec^{-1})$ values and regarding them as constant, we can construct for each plot a a plot b reflecting the dependence of the stress σ on the appropriate parameters: time, strain or number of pulses (see figs. 5.7 to 5.9). All these dependences also have a point of inflection corresponding to the maximum stress; moreover, the stresses peak, as they did before, at a constant number of acoustic pulses.

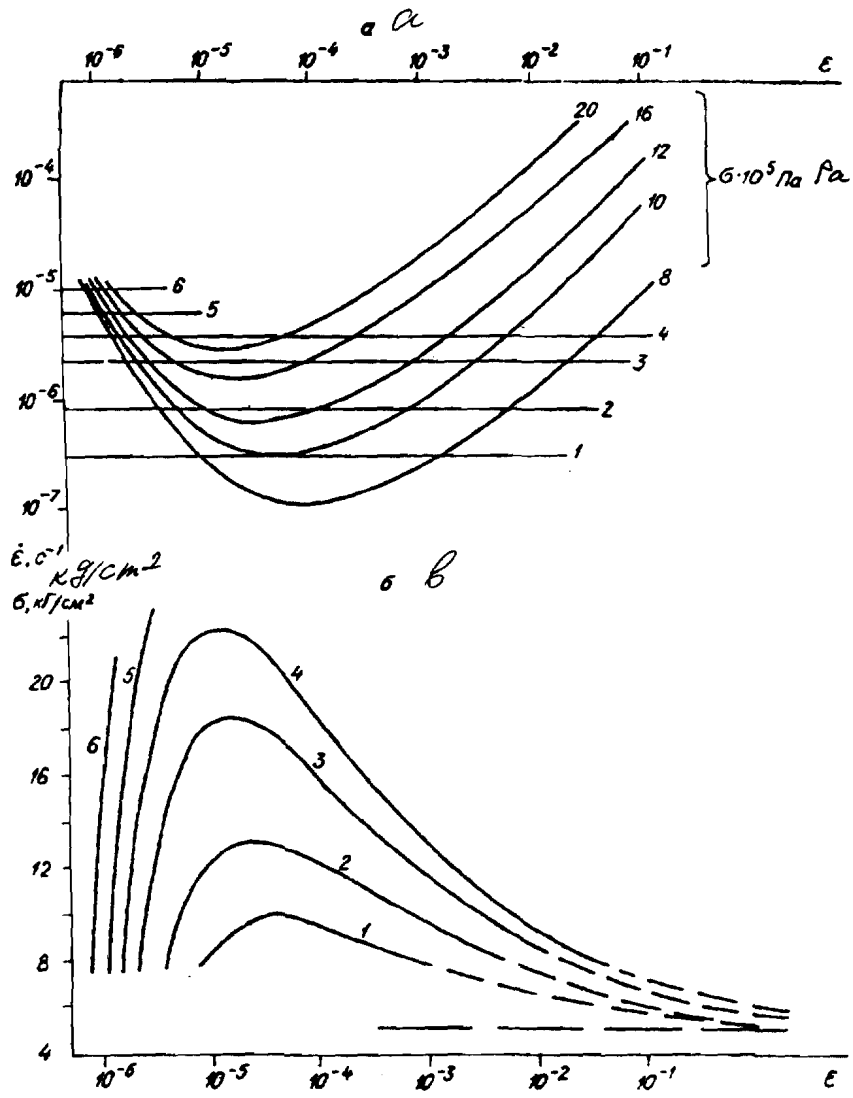

Fig. 5.8

Strain-rate as a function of deformation at σ=const (a) and load as a function of deformation (b) at $\dot{\varepsilon}$=const (θ=-4°C). Strain-rate $\dot{\varepsilon}\cdot 10^5$, sec^{-1}: 1 - 0.30; 2 - 0.83; 3 - 2.26; 4 - 3.73; 5 - 6.14; and 6 - 10.13

***

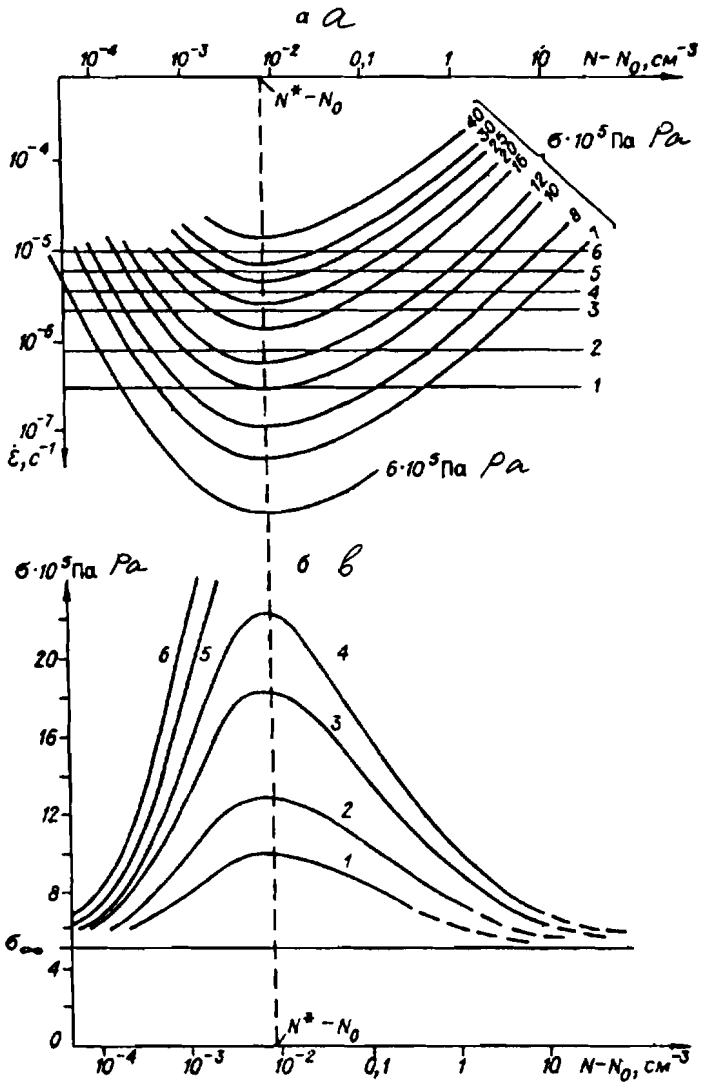

Fig. 5.9

Strain-rate as a function of the number of pulses (a) at σ=const, and stress as a function of the number of pulses (b) at $\dot{\varepsilon}$=const (θ=-4°C).

Strain-rate $\dot{\varepsilon} \cdot 10^5$, sec^{-1}: 1 - 0.30; 2 - 0.83; 3 - 2.26; 4 - 3.73; 5 - 6.14; and 6 - 10.13

***

For each temperature there is thus a certain "critical" number of defects, i.e. cracks, when the maximum stress is attained regardless of the strain-rate. This is obviously

the moment of the greatest danger for engineering structures interacting with ice, as well as for the structural continuity and stability of ice itself. In both cases recording of acoustic emission can be used as a means of monitoring the growth of stresses in ice as a method of predicting these stresses.

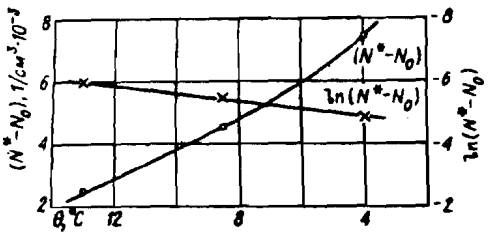

Fig. 5.10

The critical number of pulses as a function of temperature on the arithmetical and semilogarithmic scale (temperatures negative)

***

The dependence of the critical number of pulses on temperature (fig. 5.10) is nonlinear on the conventional scale, but on the semilog scale it becomes linear, i.e. is described by an exponential function.

Knowing the creep parameters for a given type of ice, it is thus possible to predict at the known stress level the magnitude and rate of deformation and the time to the transition of the ice to tertiary creep. On the other hand knowing the strain-rate of the ice interacting with an engineering structure, it is possible to predict the current and maximum stresses.

***

The results of the experiments performed can be used to verify the criterion of failure for ice during short-time creep adopted in chapter 2.

The very meaning of the term "short-time creep" implies that under any stress $\sigma > \sigma_\infty$ failure will inevitably occur at time t^{**}. Moreover, it is assumed (see section 2.2) that the limit strain ε^{**} corresponding to the maximum strain-rate $\dot{\varepsilon}^{**}$, increases with increasing failure time t^{**}, whereas the maximum number of structural defects N^{**} is a constant for ice with a given structure. The same conclusion can be drawn from the experiments of A.M.Fish [Zaretskii et al., 1975].

Since in our experiments the maximum axial deformation of the specimens was identical in all the tests (10%), the corresponding maximum number of defects decreases as the duration of the test increases (see fig.4.2). We shall therefore use an indirect method to check the criterion of long-time strength of ice.

It follows from (2.20a) that $t^{**}=\left[\frac{\kappa^{**}}{\kappa_0 T + \kappa_1} \cdot \frac{\sigma}{\sigma - \sigma_\infty}\right]^3$, and from (2.19a) that $\kappa^{**}=\frac{\ln N^{**} - \ln N_0}{\sigma_\infty}$. Then, keeping in mind the assumption that $\bar{\kappa}(T)=\sigma_\infty (\kappa_0 T + \kappa_i)$, we obtain

$$t^{**}=\left[\frac{\ln N^{**} - \ln N_0}{\bar{\kappa}(T)} \times \frac{\sigma_\infty}{\sigma - \sigma_\infty}\right]^3 . \qquad (5.5)$$

The time of failure t^{**} is determined in one of three ways.

1. As the time at which the creep curve has approached a certain angle to the vertical. This is done with the help of the graphical plots in fig. 5.7a, from which the values of t_1^{**} corresponding to the series of $\dot{\varepsilon}(t)$ curves for different stresses were taken at a selected value of the strain-rate $\dot{\varepsilon}$ (in this case $6 \cdot 10^{-2}$, sec^{-1}).

2. By extrapolating the curves showing the dependence of the number of pulses on the time (see fig. 4.2) to the selected value of N regarded as the maximum. This value of N^{**} is greater than any of its experimentally derived values (in this case it is assumed that $N^{**}=30 cm^{-3}$). The abscissae of the points of intersection of the extrapolation curves with the ordinate N=30 define the values of t_2^{**}.

3. Through calculations according to equation (5.5), in which all the values of the parameters have already been determined earlier and N^{**} is also assumed to be equal to $30 cm^{-3}$. In this manner t_3^{**} can be calculated for any stresses and temperatures.

The values of t^{**} obtained by means of the three techniques for a temperature of -4°C are shown in table 5.1.

The good coincidence of the results obtained confirms the applicability of the long-time strength (lengthy failure) criterion adopted for ice.

Table 5.1

$\sigma \cdot 10^5$, Pa	$t_1^{**} \cdot 10^5$, s	$t_2^{**} \cdot 10^5$, s	$t_3^{**} \cdot 10^5$, s
20,25		0,5	0,49
20	0,48		0,51
16	1,4	1,4	1,30
12	5,5		5,05
11,4		6,2	6,61
10	17		13,87
9,1		21,3	25,15

We shall additionally check condition (5.5) for the two tests in which a certain interval of creep was succeeded by brittle failure of the specimen. In the first of the two tests ($\theta=-8.5°C$; $\sigma=10.4 kG/cm^2$) the failure occurred 19.4 minutes after the beginning of the test; calculated $t^{**}=16.8$ minutes. In the second test ($\theta=-13°C$; $\sigma=24 kG/cm^3$) the failure occurred after 19.7 minutes; calculated $t^{**}=21.9$ minutes. In the first case the discrepancy between the experimental and calculated data was $\approx$ 15%, and in the second case it was $\approx$ 11%.

5.2. Vibrocreep and vibrostrength of ice

The development of deformations in time with the periodic variable component σ_a superposed on the constant average stress σ_m will be designated as vibrocreep.

A single change from the maximum value of stress (σ_{max}) to its minimum value (σ_{min}) and back (fig.5.11) during instant cyclic stressing is designated as the stress cycle.

When the change of stress within a single cycle follows the sine law, the cyclic stress

$$\sigma=\sigma_m + \sigma_a \sin \omega t, \qquad (5.6)$$

where ω is the cyclic frequency (1/sec), related to the frequency of the stress, λ, by the expression $\omega=2\pi\lambda$.

The cycles are symmetrical when the extreme stress values (σ_{max} and σ_{min}) are equal in absolute value, but opposite in sign, or asymmetrical, when the absolute values of the extreme stress are not equal (see fig. 5.11). The characteristics of any cycle are its amplitude $\sigma_a=\frac{\sigma_{max}-\sigma_{min}}{2}$;

average stress $\sigma_m = \frac{\sigma_{max} + \sigma_{min}}{2}$; range $2\sigma_a = \sigma_{max} - \sigma_{min}$; and asymmetry coefficient $r = \frac{\sigma_{max}}{\sigma_{min}} = \frac{\sigma_m + \sigma_a}{\sigma_m - \sigma_a}$.

The concept of fatigue (or endurance) limit is introduced for the determination of the strength of the material during cyclic stressing. The fatigue limit σ^*_{ycm} for symmetrical cycling is the greatest absolute stress magnitude at which or below which the material can sustain an infinitely great number of cycles without fracturing.

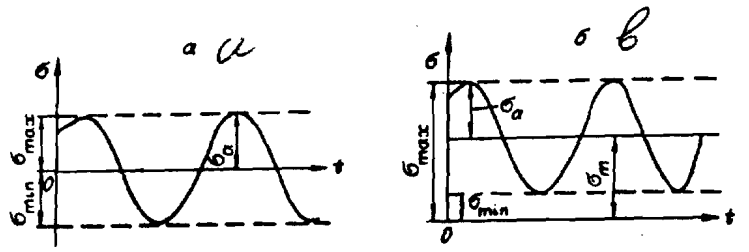

Fig. 5.11
Modes of cyclic stressing during a symmetrical (a) and an asymmetrical (b) cycle

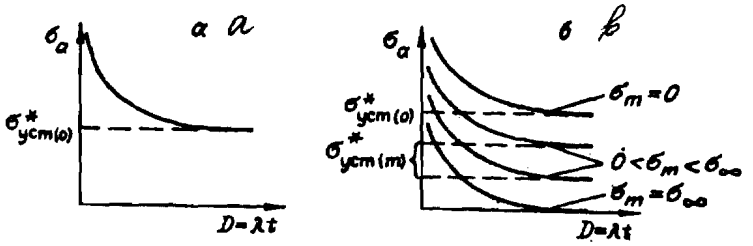

Fig. 5.12
Fatigue diagrams for a symmetrical (a) and an asymmetrical (b) cycle

*ycm= fatigue.Translator.

At alternating stresses involving changes in sign (when $\sigma_m = 0$) and having absolute values above the endurance (fatigue) limit, failure of the material will occur after a finite number of cycles D. The greater the amplitude of the applied cyclic stresses, the fewer the cycles preceding failure. Conversely, with decrease in the value of the maximum stress, the number of the stressing cycles preceding failure increases.

The dependence between the number of cycles D, at which failure occurs in a symmetrical cycle, and the amplitude of the applied cyclic stress σ_a is graphically represented in the form of a fatigue diagram (see fig. 5.12a). The asymptote of the fatigue diagram at $D=\lambda \cdot t \longrightarrow \infty$ is the fatigue limit σ^*_{ycm}.

The fatigue limit σ^*_{ycm} is regarded as the mechanical characteristic of the strength of the material defining its capacity for withstanding cyclic stresses.

Asymmetrical stressing cycles characterized by the asymmetry coefficient $r=\frac{\sigma_{max}}{\sigma_{min}}$ and stress range $(\sigma_{max}-\sigma_{min})$; or by the maximum and minimum stresses (σ_{max} and σ_{min}, respectively), or else by the static stress σ_m and the amplitude of the cyclic component σ_a, are associated with a set of fatigue diagrams (fig. 5.12b).

In this case the term fatigue limit continues to refer to the amplitude of the cyclic stress σ_a under the specified static stress σ_m which the material can sustain without fracturing even for an unlimited number of cycles D, and is designated as well as σ^*_{ycm}. The condition of indestructibility is obviously valid only for the case where the static stress σ_m is smaller than the long-time static endurance limit of the material, which corresponds for ice to its creep limit, i.e. at $\sigma_m \leq \sigma_\infty$.

Fatigue strength of a material can be related to the loss of deformation energy by internal friction.

Internal friction can be estimated from the hysteresis loops, the areas of which denote the amount of dissipated energy per cycle (fig. 5.13). The dependence of the dissipation of deformation energy on the number of cycles, asymmetry and magnitude of cyclic stresses for given plastic and structural properties of the material, and the effect of the released heat on the physical state can be derived from vibrocreep tests.

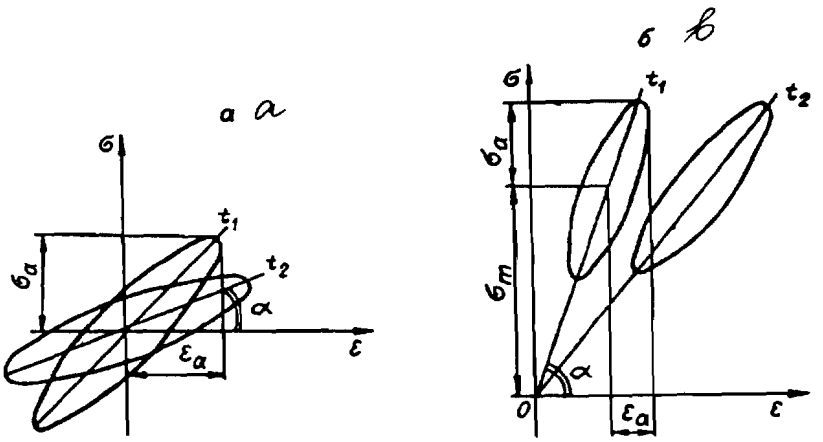

Fig. 5.13

Hysteresis loops for symmetrical (a) and asymmetrical (b) cycles

***

We shall differentiate between two domains of the deformation of materials during cyclic stressing.
The first domain is characterized by the resistance of the material to failure (i.e. by its indestructibility) regardless of the duration of stressing. In the case of a symmetrical cycle the amplitude of the effective cyclic stress is then limited to the value of the fatigue limit $\sigma^*_{ycm(0)}$, i.e.

$$\sigma_a \leq \sigma^*_{ycm(0)}. \tag{5.7}$$

In the case of an asymmetrical cycle the maximum (limit) amplitude depends on the static stress component σ_m, hence

$$\sigma_a \leq \sigma^*_{ycm(m)}. \tag{5.7a}$$

In the asymmetrical mode under cyclic stresses satisfying the conditions of (5.7), the rate of vibrocreep decreases in time in spite of the presence of an additional cyclic stress component, and the strain tends towards a constant value. In this domain vibrocreep is transient in character.

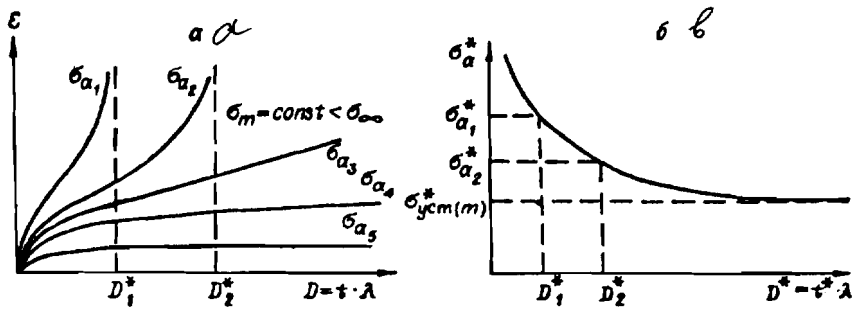

Fig. 5.14

Vibrocreep

a - development of total strain in time; b - fatigue diagram

***

The second domain may be referred to as the domain of tertiary vibrocreep. In this case a cyclic load applied to an earth material leads to its deformation progressing in time and terminating in its failure after a definite number of cycles. Moreover, the greater the amplitude of the cyclic stress σ_a, the more intensive the process of vibrocreep and the smaller the number of the cycles preceding failure of the material. Acceleration of the process of failure also depends on the value of the average static stress σ_m. The dependence

of the vibrocreep strain on the number of cycles is shown in fig. 5.14. The vibrocreep strain-rate decreases for maximum loads less than the long-time fatigue limit $\sigma^*_{ycm(m)}$, and the vibrocreep strain itself becomes stabilized (see fig. 5.14). The long-time fatigue limit $\sigma^*_{ycm(m)}$ is a function of the applied static stress σ_m. It is natural to consider smaller values of σ_m than the ultimate long-time static strength σ_∞. In the domain of transient vibrocreep, under isothermal conditions, the material hardens and its long-time static strength increases. In other words, after a specimen of the material has been "trained" by a cyclic load that does not exceed the ultimate long-time fatigue strength, failure under a static load requires a higher stress.

At stress amplitudes $\sigma_a > \sigma^*_{ycm(m)}$ the vibrocreep strain-rate increases with increasing number of cycles, and failure of the material occurs after a definite number of loading cycles. The number of cycles corresponding to failure D^* depends on the magnitude of the amplitude of the cyclic stress σ_a (see fig. 5.14b). The long-time fatigue limit of the material depends, however, in its turn on the applied static load σ_m and is meaningful only at $\sigma_m < \sigma_\infty$.

As was mentioned earlier, the phenomenon on which the process of vibrocreep is based, is hysteresis, i.e. the irretrievable loss of energy during each loading cycle. In the most general case the energy dissipated in the course of a cycle W is equal to the work done in the course of the cycle by the stress σ_a and corresponding strain amplitude ε_a:

$$W = \left| \oint \sigma_a d\varepsilon_a \right| = \left| \int_0^{2\pi/\omega} \sigma_a \cdot \dot{\varepsilon}_a dt \right|. \qquad (5.8)$$

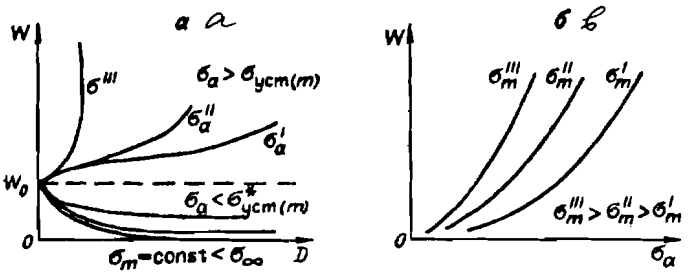

Fig. 5.15

Dependence of the energy dissipated in the course of a cycle on a) the number of cycles and the stress range, and b) the amplitude and static component of the stress

***

Moreover, whereas in the domain of transient vibrocreep the areas of the hysteresis loops corresponding to the work, W, decrease with increasing number of cycles, in the domain of tertiary creep the areas of the hysteresis loops do not decrease (fig. 5.15).

Results of the studies carried out by L.S. Lapidus et al. (1969) on soil fatigue, confirm in a way that the amount of energy dissipated over a loading cycle depends on the duration of the vibrocreep process (number of cycles). Table 5.2 is taken from that work.

As may be seen from table 5.2, in all the soil tests at stresses below the fatigue limit the area of the hysteresis loop decreased with time (with increasing number of loading cycles), whereas at amplitudes greater than the fatigue limit the energy dissipated in the course of a cycle increased with increasing number of cycles.

The use of elasticoviscous models of deformed media for describing the behaviour during cyclic stressing brings us to a general conclusion that the energy dissipated over a cycle depends on the frequency of the applied harmonic stress.

This is contradicted by the data from the literature on testing of various construction materials for which the area of the hysteresis loop is independent of the frequency of the stress and is merely a function of the range. The aforementioned conclusion should, however, be valid for ice, since the dependence of the area of the hysteresis loop on the frequency of the stress indicates that the internal inelastic resistance of the material depends on the strain-rate, and since it has already been established (see chapter 1) that the strain-rates and loading rates have a significant effect on the strength and deformation characteristics of ice.

TABLE 5.2

Earth materials	Stress	Area of the hysteresis loop, $H \cdot cm/cm^3 \cdot 10^2$		
		beginning of the test	middle of the test	end of the test
Montmorillonite	Below the fatigue limit	0.60	0.50	0.33
Montmorillonite with sand		0.50	0.32	0.30
Reddish-brown loam		0.32	0.28	0.26
Montmorillonite	Above the fatigue limit	1.0	1.47	2.15
Montmorillonite with sand		1.62	1.77	4.67
Reddish-brown loam		1.36	2.38	2.0

The energy dissipated in the course of a cycle, W, is evidently a function of the stress amplitude, the mean stress, frequency and number of cycles

$$W=W(\sigma_a,\sigma_m,\ \omega,\ D) \tag{5.9}$$

To solve the problem of failure of ice under cyclic loads it is necessary to determine the form of dependence (5.9).

It is quite obvious that the dependence of the dissipated energy on the number of cycles and on the parameters of the applied cyclic load is determined by the mechanism of the fatigue process developing in the material during vibrocreep.

Our notion of the mechanism of the fatigue process in ice is outlined below on the basis of the data on the relationship of the deformation of ice and kinetics of formation and development of structural defects discussed in preceding chapters.

The basic hypothesis is that ice, similar to all solids, contains a multitude of defects in the form of microscopic structural disturbances scattered throughout its bulk. The defects are small, yet of significant dimensions relative to the size of molecules or intermolecular spaces. These defects weaken the material: they reduce its cross-sectional areas and are the prime sites of stress concentrations, causing the occurrence of local overstresses at their edges. Under cyclic loads the local stresses near the edges of some of the microcracks increase. The enlargement of one or more of such microfractures engenders new structural defects, which subsequently coalesce into fatigue microcracks under the

continued action of a cyclic load. Failure probably occurs when the defects capable of forming major fatigue fractures attain a definite number. The kinetics of formation and development of fatigue defects is qualitatively the same as that for static conditions. It may be assumed that the formation of structural defects in the process of vibrocreep obeys the same laws as in the process of creep of ice under a static load. Proceeding from this assumption it may be argued that the dissipation of energy over a cycle is proportional to the number of the structural defects formed. The number of the structural defects formed in the process of deformation N is equal [Zaretskii and Vyalov, 1971] to the number of activated elements in the ice structure

$$N=N^{*}\exp\left[\frac{U_0 - U_t}{kT}\right], \qquad (5.10)$$

where U_0 is the initial activation energy of the structure and is a constant for a given physical state of the ice; U_t is the variation of the activation energy during creep as a result of the structural distortion; k is Boltzmann's constant; and T is the absolute temperature.

N^{*} is the number of defects corresponding to the critical degree of deformation (distortion) of the ice structure, at which the energy of activation (U_0-U_t) becomes equal to zero. Using the transition of ice to the stage of tertiary creep as the criterion of ice failure, we introduce the assumption, as was done in Yu.K. Zaretskii's work (1973), that the transition in question occurs at the time

when the energy of activation of the structural elements tends towards zero and the number of structural defects in ice attains its critical value, i.e. when

$$N \longrightarrow N^*$$

$$U_t \longrightarrow U_0. \tag{5.11}$$

The author [Zaretskii, 1973] proposes concrete forms for the analytical dependence of the activation energy on the applied stresses and time.

Juxtaposition of expressions (5.10) and (2.16) gives

$$N_0 = N^* \exp\left(-\frac{U_0}{kT}\right); \tag{5.12}$$

$$\frac{U_t}{kT} = \int_0^t \varkappa(T)\cdot\dot{\psi}(t)\cdot(\sigma - \sigma_\infty)\,dt. \tag{5.12a}$$

where σ_∞ is the long-time creep limit; $\varkappa(T)=\varkappa_0 T + \varkappa_1$; and $\dot{\psi}(t)$ is the influence function. All these quantities are determined experimentally.

The condition of failure derived from (5.11) and (5.12) has the form

$$\frac{U_{t^*}}{kT} = \frac{U_0}{kT} = \int_0^{t^*} \varkappa(T)\cdot\dot{\psi}(\tau)(\sigma - \sigma_\infty)\,d\tau. \tag{5.13}$$

The criterion formulated above can be used for determining the conditions of non failure of ice in the process of vibrocreep.

Non failure of soils during cyclic loading is obviously determined by the fact that whatever the duration of the applied load, the number of structural defects in the soils does not reach the critical value N*. In that case the number of structural defects should decrease from cycle to cycle, some of the defects should disappear ("healed"), and the areas of the hysteresis loops proportional to the number

of structural defects, should also decrease with increasing number of the load cycles.

To determine the failure limit of ice, we substitute for the variable cyclic load σ in equation (5.13) a certain equivalent constant load $\sigma^{э}$ causing failure of ice in time t^*. In that case

$$\frac{U_0}{kT} = \kappa(T)\cdot\psi(t^*)\cdot(\sigma^{э} - \sigma_\infty). \tag{5.14}$$

In accordance with (5.6),

$$\sigma^{э} = \frac{1}{t_0}\int_0^{t_0} (\sigma_m+\sigma_a \sin \omega t)dt, \tag{5.15}$$

where t_0 is the duration of the positive half of the loading cycle, during which plastic deformation occurs and defects accumulate, $t_0 = \Pi/\omega$. In that case

$$\sigma^{э} = \sigma_m + 2\sigma_a/\pi. \tag{5.16}$$

It follows from (5.14) and (5.16) that

$$\sigma_a^* = (\pi/2)(\sigma_\infty - \sigma_m) + \frac{(\pi/2)A}{\psi(t^*)}, \tag{5.17}$$

where $$A = \frac{U_0}{kT\cdot\kappa(T)}.$$

In equation (5.17) the time of failure (acceleration of creep) t^* appears only on the right-hand side in a term that tends to zero as $t^* \longrightarrow \infty$. The limit failure condition for ice during cyclic loading is thus the value of the maximum cyclic load

$\sigma_a = \sigma^*_{ycm(m)}$, at which equality $\sigma^*_{ycm(m)} = \frac{\Pi}{2}(\sigma_\infty - \sigma_m)$ (5.18)

is fulfilled.

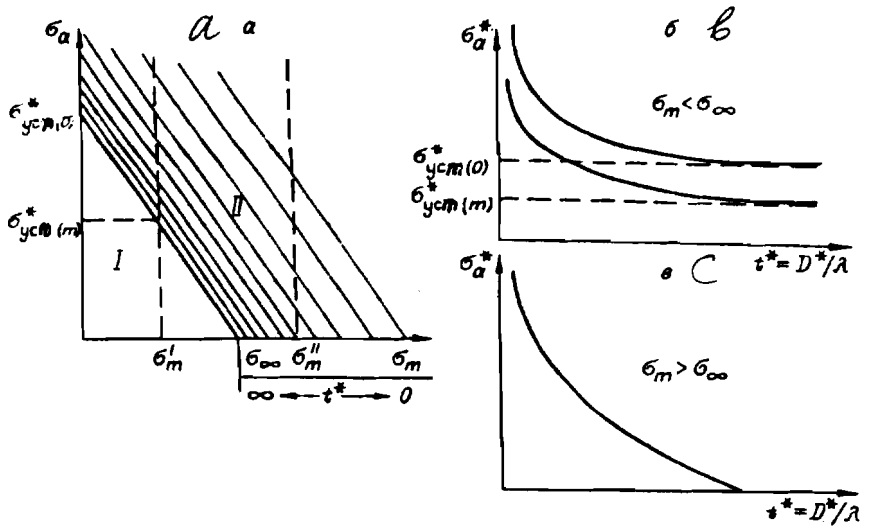

Fig. 5.16

Vibrocreep

a - strength diagram; b - fatigue diagrams

***

For a given static load σ_m, vibrocreep is transient in character only when the amplitude of the cyclic stress does not exceed the value specified by equality (5.18).

Equality (5.18) can be used to calculate theoretically the fatigue limit of ice if its long-time creep limit is known, and, in the case of an asymmetrical cycle, if the static component of stress is also known. The non failure condition for ice is defined in the σ_a-σ_m coordinates by the region enclosed between the coordinate axes and the straight line defined by (5.18). The intercept on the σ_m axis gives the long-time creep limit σ_∞, and on the Y-axis the long-time endurance limit during a symmetrical cycle, i.e. $\sigma^*_{ycm(0)}=1.57\sigma_\infty$ (fig. 5.16a).

The two domains are shown in fig. 5.16a. At certain combinations of the cyclic load amplitudes σ_a and static stress component σ_m the ice may be either in the region of transient vibrocreep (domain I), or in the tertiary vibrocreep region (domain II). Moreover, each line in the diagram shown in fig.5.16a corresponds to a definite value of failure time t*.

Dependences of fatigue strength on the number of cycles plotted on the Y-axis of the diagram in fig. 5.16a, are presented in figs 5.16b and c. At static stress components $\sigma_m < \sigma_\infty$ the asymptotes of the long-time fatigue curves (fig. 5.16b) characterize the long-time fatigue limits $\sigma^*_{ycm(m)}$ that are different for each asymmetrical cycle, i.e. for each value of σ_m. At $\sigma_m > \sigma_\infty$ the long-time fatigue curves (fig. 5.16c) cut across the X-axis at a definite time value. This means that failure of ice can be caused at that time by the static stress component alone.

The diagram examined is universal in character, since it covers breaking and non-breaking, static and dynamic stresses, as well as their combinations.

5.3. Testing of ice under cyclic loads

To verify experimentally the theoretical propositions outlined in section 5.1, a series of tests was performed with ice specimens in a uniaxially stressed state at different combinations of static and cyclic loads.

A mechanical vibrator generating vertical vibrations at a frequency of 12 to 100 Hz and an amplitude of 0.05 to 1 mm,

was used in the tests. A cylindrical ice specimen (diameter 50.5mm, height 100mm) placed on a vibrating table was subjected to static axial compression with a hydraulic jack. The jack was supported by a frame that was also secured to the table of the vibrator. An inertia mass for generating alternating stresses in the sample during the vibrations of the table was placed between the jack and the specimen. The amplitude of the alternating load σ_a was determined by the magnitude of the inertia mass, as well as by the range and frequency of vibrations of the table. The static component of the load σ_m consisted of the force generated by the jack and the weight of the inertia mass. A constant average load was maintained throughout the test using an air and oil compensator connected to the hydraulic system pump for the jack.

The ice tested was natural fresh-water lake ice with a columnar-grained structure, macrocrystalline, with a vertical orientation of the crystals measuring up to 40-70cm in length and 40-60 to 100-120cm^2 in cross-sectional area. The value of $\sigma_\infty = 8.10^5$ Pa was determined for the ice from the long-time strength curve obtained under static load. All the tests were carried out at a temperature of -4° C. The tests were performed using VI*6-5MA* equipment for measuring vibrations and of a tensodynamometer.

A block diagram of the measurements during the cyclic uniaxial tests is shown in fig. 5.17. The tensodynamometer is

* Transliteration. Translator.

located between the specimen and the table of the vibrator and senses all the forces transmitted to the specimen. Two displacement gauges are rigidly attached to the upper platen; one of the gauges records the total strain and the other the cyclic axial deformation.

Prior to loading the specimen the vibrator was turned on at the specified frequency and at the minimum amplitude of vibrations, and the required pressure was generated in the air and oil compensator with the valve of the jack in the off position. At the beginning of the test the valve of the jack was turned on and the amplitude of vibrations of the table was simultaneously raised to the required value. The time count began at that moment. The signals from the gauges were recorded by the oscillograph at the end of 5, 15, and 30 seconds, 1, 2, 3, 5, 10, 15 and 20 minutes from the beginning of the test, then every 10 minutes to the end of the hour and every 15 minutes after that. At each increase of 5% in the cross-sectional area of the specimen the axial load was increased so as to return the stress to the originally applied level. If the rate of deformation of the specimen increased, the experiment was terminated when the total axial deformation of the sample exceeded 10%. In the case of a decreasing or constant deformation rate the experiment continued for at least 4.0-4.5 hours (safe life of the equipment during continuous operation).

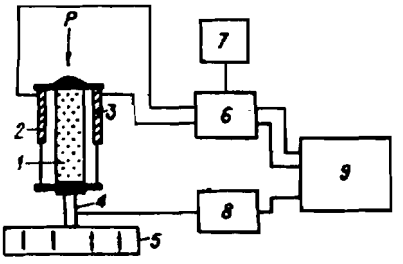

Fig. 5.17

Block diagram of measurements during cyclic tests

1 - Specimen; 2 - Total strain gauge; 3 - Cyclic strain gauge; 4 - Tensodynamometer; 5 - Vibrator; 6 - VI6-5MA amplifier; 7 - Power source; 8 - Tensoamplifier TA*-5; 9 - Oscillograph H*-105

***

From the oscillograms the frequency, amplitude and mode of application of the cyclic load (cyclic loading program) can be controlled, the graphical plots depicting the increase of the total strain in time (creep curves) can be constructed, and the paired values stress-cyclic strain can be obtained for any time. These pairs are read off every 10^{-3} sec and can be used to present graphically the hysteresis loops characterizing the amount of the deformation energy dissipated over the cycle.

In interpreting the results of the experiments we differentiated between two cases of deformation of the materials tested under cyclic loads.

In the first case the material does not fail regardless of the number of the loading cycles D to which it is subjected.

---

* Transliteration. Translator.

To satisfy that condition the amplitude of the cyclic loading σ_a must be smaller than a certain limiting value designated as the fatigue limit σ^*_{ycm}. The fatigue limit depends on the applied static load σ_m and is meaningful only if it has a smaller value than the long-time creep limit σ_∞; ($\sigma_m < \sigma_\infty$), since at $\sigma_m > \sigma_\infty$ the deformation invariably enters the tertiary stage and causes failure in the presence, as well as in the absence of a cyclic load.

In the second case the combination of static and cyclic loads (σ_m and σ_a, respectively) leads to progressive deformation (tertiary creep) and failure of the material after a definite number of cycles. That number is smaller, the greater the amplitude of the cyclic loading σ_a for the same value of σ_m.

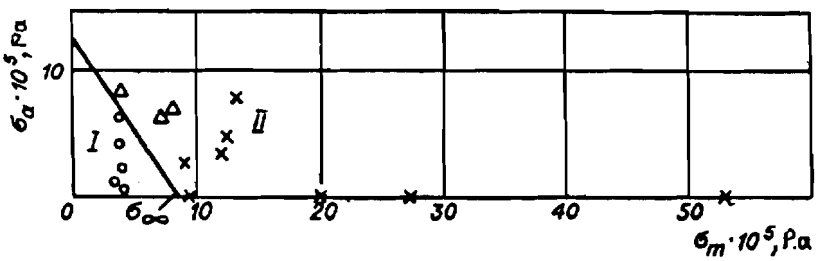

Fig. 5.18

Strength diagram of lake ice, $\theta = -4°C$

***

An analytical dependence of the activation energy of the structural elements on the applied stresses and time of the process is proposed in section 5.2. The dependence is based on assumptions regarding the relationship between the deformation of ice and kinetics of development of structural

defects. Proceeding from that dependence the fatigue limit at the given static load (designated as $\sigma^*_{ycm(m)}$) is defined by expression (5.18).

If the creep limit of ice σ_∞ is known, expression (5.18) can be used to plot for the given ice a long-time static and cyclic strength diagram, on the basis of which its failure or endurance can be predicted for any combination of static and cyclic loads (fig.5.18)

Domain I demarcated by the coordinate axes and the straight line (fig. 5.18), is the region of transient vibrocreep (i.e. indestructibility) of ice, since within that region the condition of non-failure (indestructibility) of ice $\sigma_a < \sigma^*_{ycm(m)}$ is fulfilled and the life-span of the ice specimen at any combination of the loads is theoretically infinite.

Domain II situated outside the straight line (5.18), may be designated as the region of tertiary vibrocreep. Any combination of the loads σ_m and σ_a corresponding to domain II, causes the vibrocreep strain-rate to rise and ultimately leads to failure of the material.

Results of the tests performed with specimens of lake ice are plotted in the diagram in fig. 5.18. The tests which ended in failure of the specimens or in transition to the stage of tertiary creep are marked with "*". The tests in which decreasing or constant strain-rates were obtained, are marked with "o". The points located on the σ_m axis were obtained from the static tests, and the position of the boundary between

the domains I and II, the value of $\sigma^*_{ycm(0)}$, by calculations according to equation (5.18). The disposition of the points within "their own" domains confirms the validity of the principle proposed as a basis for plotting strength diagrams.

The points marked with "Δ" should be mentioned separately. In these tests no failure of the specimens occurred, but neither was there any perceptible increase in the vibrocreep rate. The stage of transient creep was, however, exceeded in these tests and the deformation proceeded at an approximately constant rate. It may be assumed that these tests were discontinued before the creep had the opportunity to acquire a clearly defined accelerating character.

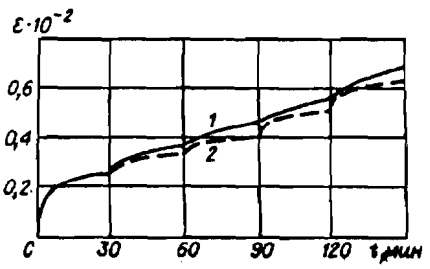

Fig. 5.19

Development of deformations in time during loading in stages, $\theta=-4°C$

1 - Static loading; $\sigma_1=4 \times 10^5$Pa; $\Delta\sigma=2\cdot10^5$Pa; 2-Cyclic loading; $\sigma_m=4\cdot10^5$Pa; $\Delta\sigma_a=2\cdot10^5$Pa

***

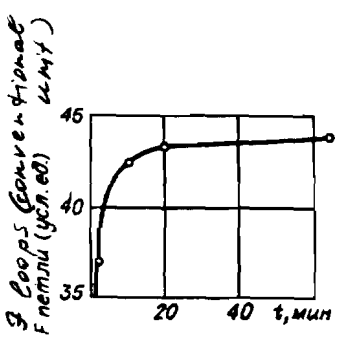

Fig. 5.20

Hysteresis loop as a function of time. $\theta=-4°C$; $\sigma_m=8.7\cdot10^5$Pa; $\sigma_a=2.2\cdot10^5$Pa; $\lambda=42$Hz

***

Figure 5.19 illustrates the apparent contradiction in the results of two tests with the same ice with loading in stages (fig. 5.19). At the initial stage the load was static $\sigma_1=\sigma_m$ in both tests, but after that in the first test it increased by $0.5\sigma_m$ at each successive stage, while in the second test the subsequent stages were applied in the form of a cyclic load that also increased from stage to stage by $\sigma_a=0.5\sigma_m$. The duration of each individual stage was 30 minutes. Fig. 5.19 combines the plots of the initial stages for the two tests.

It was found that in the test with cyclic loading the deformations became attenuated at all the stages, except the last one, whereas in the static test the deformation was of the transient kind only at the first two loading stages, while at the third stage the deformation rate was constant and at the last two stages it increased. Comparison of the results of these tests with the strength diagram for that ice shows that in the static test the first two loading stages were in domain I (i.e. in the region of non failure), the third one corresponded roughly to the boundary between domains I and II, and the last two stages were in domain II, i.e. in the region of tertiary creep. Examination of the dynamic loading stages shows that nearly all of them were in domain I, hence the attenuation of deformations observed in the test was as it should be. The rate at which the deformation developed during the last stage of that test did not decrease, which was consistent with the location of that stage in domain II.

It has been demonstrated in section 5.2 that from the viewpoint of energy the process of vibrocreep is determined by the amount of the loss of energy during each loading cycle. The area of the hysteresis loop plotted in the coordinates stress-cyclic strain, is equivalent to the energy dissipated in the material in the course of a loading cycle.

During transient deformation the rate of dissipation of the energy decreases and, as the number of the stressing cycles increases, the area of the hysteresis loop tends towards zero so that the loop itself degenerates into a straight line. This indicates that the deformation becomes purely elastic. In the region of tertiary vibrocreep the areas of hysteresis loops do not decrease.

The data from one of the tests which ended in tertiary creep and failure, were used to plot hysteresis loops for a series of times: 2, 10, 20, 40 and 64 minutes from the beginning of the test. As may be seen from fig. 5.20, the areas of the hysteresis loops increase in time (with increasing number of loading cycles). This indicates that the dissipation of energy increases over the loading cycle, which should cause failure of the specimen, and this is precisely what happened in reality.

CHAPTER 6

ALGORITHM OF THEORETICAL CALCULATIONS OF SHORT-TIME CREEP OF ICE

6.1. Fundamental equations of short-time creep of ice

The fundamental equations from which the short-time creep process in ice can be predicted theoretically are presented here in brief. The rather narrow problem of determining the stressed-strained state of an ice mass at constant temperature and subjected to the action of forces is discussed. As is well known, the problem specified is reduced in this case to solving the so-called boundary value problem with the fundamental system of equations consisting of a) equations of motion; b) equations of consistency (compatibility) of strains; c) equations of state, and of suitably formulated boundary (boundary value) and initial conditions. Subsequently the algorithm for the boundary value problem is constructed for strain-rates. Therefore only the following equations will be needed:

a. The law of conservation of mechanical energy

$$\dot{L} = \frac{d}{dt}(K+P), \tag{6.1}$$

where $\dot{L}$ is the output of the mechanical work done by the volume and surface forces of the system; K stands for the kinetic energy, and P for the potential internal energy.

For an element of volume this law leads to the system of equations (2.9) written as follows in the tensor form*:

* Compressive stresses and, accordingly, compressive strains are assumed here to be positive.

$$\sigma_{ij,j} = \delta_{j3} \cdot pg + \rho \dot{U}_i . \qquad (6.1a)$$

b. The kinematic relation between the strain-rate and the translational velocity gradient. The simplest relation has been adopted in this work:

$$\dot{\varepsilon}_{ij} = \frac{1}{2} \left(\dot{U}_{i,j} + \dot{U}_{j,i} \right). \qquad (6.2)$$

c. Equations of state. It is assumed that the strain-rates of ice are composed of elasticoviscous strain-rates $\dot{\varepsilon}^{(e)}_{ij}$ and viscoplastic strain-rates $\dot{\varepsilon}^{(p)}_{ij}$, i.e.

$$\dot{\varepsilon}_{ij} = \dot{\varepsilon}^{(e)}_{ij} + \dot{\varepsilon}^{(p)}_{ij} \qquad (6.3)$$

Then elasticoviscous strains* alone develop in the subcritical region, i.e. at stresses below the long-time creep limit of ice $\sigma_i \leq \sigma_{i(\infty)}$:

$$\dot{\sigma}_{ij} = \frac{d}{dt} \left[2G\varepsilon^{(e)}_{ij} + \delta_{ij} \left(K - \frac{2}{3} G \right) e^{(e)}_v \right], \qquad (6.4)$$

where G designates the shear modulus and K stands for the bulk modulus. A feature characteristic of ice is that its bulk modulus depends only on temperature and ice structure, whereas its shear modulus varies with time and is temperature-sensitive, being given by:

$$G = G_1 \cdot t^{-r}; \; G_1 = G_0(1 \pm |\theta|); \; r \leqslant 1; \; \theta < 0^\circ C. \qquad (6.5)$$

In this case relations (6.4) are written as

$$\dot{\sigma}_{ij} = 2G_1 \cdot t^{-r} \left(\dot{e}^{(e)}_{ij} - \frac{1}{3} \delta_{ij} \dot{e}_v \right) - 2rG_1 t^{-r-1} \left(e^{(e)}_{ij} - \frac{1}{3} \delta_{ij} e^{(e)}_v \right) + \delta_{ij} K \dot{e}^{(e)}_v; \qquad (6.4a)$$

$$\dot{\sigma}_i = G_1 t^{-r} \cdot \dot{e}^{(e)}_i - rG_1 t^{-r-1} \cdot e^{(e)}_i; \quad \dot{\sigma} = K \dot{e}^{(e)}_v .$$

* Any suitable elasticoviscosity model can be used

In the region of short-time creep, where there develop predominantly viscoplastic strains, the strain-rates are determined as the sum of the elasticoviscous and viscoplastic strain-rates. Viscoplastic strain-rates are calculated from the mathematical model of viscoplastic flow of ice formulated in chapter 2

$$\dot{e}_{ij}^{(p)} = \dot{h}\frac{\partial \Pi}{\partial \sigma_{ij}} = \dot{h}\left[\frac{\partial \Pi}{\partial \sigma_i}\cdot\frac{S_{ij}}{2\sigma_i} + \delta_{ij}\frac{1}{3}\frac{\partial \Pi}{\partial \sigma}\right], \tag{6.6}$$

where the loading function is given by the equation*

$$\Pi = \sigma_i - \sigma^*_{i(t)} - \frac{m}{\varkappa(T)\cdot\psi(t)}\ln\frac{\dot{e}_i^{(p)}}{\dot{e}_i^*}. \tag{6.7}$$

In this equation $\sigma^*_{i(t)}$ is expressed through the long-time creep limit of ice $\sigma_{i(\infty)} = c_\infty + \sigma\,\mathrm{tg}\varphi_\infty$ in the form

$$\sigma^*_{i(t)} = \sigma_{i(\infty)}\left[1 + \frac{\varkappa^*(T)}{\varkappa(T)\cdot\psi(t)}\right]. \tag{6.8}$$

The loading function can alternatively be written as

$$\Pi = \sigma_i - c_t - \sigma\cdot\mathrm{tg}\varphi_t, \tag{6.9}$$

where

$$\begin{aligned} c_t &= c_\infty\left[1 + \frac{\varkappa^*(T)}{\varkappa(T)\cdot\psi(t)}\right] + \frac{m}{\varkappa(T)\psi(t)}\cdot\ln\frac{\dot{e}_i^{(p)}}{\dot{e}_i^*}; \\ \mathrm{tg}\,\varphi_t &= \mathrm{tg}\,\varphi_\infty\left[1 + \frac{\varkappa^*(T)}{\varkappa(T)\psi(t)}\right]. \end{aligned} \tag{6.10}$$

---

* In section 2.3 the loading function (2.21a) differs from the function presented in (6.7) because of the multiplier which depends only on time. It can be easily demonstrated that loading functions differing in the multiplier that is independent of the stress components and hardening parameters, e.g. the loading functions Π and $a(t)\cdot\ $, are equivalent and that the factor a(t) does not affect the determination of the increments of plastic strains.

Viscoplastic strain-rates in the region $\sigma_i \geq \sigma_{i(\infty)}$ are thus fully defined by relations (6.6), (6.9) and (6.10), and the rates of the elasticoviscous strains occurring for $\sigma_i < \sigma_{i(\infty)}$, as well as for $\sigma_i \geq \sigma_{i(\infty)}$ are determined on the basis of formulas (6.4) and (6.5)*.

The above equations suffice for solving problems of mechanics for ice under isothermal conditions, if the boundary and initial conditions are added to them.

In conclusion the experimentally measurable functions and parameters forming part of the model for plastic flow of ice, are listed below.

1. Long-time creep limit $\sigma_{i(\infty)}$ dependent on the sum of the principal stresses $\sigma_{i(\infty)} = c_\infty + \sigma \mathrm{tg}\varphi_\infty$, or, in a more general form, $\sigma_{i(\infty)} = \Phi(\sigma)$.
2. Bulk modulus K and shear modulus $G=G_o(1+|\vartheta|)\cdot t^{-r}$, where ϑ is the negative temperature of the ice (°C); the values of the parameter r vary within the range of $1/3 \leq r < 1$.
3. Function of time $\psi(t)=t^{\delta_1}$; parameter $\delta_1 < 1$ is often equal to 1/3.
4. Functions of temperature $\kappa(T)$ and $\kappa^*(T)$ within a narrow temperature range ($250K<T<270K$) are taken in the form of linear functions.

---

* The possible plastic strains in the precritical state can be estimated on the basis of the works by Zaretskii et al. (1978a) and Zaretskii (1980).

5. The minimum flow rate of ice e_i^* characterizing the transition to the critical state under conditions of creep at constant stresses, is determined by the dependence

$$e_i^* = \frac{1}{\eta_0}\dot{\psi} = \frac{\delta_1}{\eta_0} t^{\delta_1 - 1}.$$

6.2. Algorithm for determining viscoplastic deformations

As was pointed out in the preceding section, determination of the stressed-strained state of an ice mass involves analysis of a certain system of differential equations. It follows from the system of equations of motion that the components of the total displacement velocity vector U_i, hence the components of the total strain-rate [in accordance with (6.2)] can be determined for the time $t+\Delta t$ if the components of the total displacement velocity vector for the preceding time step t and those of the stress tensor for the same time σ_{ij}^t are known. This can be easily demonstrated by substituting the finite difference approximation for the second derivative in time in the system of equations (6.1a), i.e.

$$\dot{U}_i^{t+\Delta t} = \dot{U}_i^t + \Delta t\left(\frac{1}{\rho}\sigma_{ij,j}^t - \delta_{i3}g\right). \tag{6.11}$$

However, the components of the stress tensor σ_{ij}^t for time t are known only if the components of elasticoviscous strains are known for that time, since (6.4a) gives a unique relation which is as follows in the finite-difference form:

$$\left.\begin{aligned}
&\sigma_{ij}^t = \sigma_{ij}^{t-\Delta t} + \Delta t\left[2G_1 t^{-r}\left(\dot{e}_{ij(t)}^{(e)} - \frac{1}{3}\delta_{ij}\dot{e}_{v(t)}^{(e)}\right) - \right.\\
&\qquad\left. - 2rG_1 t^{-r-1}\left(e_{ij(t)}^{(e)} - \frac{1}{3}\delta_{ij}e_{v(t)}^{(e)}\right) + \delta_{ij}K\dot{e}_{v(t)}^{(e)}\right];\\
&\sigma_i^t = \sigma_i^{t-\Delta t} + \Delta t\left[G_1 t^{-r}\dot{e}_{i(t)}^{(e)} - rG_1 t^{-r-1}e_{i(t)}^{(e)}\right];\\
&\sigma^t = \sigma^{t-\Delta t} + \Delta t\,\dot{e}_{v(t)}^{(e)};\quad e_{ij(t)}^{(e)} = e_{ij(t-\Delta t)}^{(e)} + \Delta t\,\dot{e}_{ij(t)}^{(e)}.
\end{aligned}\right\} \tag{6.46}$$

Since only the total strain-rates are known for time $\underline{t}$, the main problem is to work out an algorithm with the help of which the total strain-rates can be broken up into the sum of elasticoviscous and viscoplastic strain-rates (6.3). Once the elasticoviscous strain-rates have been determined, the stress components are calculated according to formulas (6.4b), after which the components of the displacement velocity vector are found for the next point in time on the basis of (6.11). This sequence of operations permits us to determine the stressed-strained for a given loading condition in the time interval that is of interest to us, beginning with time $t=0$, at which the initial conditions are set. This method of solving the problem has been proposed by V.N. Lombardo (1973), and the algorithm for determining plastic strains has been published by Zaretskii et al. (1979c and d; Zaretskii et al., 1979). Following the general principles of the method developed, we shall briefly examine the sequence of operations with the help of which the elasticoplastic and viscoplastic components of the plastic flow of ice are determined from the known total strains of the ice mass on the basis of the model proposed for plastic flow of ice.

Thus let the total displacement vector, the total strain components $\varepsilon_{ij(t-\Delta t)}$ and the components of viscoplastic strains $\varepsilon^{(p)}_{ij(t-t)}$ be known for the time step $t-\Delta t$. Only the combined displacement vector has been determined for step $\underline{t}$, hence the values of $\varepsilon_{ij(t)}$ are known. At step $\underline{t}$ the combined (total) strains must be separated into their elasticoviscous and

viscoplastic constituents, whereby the stress components will also be determined. In other words, at step $\underline{t}$ it is necessary to determine $\varepsilon^{(p)}_{ij(t)}$, $\varepsilon^{(p)}_{ij(t)}$ and σ^{t}_{ij}.

The sequence of operations in that algorithm is as follows.

1. It is assumed that no viscoplastic strains occurred during the step t-Δt to t. The strain difference

$$\varepsilon_{ij(t)} - \varepsilon^{(p)}_{ij}\ (t - \Delta t)$$

defines then conditionally the elasticoviscous strain designated by $\tilde{\varepsilon}_{ij}$, and the stresses are found from formulas

$$\tilde{\dot{S}}_{ij} = 2(G\tilde{\dot{e}}_{ij} + \dot{G}\tilde{e}_{ij});\ \tilde{\dot{\sigma}} = K\tilde{\dot{e}}_{v}. \tag{6.12}$$

The conditional elasticoviscous strain-rate, however, is equal in reality to $\tilde{\dot{\varepsilon}}_{ij} = \dot{\varepsilon}_{ij(t)} - \dot{\varepsilon}^{(p)}_{ij(t-\Delta t)} = \dot{\varepsilon}^{(e)}_{ij(t)} + \dot{\varepsilon}^{(p)}_{ij}$. The components of the stress tensor determined from (6.12) and its invariants are therefore equal to

$$\dot{\sigma}_{i(t)} = \tilde{\dot{\sigma}}_i - \left(G\dot{e}^{(p)}_i - \dot{G}\dot{e}^{(p)}_i dt\right) = \tilde{\dot{\sigma}}_i - G_2\dot{e}^{(p)}_i;$$
$$\dot{\sigma}_{(t)} = \tilde{\dot{\sigma}} - K\dot{e}^{(p)}_v, \tag{6.13}$$

where $G_2 = G\left(1 + \frac{r \cdot dt}{t}\right)$ and G is given by formula (6.5).

2. The position of the point with the coordinates $\{\tilde{\sigma}_i;\ \tilde{\sigma}\}$ is determined from the values of the invariants of the conditional stress tensor in the plane $\sigma_i \div \sigma$. The position of that point relative to the loading surface is analysed. If the point $\{\tilde{\sigma}_i;\ \tilde{\sigma}\}$ is inside the region demarcated by the σ axis and by the loading surface $\Pi=0$, these stresses are regarded as true, since in fact no increment of viscoplastic strains occurred in this case during the step t-Δt to t. In

the opposite case viscoplastic strains did arise during that loading step and the true stresses must be determined from formula (6.13). The true values of the invariants of the stress tensor are then found from the condition that the point sought must be on the loading surface and must satisfy the condition $\Pi=0$.

Determination of the true values of σ_i and σ is graphically illustrated in fig. 6.1. Once the values of σ_i and σ have been determined from the formulas derived from (6.13), the values of $\dot{e}_i^{(p)}$ and $\dot{\varepsilon}_v^{(p)}$ can be found. This is written analytically as follows. Relations (6.13) can be rewritten on the basis of the unified flow law as

$$\sigma_i = \tilde{\sigma}_i - G_2 \dot{h} \Delta t; \quad \sigma = \tilde{\sigma} + K \dot{h} \Delta t. \tag{6.13a}$$

Substituting (6.13a) into the loading surface equation $\Pi=\sigma_i - c_t - \sigma \operatorname{tg}\varphi_t$, we obtain

$$d\lambda \equiv \dot{h} \cdot \Delta t = \frac{\tilde{\sigma}_i - \tilde{\sigma} \operatorname{tg}\varphi_t - c_t}{G_2 + K \cdot \operatorname{tg}^2 \varphi_t}. \tag{6.14}$$

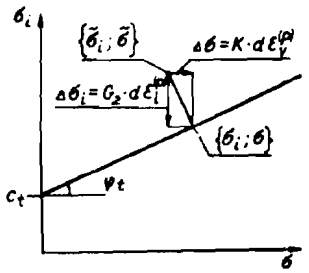

Fig. 6.1

Determination of the increments of plastic strains during loading

* * *

To determine the plastic factor $d\lambda$ it must be taken into consideration that the magnitude c_t can be represented in its turn in the form of (6.10), and that the intensity of the plasticoviscous strain-rate $\dot{e}_1^{(p)}$ is equal to $\frac{d\lambda}{dt}$. Taking into account the latter comments and formula (6.14), we can find

the plastic factor by solving the incremental equation

$$\Delta\lambda = A - mB \ln\left(\frac{1}{\dot{e}_i^*}\frac{\Delta\lambda}{\Delta t}\right), \tag{6.15}$$

into which we incorporate the following notations:

$$A = \frac{\tilde{\sigma}_i - (c_\infty + \tilde{\sigma}\,\mathrm{tg}\,\varphi_\infty)\left(1 + \frac{\varkappa^*}{\varkappa(T)\cdot\psi(t)}\right)}{G_2 + K\cdot\mathrm{tg}^2\varphi_\infty\left(1 + \frac{\varkappa^*}{\varkappa(T)\cdot\psi(t)}\right)^2};$$

$$B = \frac{1}{\left[G_2 + K\,\mathrm{tg}^2\varphi_\infty\left(1 + \frac{\varkappa^*}{\varkappa(T)\cdot\psi(t)}\right)^2\right]\varkappa(T)\cdot\psi(t)};$$

$$\frac{1}{\dot{e}_i^*} = 3\eta_0\cdot t^{2/3};$$

$$G_2 = G\left(1 - \frac{r}{t}\Delta t\right).$$

A special subprogram for solving equation (6.15) has been written for the computer program.

Once the value of $d\lambda$ has been calculated, the stress components can be readily found from formulas (6.13), after which the components of the tensor of the viscoplastic strain-rates $\dot{\varepsilon}^{(p)}_{ij(t)}$ can be calculated from the formulas of the unified plastic flow law

$$\dot{e}^{(p)}_{ij} - \frac{1}{3}\delta_{ij}\dot{e}^{(p)}_v = \dot{e}^{(p)}_{ij} = \frac{S_{ij}}{2\sigma_i}\frac{d\lambda}{dt};$$
$$\dot{e}^{(p)}_i = \frac{d\lambda}{dt}; \quad \dot{\varepsilon}^{(p)}_v = -\,\mathrm{tg}\,\varphi_t\cdot\dot{e}^{(p)}_i. \tag{6.16}$$

By using the algorithm presented above the stresses and the components of viscoplastic and viscoelastic strains can thus be determined as unique values for time t. As was mentioned earlier, the determination of the value sought for the next point in time $t+\Delta t$ involves once again solving an equation of the type of (6.11).

In conclusion we shall discuss in somewhat greater detail the solution of the equation of motion. It must be borne in

mind that the most convenient way of obtaining a numerical solution to equation (6.1a) is by using an explicit time formulation. The terms from the right-hand part of the equation comprising the stress gradients should be replaced by their difference analogue. To solve the problems of statics, it is proposed that equation (6.1a) be supplemented with a fictitious dissipative term and that the system of equations be written in the form

$$\rho\ddot{U}_i + n\dot{U} = \sigma_{ij,j} - \delta_{i2}g\rho, \tag{6.1б}$$

where n is a fictitious attenuation factor introduced for the sole purpose of ensuring that the static problem is derived from the steady-state solution of the dynamic system [Lombardo, 1975].

Discretization of the calculated area into elements of the kind shown in fig. 6.2 permits us to write equation (6.1b) in the following finite-difference approximation:

$$\dot{U}_i^{t+\Delta t} = \left\{\dot{U}_i^t + \Delta t\left[\frac{R_i}{\rho\Omega} - \delta_{i2}g\right]\right\}\frac{1}{1+\frac{n\Delta t}{\rho}}. \tag{6.1в}$$

where R_i is the projection on the i-axis of the stress resultant along the contour of the discretization element of the calculated area, and Ω is the volume of the element.

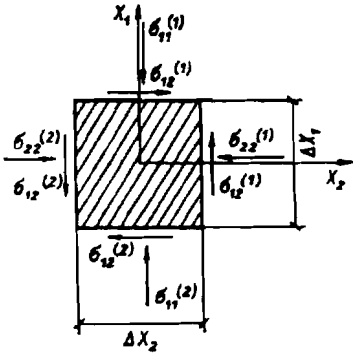

Fig. 6.2

Element of the calculated area

***

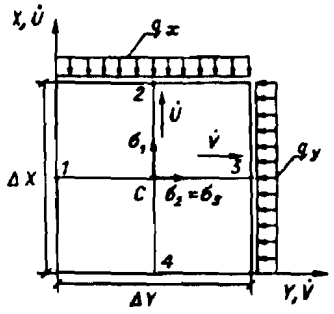

Fig. 6.3

Stresses and strains in the specimen during the triaxial compression test

***

6.3. Results of numerical modelling of uniaxial and triaxial compression of ice under conditions of short-time creep

The mathematical model proposed for the viscoplastic flow of ice, and the algorithm developed for solving numerically the problems involved in it, were tested first of all with the data from short-time creep tests of ice specimens. For that purpose M.E. Groshev wrote using the algorithm presented in the preceding section a computer program applicable to tests with ice in a triaxial compression apparatus. In the tests the stressed state is regarded as uniform and independent of the coordinates. In this case the result of numerical calculations should not depend on the density of the finite difference grid, and it is therefore possible to restrict ourselves to the grid shown in fig. 6.3. The vertical component of velocity $\dot{U}$ is determined from the X-axis at intercept 2, the horizontal component of velocity $\dot{V}$ is determined from the Y-axis at intercept 3, and the stresses $\sigma_{xx} = \sigma_1$, $\sigma_{yy} = \sigma_{zz} = \sigma_2 = \sigma_3$ and $\sigma_{xy} = \sigma_{xz} = \sigma_{zy} = 0$ are determined at intercept C. The principal strain-rates are

$$\dot{\varepsilon}_1 = \frac{\dot{U}}{\Delta X}; \quad \dot{\varepsilon}_2 = \dot{\varepsilon}_3 = \frac{\dot{V}}{\Delta Y}, \tag{6.17}$$

while the vertical velocities at point 4 and the horizontal velocities at intercept 1 are equal to zero according to the conditions of symmetry of the specimen. The finite difference equations of motion (disregarding the forces of gravity) will have the form [see formula (6.1c)]

$$\dot{U}^{t+\Delta t} = \left[\dot{U}^t + 2\Delta t\left(\frac{q_x - \sigma_1}{\rho \Delta X}\right)\right]\frac{1}{1+\frac{n}{\rho}\Delta t};$$
$$\dot{V}^{t+\Delta t} = \left[\dot{V}^t + 2\Delta t\left(\frac{q_y - \sigma_2}{\rho \Delta X}\right)\right]\frac{1}{1+\frac{n}{\rho}\Delta t}. \tag{6.18}$$

Equations (6.17) and (6.18) fully define the solution to the problem specified. The external load q_x and q_y is imposed by the path selected for loading the specimen. In the case of uniaxial compression $q_y=0$.

The program presented below (fig. 6.4) is written in FORTRAN. The designations adopted in that program are as follows:

XX and YY - external loads q_x and q_y (MPa);

SSR - argument of the functions $c_\infty(\sigma)$ and $tg\varphi_\infty(\sigma)$ specified in a tabulated form;

СЦД and ТФД - parameters of the viscoplastic yield c_∞(MPa) and $tg\varphi_\infty$;

X and Y - internal stresses σ_1 and $\sigma_2=\sigma_3$ (MPa);

SI and S - invariants of the stresses σ_1 and σ (MPa);

U and V - velocities of displacement $\dot{U}$ and $\dot{V}$ (m/sec);

EX and EY - strain-rates $\dot{\varepsilon}_1$ and $\dot{\varepsilon}_2=\dot{\varepsilon}_3$($sec^{-1}$);

E1 and E2 - strains ε_1 and $\varepsilon_2=\varepsilon_3$;

EI and EV - strain-rates $\dot{e}_i$ and $\dot{\varepsilon}_v$ (sec^{-1});

EI1 - elasticoviscous strain $e_t^{(e)}$;

DL - viscoplastic strain constituent $d\lambda$;

СДВ and ОБ - strains e_i and ε_v;

T - current time (sec.);

DT1 - calculated time step Δt_1 sec.);

TK - output interval (sec.);

LL - number of outputs;

A - time scale.

CONSTANTS

Reference constants

G1 - initial shear modulus G_1(MPa);

AK - bulk modulus K(MPa);

RO - density of ice p (g/cm^3);

ЭН - attenuation coefficient n ($g/cm^3 \cdot sec.$);

Experimental constants

APP - κ^* (MPa^{-1});

AP - κ(MPa^{-1});

ЭТ - $3\eta_o$ ($sec^{1/3}$);

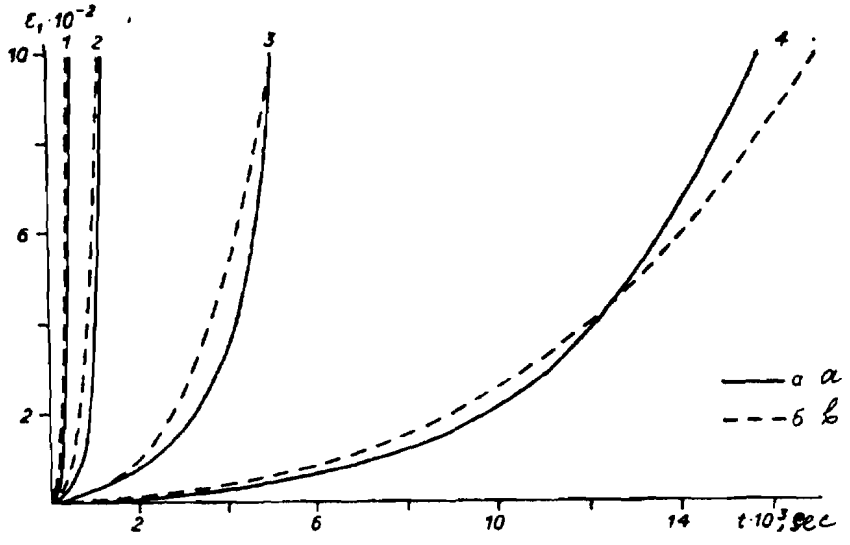

Fig. 6.5

Creep curves during uniaxial compression (θ=-4°C)
a - Experimental data; b - Calculations from the model of plastic flow.
1 - σ_1=2.02MPa; 2 - σ_1=1.6MPa; 3 - σ_1=1.14MPa; 4 - σ_1=0.91MPa

***

```
      PROGRAM ПОЛЗУЧЕСТЬ CREEP
      COMMON/BL1/DL,AS,B,СЦ
      DIMENSION XX(1),УУ(1),ТФД(100),СЦД(100),SSR(100)
      READ 1,NS◊PRINT1, NS
    1 FORMAT (I4)
      READ 2,(SSR(I),I=1,NS)◊READ 2,(СЦД(I),I=1,NS)
      READ 2,(ТФД(I),I=1,NS)
    2 FORMAT (7F7.4)
      PRINT 2 (SSR(I),I=1,NS)◊PRINT 2,(СЦД(I),I=1,NS)
      PRINT 2 (ТФД(I),I=1,NS
      PEAD 4,RO,ЭН,G1,AK,APP,AP,ЭТ,TK,LL
    4 FORMAT (7F10.4)
      PRINT 5,RO,ЭН,G1,AK,APP,AP,ЭТ,TK,LL
    5 FORMAT (9X,1F10.4)
      DT1=0.9/SQRT(2.*(4.*G1/3.+AK)/RO)
      AR=ЭН*DT1◊DT=TK*DT1*LL◊N=1/LL/DT1◊A=DT/DT1◊СЦ1=ЭТ/DT1
      READ 6,XX,УУ◊PRINT 6,XX,УУ
    6 FORMAT (2F9.7)
      SI=(XX-УУ)/SQRT(3. )◊S=(XX+2.*УУ)/3.◊E11=SI/G1◊T=1
      I0=1./3.◊I01=2./SQRT(3.)◊I02=SQRT(3.)/3.◊I04=2./(A*RO)◊I05=1.+AR/RO
      DO 21 I=1,LL◊DO 11 L=1,N◊T=T+DT◊R2=T**I00◊R1=1.+APP/(AP*R2)
      G=G1/SQRT(T)◊EX=Ц/A◊EУ=V/A◊EI=(EX-EУ)*I01◊EV=EX+2.*EУ
      СЦ=СЦ1*R2**2.◊G2=G*(1.-DT/2./T)
      SI=SI+DT*(G2*EI-E11*G/2./T/A)◊S=S+EV*AK*DT
      CALL SPA(SSR,СЦД,S,NS,SM)◊CALL SPA(SSR,ТФД,S,NS,TD)
      C=SM*R1◊TF=TD*R1◊ZN=AK*TF**2+G2◊AS=(SI-TF*S-C)/ZN◊B=1./(ZN*AP*R2)
      DL=0.◊IF(AS.GT.0.)CALL DLL◊SI=SI-DL*G2◊S=S+DL*TF*AK
      X=S+I01*SI◊У=S-SI*I02◊E1=E1+U*DT◊E2=E2+V*DT◊EI1=EI1+EI*DT-DL
      U=(U+DT*(XX-X)*I04)/I05◊V=(V+DT*(УУ-У)*I04)/I05
   11 CONTINUE
      ОБ=E1+2.*E2◊СДВ=(E1-E2)*I01
      PRINT 3,T,E1,ОБ,СДВ,SI,S,U,EX
   21 CONTINUE
    3 FORMAT(1X,8F15.8)
      STOP◊END
      SUBROUTINE DLL
      COMMON/BL1/DL,A,B,C
      XL=0.1E-14◊XP=EXP(A/B)/C
    1 X=(XL+XP)/2◊IF(XP-XL.LT.0.1E-9)GOTO 5
      R=X-A+B*ALOG(C*X)◊IF(R)4,5,6
    6 XP=X◊GOTO 1
    4 XL=X◊GOTO 1
    5 DL=X◊RETURN◊END
      SUBROUTINE SPA(X,У,R,L,SP)
      DIMENSION X(L),У(L)◊K=2◊DO 1 I=2,L
      IF((X(I).GT.R)AND.(X(I-1).LE.R))K=I
    1 CONTINUE
      IF(R.GT.X(L-1))K=L
      SP=У(K-1)+(R-X(K-1))*(У(K)-У(K-1))/(X(K)-X(K-1))
      RETURN◊END
```

Fig. 6.4

BESM-6 computer program for calculating short-time creep of ice

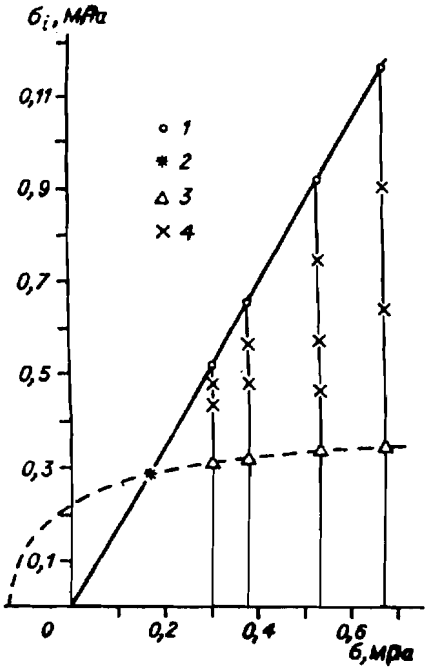

Fig. 6.6

Stresses in tests at $\theta=-4^{\circ}C$:

1 - the points of the real and numerical uniaxial compression tests; 2 - the values of the long-time creep limit $\sigma_{i(\infty)}$ determined from uniaxial compression tests; 3 - the points of the envelope function $\sigma_{i(\infty)}(\sigma)$; 4 - the points of numerical experiments in a composite stressed state.

***

Short-time creep of ice at a temperature of $\theta=-4^{\circ}C$ and under different external loads q_x was calculated with the help of the proposed program. The calculations were done with the following values of the parameters: $\kappa^*=71$ MPa^{-1}, $\kappa=1.48$ MPa^{-1}, $G=10^4$ MPa; $K=2.37\cdot10^4$ MPa; $\rho=0.9$ g/cm^3; $n=1000$ g/cm$^3\cdot$sec. (the factor 10^{-3} was introduced into the values of $\underline{p}$ to satisfy dimensional requirements);

$3\eta_0 = 1.6 \cdot 10^4 \cdot \sec^{1/3}$. It follows from fig. 5.7 that the points corresponding to the minima of the axial strain-rates at different stresses agree well with a line with the gradient 2/3. The segment intercepted by that line on the t=1 (in t=0) axis corresponds for the axial strain-rate to the value $3\eta_0 = 1.6 \cdot 10^5$ $\sec^{1/3}$, and for the shear strain intensity rate to a value that is roughly an order smaller.

The values of c_∞ and $tg\varphi_\infty$ presented below characterize the nonlinear dependence of the long-time creep limit $\sigma_{i(\infty)}$ on the sum of the principal stresses, which is commonly observed in strength tests of ice [Fokeev, 1976]. This nonlinearity is related to the fact that at small σ ice behaves like a material whose tensile strength differs sharply from its compressive strength, while at fairly large values of σ ice exhibits properties of a perfectly elastic material.

$\sigma(\cdot 10^{-5})$ Pa	1,667	3,033	3,8	5,333	6,733
$c_\infty(\cdot 10^{-5})$ Pa	2,48	2,70	2,78	2,92	3,0
$tg\varphi_\infty$	0,245	0,147	0,121	0,093	0,0739

Results of the calculations and their juxtaposition with experimental creep curves are shown in fig. 6.5. The good agreement of these data illustrates the possibilities offered by the model formulated for plastic flow of ice.

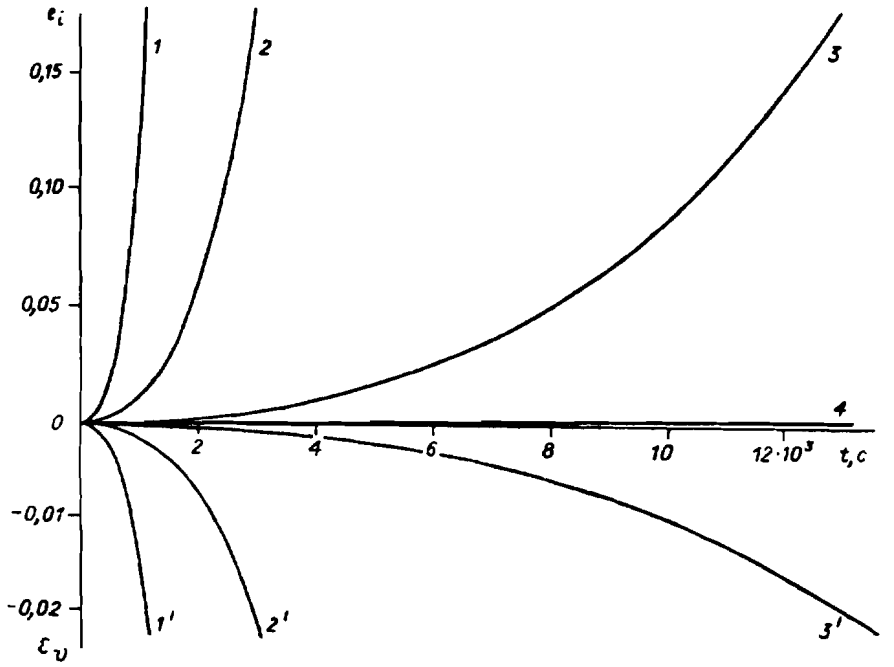

Fig. 6 7

Development of shear and volume strains (e_i and e_v, respectively) in time

Calculation at o=0.533 MPa; 0=-4°C:

1 and 1' - σ_i=0.923 MPa (σ_3=0.0; σ_1=1.6 MPa);

2 and 2' - σ_i=0.750 MPa (σ_3=0.1 MPa; σ_1=1.4 MPa);

3 and 3' - σ_i=0.577 MPa (σ_3=0.2 MPa; σ_1=1.2 MPa);

4 and 4' - σ_i=0.475 MPa (σ_3=0.26 MPa; σ_1=1.08 MPa).

***

The computer program proposed here was used in a series of numerical experiments simulating triaxial short-time creep tests of ice. The data from these experiments are combined in fig.6.6, where the loads applied to the ice specimen are given in the form of invariant stresses $\sigma_i=(q_x-q_y)/\sqrt{3}$; and $\sigma=(q_x+2q_y)/3$. At all the points in fig. 6.6, those

corresponding to experimental uniaxial loads (symbol 1), as well as those denoting arbitrary combinations of stresses (symbol 4), the loading procedure in the numerical tests was the same as in the real creep tests: the load was applied instantaneously and was maintained constant throughout the test. Some of the results obtained from the calculations for a number of points of the so-called purely deviatory path, i.e. at σ=const, are shown in fig. 6.7 in the form of dependences of the shear and volume deformation on time. Figure 6.7 shows that according to the proposed model of viscoplastic flow of ice, the volume deformation for the deviator stress $\sigma_i > \sigma_{i(\infty)}$ is "dilatational" due to the development and accumulation of structural defects. As may be seen from the plots, hydrostatic pressure significantly reduces the rate of accumulation of plastic deformations. Both these conclusions fully agree with the experimental results obtained from triaxial tests of ice specimens [Goughnour and Andersland, 1968; Jones, 1978].

It should be noted that in the examples discussed the calculations were done for the case of creep at constant stress (σ_i=const.). If it is necessary to calculate creep at a stress varying in time, the computer program should be able to accommodate appropriate data on the values of the loads q_x and q_y for any time. Any path in the plane (σ_1-σ) and any loading program can then be explored with the help of that program.

CONCLUSION

In this work the results of the recent theoretical and experimental studies by the author on the patterns of deformation and failure of ice during short-time creep are discussed. One of the variants of the theory of plastic flow for elastico-viscous-plastic media with contribution from the molecular-kinetic concepts of failure formed the theoretical basis of these studies. Short-time creep tests of fresh-water columnar-grained ice under compression at temperatures of -4, -8.5 and -13°C were performed with simultaneous recording of the acoustic emission accompanying microfracturing, crystallo-optic observations and quantitative analyses of the deformation-related metamorphism of the ice structure. Furthermore, vibrocreep tests of ice were carried out in uniaxial compression with cyclic loading of the ice specimens.

The integrated studies performed have confirmed the existence of a long-time creep limit for ice, i.e. of the stress below which the creep strain-rate decreases tending towards zero or a certain minimum, but above which the strain-rate steadily increases. It has been established that the initial appearance of brittle deformations (defects) in the ice structure and the attendant propagation of elastic oscillations (acoustic emission) correspond to the point at which the long-time creep limit is exceeded. It has been established that within the temperature range explored the creep limit σ_∞ is a constant characteristic of ice of the given structure. Under failure loads $\sigma > \sigma_\infty$ the deformation of ice is controlled mainly by the accumulation and development

of structural defects in ice, i.e. failure is a time-dependent process composed of discrete events involving the occurrence and progressive development of defects in the crystal structure of ice. The amount of the total deformation of ice is proportional to the combined total surface of the microdefects formed in the process of tertiary creep. The probability of occurrence of an isolated structural defect in ice is as many times greater than the probability of its healing as the applied stress is greater than the creep limit of the given ice. The statistical mean of the size of a defect (microcrack) increases from a certain minimum in proportion to the number of the microfractures formed in the process of creep, and does not depend either on the temperature of the ice, or on the stress acting on it. The number and surface area of the ice crystals are directly proportional to the number of cracks; moreover, that dependence is the same for all the temperatures and stresses.

The total number of microdefects per unit volume of ice tends towards a limit that is constant for ice of the given structure. This tendency can be used as the criterion of failure of ice during tertiary creep. In the event of long-time failure of ice under combined static and cyclic loads the amount of energy imparted by the vibrational action and dissipated in ice, hence the rate of the process of failure, are determined by the mechanism controlling the development of defects in the crystal structure of ice, as they are in statics. The criterion of ice failure adopted in statics, i.e. a critical number of defects, is also valid for tertiary vibrocreep.

By treating the macroprocess of short-time creep as a process dependent on the development and accumulation of discrete acts of microfracturing, it is possible to predict the viscoplastic deformations developing in ice by constructing an appropriate loading function on the basis of the theory of plastic flow.

The prospects for further investigations are both exciting and obvious. It is important to study the nature of the deformation and failure of ice under conditions of multiaxial (triaxial) stress states with arbitrary loading paths and programs, and the effect of the total principal stresses on the processes of microfracturing, strength of ice and rate of accumulation of plastic deformations. This information is required to confirm or elaborate more precisely the formulation of the loading function for algorithms and computer programs that can be used to calculate important practical engineering problems related to the buildup of ice against support structures, construction of foundations on buried ice or of ice structures, as well as problems pertaining to rapid advances of glaciers, operation of ice-breakers in pack or hummocky ice, etc. It should also be pointed out that the acoustic emission method used in our work under laboratory conditions can be effectively adapted for monitoring the interaction of ice with engineering structures, as well as for analysing and predicting stresses and strains of natural ice masses.

REFERENCES

Берденников В. П., Хаминов П. А., Шматков В. А. Инструментальное изучение сжатия ледяного покрова оз. Байкал.— Науч. тр. Гидрологического ин-та, 1968, вып. 159, с. 15—22.

Богородский В. В., Гаврило В. П., Гусев А. В. Звукообразование при разрушении образцов льда в жидкости.— В кн.: Труды VI Всесоюз. акустической конференции. М., 1968, с. 4.

Богородский В. В., Гусев А. В., Хохлов Г. П. Физика пресноводного льда. Л., Гидрометеоиздат, 1971. 227 с.

Богородский В. В., Гаврило В. П., Григорьев В. С. и др. Напряженное состояние ледяного покрова и сопутствующий ему акустический эффект.— Науч. тр. Ин-та Арктики и Антарктики. Т. 324. Л.: Гидрометеоиздат, 1974.

Бутягин И. П. Прочность льда и ледяного покрова. Новосибирск: Наука, 1966. 154 с.

Вейнберг Б. П. Лед. М.— Л.: Гостехтеориздат, 1940. 524 с.

Виноградов С. Д. Акустические наблюдения процессов разрушения горных пород. М.: Наука, 1964. 84 с.

Войтковский К. Ф. Механические свойства льда. М.: Изд-во АН СССР, 1960. 100 с.

Войтковский К. Ф., Голубев В. Н. Зависимость механических свойств льда от его структуры.— В кн.: Лед и его воздействие на гидротехнические сооружения. Л., 1972, с. 3—8.

Вялов С. С. Закономерности деформирования льда.— В кн.: Сов. антаркт. экспедиция. Т. 10. Л.: Морской транспорт, 1960.

Вялов С. С. Реология льда.— В кн.: Материалы гляциол. исследований. Хроника, обсуждения. Вып. 22. М., 1973, с. 39—44.

Вялов С. С. Кинетическая теория деформирования грунтов.— В кн.: Труды II Всесоюз. симпозиума по реологии грунтов. Ереван, 1976, с. 22—40.

Вялов С. С., Докучаев В. В., Шейнкман Д. Р. Подземные льды и сильнольдистые грунты как основания сооружений.— Л.: Стройиздат, 1976. 168 с.

Вялов С. С., Зарецкий Ю. К., Максимяк Р. В., Пекарская Н. К. Кинетика структурных деформаций и разрушения глин.— В кн.: Труды VIII Междунар. конгресса по механике грунтов и фундаментостроению. М.: Стройиздат, 1973.

Вялов С. С., Пекарская Н. К., Максимяк Р. В. О физической сущности процессов деформирования и разрушения глинистых грунтов.— Основания, фундаменты и механика грунтов, 1970, № 1.

Вялов С. С., Чернигов В. А. Зависимость между напряжением и деформацией льда с учетом фактора времени.— В кн.: Сов. антаркт. экспедиция. Т. 10. Л.: Морской транспорт, 1960.

Гайдаенко Е. И. Исследование льдов в качестве основания сооружений. Новосибирск: Наука, 1978. 81 с.

Грешников В. А., Дробот Ю. Б. Акустическая эмиссия. Применение

для испытаний материалов и изделий. М.: изд. Стандартов, 1976. 272 с.

Зарецкий Ю. К. Неустановившаяся ползучесть и прочность мерзлых грунтов.— В кн.: Тезисы докладов Всесоюз. совещ. по мерзлотоведению. М.: Изд-во Моск. ун-та, 1970.

Зарецкий Ю. К. Длительная прочность грунтов.— В кн.: Труды I Всесоюз. симпозиума по реологии грунтов. Ереван, 1973, с. 43—68.

Зарецкий Ю. К. Новая концепция упруго-вязкопластического поведения грунтов.— В кн.: Труды III Всесоюз. симпозиума по реологии грунтов. Ереван, 1980, с. 58—73.

Зарецкий Ю. К., Вялов С. С. Вопросы структурной механики глинистых грунтов.— Основания, фундаменты и механика грунтов, 1971, № 3, с. 1—5.

Зарецкий Ю. К., Фиш А. М. и др. Вопросы кратковременной ползучести льда и кинетика микротрещинообразования.— Науч. тр. Ин-та Арктики и Антарктики, 1975, т. 326, с. 197—204.

Зарецкий Ю. К., Соломатин В. И., Чумичев Б. Д. К вопросу о микромеханизме деформирования льда под нагрузкой.— В кн.: Труды II Всесоюз. симпозиума по реологии грунтов. Ереван, 1976, с. 200—210.

Зарецкий Ю. К., Чумичев Б. Д. Реологические свойства льда.— В кн.: Инженерное мерзлотоведение. М.: Наука, 1979а, с. 179—191.

Зарецкий Ю. К., Чумичев Б. Д., Соломатин В. И. и др. Разрушение льда в условиях кратковременной ползучести.— В кн.: Инженерное мерзлотоведение. Новосибирск: Наука, 1979б, с. 115—127.

Зарецкий Ю. К., Ломбардо В. Н., Грошев М. Е. Пластическое течение грунтовых массивов.— Известия вузов. Строительство и архитектура. 1979в, № 2, с. 3—23.

Зарецкий Ю. К. и др. Алгоритмы расчета водонасыщенных грунтов.— Изв. ВНИИГ, 1979г, т. 130, с. 26—34.

Картер Д. С. Хрупкое разрушение поликристаллического льда при сжатии.— В кн.: Лед и его воздействие на гидротехнические сооружения. Л., 1972, с. 69—79.

Классен-Неклюдова М. В. Механическое двойникование кристаллов. М.: Изд-во АН СССР, 1960.

Койтер В. Т. Общие теоремы теории упруго-пластических сред. М.: ИЛ, 1961.

Константинова А. Г. Сейсмоакустические исследования предвыбросных разрушений угольных пластов. М.: Наука, 1977. 132 с.

Коржавин К. Н. Воздействие льда на инженерные сооружения. Новосибирск: Изд-во СО АН СССР, 1962.

Коржавин К. Н., Птухин Ф. И. К оценке предела прочности льда на сжатие при кратковременных быстровозрастающих нагрузках.— В кн.: Материалы VIII Всесоюз. совещ. по геокриологии. Вып. 5. Якутск, 1966, с. 61—72.

Лавров В. В. Деформация и прочность льда. Л.: Гидрометеоиздат, 1969. 206 с.

Лапидус Л. С., Самсонова С. И., Стороженко В. И. Исследование усталости грунтов.— В кн.: Динамика оснований и фундаментов. (Труды II конф.). Т. I. М., 1969.

Ломбардо В. Н. Алгоритмы численного решения плоских динамических и статических задач теории упругости.— Изв. ВНИИГ, 1973, т. 103, с. 152—163.

Петров И. Г. Выбор наиболее вероятных значений механических характеристик льда.— Науч. тр. Ин-та Арктики и Антарктики, 1976, т. 331, с. 4—41.

Птухин Ф. И. Влияние скорости деформирования на предел прочности речного льда.— Тр. ТЭИ СО АН СССР, Новосибирск, 1962, вып. 15.

Рамсейер Р. О., Дикинс Д. Ф. Новые методы натурных и лабораторных испытаний прочности поликристаллического пресноводного льда на растяжение, сжатие и изгиб.— В кн.: Лед и его воздействие на гидротехнические сооружения. Л., 1972, с. 164—169.

Регель В. Р., Слуцкер А. И., Томашевский Э. Е. Кинетическая природа прочности твердых тел. М.: Наука, 1974. 560 с.

Савельев Б. А. Строение, состав и свойства ледяного покрова морских и пресных водоемов. М.: Изд-во Моск. ун-та, 1963.

Савельев Б. А., Гуликов А. Е. Изменение структуры льда под действием нагрузки.— В кн.: Мерзлотные исследования. Вып. IV. М.: Изд-во Моск. ун-та, 1964, с. 391—396.

Сериков М. И. Определение модуля упругости льда резонансным методом.— В кн.: Проблемы Арктики и Антарктики. Вып. 6. Л.: Морской транспорт, 1959, с. 81—87.

Соломатин В. И., Зарецкий Ю. К., Чумичев В. Д. и др. Исследование структурных процессов в деформируемом льде.— В кн.: Инженерное мерзлотоведение. Новосибирск: Наука, 1979, с. 188—191.

Фокеев Н. В. Определение прочности искусственных образцов льда различной солености на сжатие в условиях сложного нагружения.— Труды ААНИИ, 1976, т. 331, с. 189—202.

Фредеркинг Р. Предварительные данные по плоским деформациям при испытании столбчато-зернистого льда на сжатие.— В кн.: Лед и его воздействие на гидротехнические сооружения. Л., 1972, с. 20—30.

Фукуда А., Хигаши А. Исследования деформации монокристаллов льда топографическим методом дифракции рентгеновских лучей.— В кн.: Физика льда. Л.: Гидрометеоиздат, 1973, с. 61—64.

Черепанов Н. В. Классификация льдов природных водоемов.— Науч. тр. Ин-та Арктики и Антарктики, 1976, т. 331, с. 77—99.

Шамина О. Г. Упругие импульсы при разрушении образцов горных пород.— Изв. АН СССР. Сер. геофиз., 1956, № 5, с. 513—518.

Шульман А. Р. Текучесть поликристаллического льда.— Науч. тр. Гидрологического ин-та, 1948, вып. 7.

Шумский П. А. Основы структурного ледоведения. М.: Изд-во АН СССР, 1955. 492 с.

Шумский П. А. Механизм деформирования и перекристаллизации льда.— В кн.: Исследования по физике и механике мерзлых грунтов. Сб. 4. М.: Изд-во АН СССР, 1961, с. 129—136.

Шумский П. А. Динамическая гляциология. М., 1969.

Шушерина Е. П. Коэффициент поперечной деформации и объемные деформации льда в процессе ползучести.— В кн.: Мерзлотные исследования. Вып. VII. М.: Изд-во Моск. ун-та, 1967, с. 251—257.

Шушерина Е. П., Гуликов А. Е. Влияние строения льда на его механические свойства.— В кн.: Мерзлотные исследования. Вып. 4. М.: Изд-во Моск. ун-та, 1964, с. 376—390.

Brown E. Experiments on strength of ice. St. Lawrence Waterway Project.— In: Report on Joint Board of Engineers. App. F, 1926, p. 423—453.

Dillon H. B., Andersland O. B. Deformation rates of polycrystalline ice.— In: Phys. Snow and Ice. Sapporo, Intern. Conf. on Low Temperat. Sci., 1967, vol. 1, p. 313—328.

Dunegan H. L., Tatro C. A. Acoustic Emission Effects During Mechanical Deformation.— In: Techn. of Metal Research, vol. 5, Interscience Publishers, N. Y., 1971.

Glen J. W. The creep of polycrystalline ice.— Proc. Roy. Soc. Ser. A., 1955, vol. 288, N 1175, p. 519—538.

Glen J. W. The mechanical properties of ice.— Advances in physics, 1958, vol. 7, N 26, p. 254—265.

Glen J. W., Perutz M. F. The growth and deformation of ice crystals.— J. Glaciol., 1954, vol. 2, N 16, p. 397—403.

Gold L. W. The cracking activity in ice during creep.— Canad. J. of Phys., 1960, vol. 38, N 9, p. 1137—1148.

Gold L. W. Dependence of crack formation on crystallographic orientation for ice.— Canad. J. of Phys., 1966, vol. 44, p. 2757—2764.

Gold L. W. Elastic and strength properties of fresh water ice.— Techn. Pap. N 283, NRC of Canada, Div. Build. Res., 1968, p. 13—23.

Gold L. W. Crack formation in ice during creep.— Scripta Metallurgia, 1969, vol. 3, N 6, p. 178—184.

Gold L. W. The process of failure of columnar—grained ice.— Phil. Mag. (G. B.), 1972a, vol. 26, N 2, p. 311—328.

Gold L. W. The failure process in columnar—grained ice.— Techn. Pap. N 369, NRC, Div. Build. Res., Ottawa, 1972b. 138 p.

Gold L. W., Krausz A. S. Investigation of the mechanical properties of St. Lawrence River ice.— Canad. Geotechn. J. 1971, vol. 8, № 163.

Goughnour R. R., Andersland O. B. Mechanical Properties of a Sand Ice System.— J. Soil. Mech. and Foundat. Div., Proc. Amer. Soc. Civ. Eng., 1968, vol. 94, N 4, p. 923—950.

Hawkes I., Mellor M. Deformation and fracture of ice under uniaxial stress.— J. Glaciol., 1972, vol. 11, N 61, p. 103—131.

Higashi A. Mechanical Properties of Ice Single Crystals.— In: Physics of Ice. Proc. Intern. Symp. Münich, Germany, 1968, N. Y., 1969.

Jones S. J. Triaxial testing of polycrystalline ice.— In: Third Intern. Conf. on permafrost, Proc., vol. 1. Ottawa, 1978, p. 671—674.

Ketcham W. M., Hobbs P. V. An Experimental Determination of the Surface Energies of Ice.— Philos. Mag., 1969, vol. 19, N 162, p. 1161—1173.

Koerner R. M., Lord A. E. Acoustic emission monitoring of earth dam stability.— Water Power and Dam Constr., 1976, vol. 28, N 64, p. 45—49.

Krausz A. S. Plastic deformation of fresh water ice.— Techn. Pap. N 284, Nat. Res. Council of Canada. Div. Build. Res., Ottawa, 1968, p. 5—12.

Mellor M., Smith J. H. Creep of snow and ice.— In: Physics of Snow and Ice. Intern. Conf. on Low Temperat. Sci. Sapporo, 1967, vol. 1, pt. 2, p. 843—855.

Naghdi P. M., Murch S. A. On the mechanical behaviour of viscoelastic/plastic solids.— J. Appl. Mech., 1963, vol. 30, p. 321—328.

Nakaya N. Mechanical properties of single ice crystals. SIPRE Res. Rep. 28. CRREL US Army, 1958.

Neave K. G., Savage J. C. Icequakes on the Athabaska Glacier.— J. of Geophys. Res., 1970, vol. 75, N 8, p. 1351—1362.

Steinemann S. Results of preliminary experiments on the plasticity of ice crystals.— J. Glaciol., 1954, vol. 2, N 16, p. 404—413.

Webb W. W., Hayes C. E. Dislocations and plastic deformation of ice.— Philos. Mag., 1967, vol. 16, N 143.

Weertman J. The Eshelby-Schoeck viscous dislocation damping mechanism applied to the steady-state creep of ice.— In: Ice and Snow. Properties, Processes and Applications. Chap. 3, Cambridge (Mass.), 1963, p. 28—33.

Weertman J. Creep of ice.— In: Phys. and Chem. of ice. Canad. Roy. Soc., Ottawa, 1973, p. 320—327.

Zaretsky Yu. K., Lombardo V. M., Groshev M. E. The plastic flow of soils and analysis of stability of earthen structures.— In: 3d Intern. Conf. on Numerical Methods in Geomechanics. (Aachen, 2—6 April, 1979), 1979.